The Sensitivities of Blast Parameters in Predicting TNT Equivalence from Experimental Data

Lisa Witty

24th March 2023

University of Sheffield

with

DNV Spadeadam Research and Development

For the Spadeadam C Pad Team, it would all be nothing without you.

Abstract

When an explosive detonates, whether a high explosive, or a flammable gas or vapour, a high pressure shock wave is produced that expands rapidly away from the initiation point. For anything caught in the path of this shock wave, the initial peak pressure and the impulse loading can cause severe damage to occur. In order to facilitate a safer built environment, modern architectural design requires an accurate and complete understanding of the response of structures to shock waves caused by a variety of explosives and explosive fuels.

When modelling the range of possible explosives, a TNT equivalence factor is usually considered. This equivalence factor relates the amount of energy released of any explosive or fuel directly to the equivalent energy of TNT. To be able to accurately assess and effectively utilise this equivalence, it is imperative that the parameters are not only measured and calculated using accurate and reliable methods, but that the shortcomings and caveats of the TNT equivalence model is well understood. Effective modelling requires an understanding of how the different parameters measured with a pressure wave can vary relative to each other depending on factors such as the unique behaviour of different types of explosives; conditions such as the size or casing of the explosive; or the positioning of the explosive relative to the structure under consideration.

To enable this thesis to examine the behaviour of explosions in a significantly more thorough and scientific approach than previously possible, the author has conducted in excess of ninety explosive tests using ANFO, PE4 Nitromethane and Hydrogen, resulting in approximately 950 data points. The data produced from these trials permits an in depth examination of the sensitivities involved with measuring blast parameters during experimental trials, allowing an evaluation of the factors to be considered in order to produce accurate and reliable data.

Key findings of this research identifies the superiority of using pencil gauges for freefield pressure measurement; ensuring reflected gauges are installed within targets that are either appropriate for the trial or as large as possible to reduce clearing effects; and reducing interactions between targets in a single arena. This thesis also demonstrates the value of applying a Friedlander curve-fit to experimental pressure data as a way to produce a repeatable and reliable way to identify key parameters from the data.

Applying these recommendations, further trials were conducted, producing a second data set, shown through assessment of the uncertainty factors and coefficient of variation to be both highly repeatable and accurate. This data set was then used to validate Air3D and ConWep as computer models for use in predicting blast parameters, finding excellent agreement between the experimental data and the outputs from the models. This work stands as the largest experimental comparison seen in literature.

The expansive experimental data set was then used to validate the Hopkinson-Cranz scaling law, proving its use for a range of charge sizes and scaled distances for PE4 and ANFO. It was also used to validate the calculation of energy flux using the Grisaro method for PE4, ANFO, Nitromethane and Hydrogen. This method had only previously been investigated by Swisdak and Grisaro using very limited data and for neither commercial explosives nor gas. Using the calculated energy flux, the author compared these values to that from TNT to allow calculation of TNT equivalences. This produced values found to be independent of charge size and stand-off, and in good agreement with current literature: 1.2 for PE4, 0.81 for ANFO and 25 for Hydrogen.

In summary, this thesis explores how the sensitivities of blast parameters can vary within experimental trials and makes recommendations for producing reliable data. It also suggests a new method for producing a value for TNT Equivalence. While there remain a great number of complexities which offer potential for further investigation, it is believed that the work presented here will both enhance the reliability and accuracy of explosive testing, and will act as a springboard for further research.

Acknowledgements

Firstly, I'd like to thank my supervisors Prof. Andy Tyas and Dr. Sam Rigby, for their support and guidance throughout this journey. Their insights and challenging questions allowed me to explore avenues and produce the best work I could, especially trying to take the commercial hat off and put the academic hat back on.

I would like to thank the whole team at Spadeadam, but especially the C-Pad team: Adam, Willy, Gareth and Fraser for the never ending enthusiasm in the running of trials, no matter how stressful it got and no matter how much it rained. Alastair for the what probably felt like endless questions and queries, especially as I approached the end. Celebrating when I produced a graph I loved, and providing support when I hit setbacks. Paul, Mike and Dan for their technical reviews and for questioning why at every stage.

Mum, Dad and my brother Paul for the encouragement and support throughout. Dad, I'm sorry I kept making the same grammatical errors again and again. You're a huge inspiration to me and one of the first reasons I wanted to achieve this PhD.

Finally to my fantastic running coach Peter, and my running friends - too many to mention individually, who gave me an escape when the work was getting me down, but who also understood and encouraged me when I had to stay in and knuckle down.

Forever grateful, Lisa

Contents

List of Figures

List of Tables

1 Introduction

Explosive use has long been a keen interest of the military community and, with the onset of global terrorism, the understanding of the complexities of explosives has never been more important. Since 2007, despite many counter-measures, neither the number of countries affected, nor the number of deaths associated with terrorism, show little signs of slowing down or reducing, as seen in the Global Terrorism Index 2022 (Figure 1.1). Due to that trend, the ongoing need for the analysis of explosive effects for different explosive types, charge sizes and stand-offs is important for numerous purposes, such as designing protective measures for buildings and public spaces and the investigations of terrorist attacks.

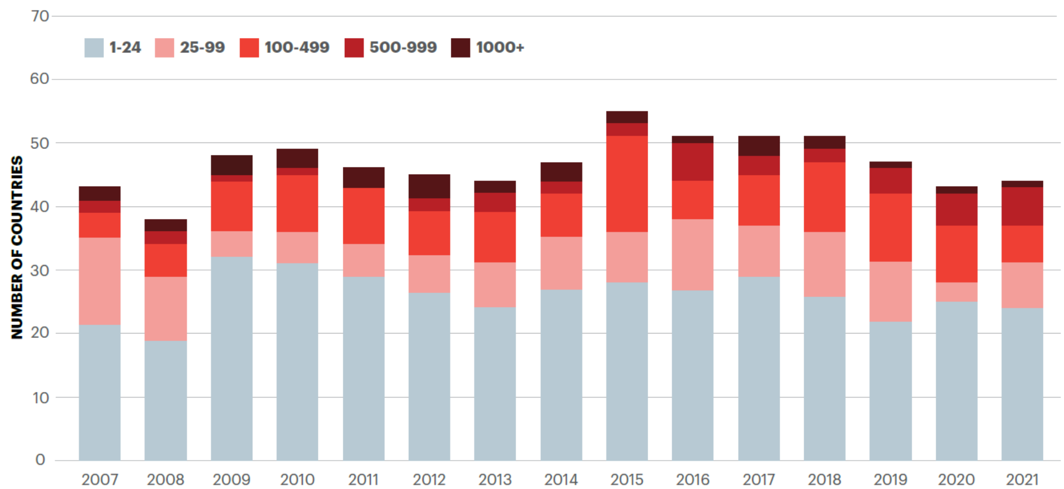

Figure 1.1: Distribution of deaths from terrorism 2007- 2021 [82]

Arguably one of the best methods for understanding explosive effects is full scale replica trials. However, full scale trials can be expensive, time consuming and often impractical to carry out. Alternatively, understanding can be found either by being able to model and calculate with reasonable accuracy how a target may react to an explosive charge or by carrying out a scaled down version of a trial. Even when a full scale trial is required, the scenario may well be modelled or calculated prior to the trial in order to determine the charge size and stand-off required to impose the required pressure and impulse upon a target based upon a known threat (e.g. personnel bomb or car bomb). As so much relies on both the ability to scale and the confidence in the calculations, it is important that the parameters, including the TNT equivalence of an explosive, that are to be used are appropriate; and that the model will closely reflect the actual experimental trial and real-world scenario. The TNT equivalence of an explosive is a standard way of expressing the effects released by an explosive in relation to that of TNT. Explosive attacks rarely use commercially available, well documented and understood explosives, instead often relying on home-made concoctions. Therefore it is important to be able to approximate an equivalent amount of a known quantity of explosive such as TNT to estimate a value of explosive charge size that is relevant to the size of the effects from the blast. This is relevant not just for terrorist attacks, but also for accidental industrial incidents such as the Beirut explosion in 2020 and Buncefield in 2005.

As many of the current principles and knowledge are based upon poor quality and subjective experimental trials, improving this this forms the motivation for this thesis. The output of this thesis will produce one of the largest datasets of experimental trials to allow for a more prescriptive method for the execution of blast trials, using a relevant and updated methodology that is appropriate for the objectives of the trial. This thesis will also use this data to newly validate current computational models for estimating both free-air blasts and TNT equivalences to allow the models to be used appropriately for modelling trials. This aim of this thesis is to provide a new opportunity for the critical analysis, advancement and understanding of the fundamentals of free-air blast tests, identifying issues with the current methods of calculating TNT equivalence factors and provide a new methodology utilising energy flux calculations to produce a single factor for equivalence independent of scale.

1.1 Why Do We Conduct Experimental Blast Tests?

The requirement for a blast test usually results from the assessment of a threat on a new product, on an existing product in a new scenario or a new threat. If a malicious or accidental blast has occurred, blast tests may be conducted with the intent of producing comparable damage in order to prove incident theories, aid in future incident investigation or for emergency services and forensics training [redacted][86]. If possible, a desktop assessment is made prior to blast testing to determine if a full scale or scaled down test is required. In many cases, computer modelling or previous results may be used to assess and sometimes certify a product. When all these other methodologies have been considered and decided to be impractical, inaccurate or not sufficient for certification, a blast test of some sort is usually the answer. This could be due to the complex nature of the target being tested, e.g. something new and novel like a large curved glass facade or a lightweight armoured car. Although there are many advanced computer modelling programmes such as VIPER and LS-DYNA, they may not be considered sufficient to predict real world effects [33]. Organisations with new products may also want to produce high quality marketing materials showing their products undergoing a blast test as a key selling point. Although a blast test is often conducted as the last resort, it is important that the blast test conducted is as appropriate and scientific as possible to ensure requirements are met and performance proved or disproved.

1.2 What Can Impact Upon the Sensitivities of an Experimental Blast Test?

Once it has been determined that a blast test has to be carried out, there is usually a set of requirements that need to be met. These may include testing to a standard such as ISO 16933:2007 [1] which details the peak pressures and impulses that must be met. Alternatively, it could be a specific threat of x explosive charge at y metres with z fragmentation. Key requirements will almost always include:

- Mass and type of explosive used and the value of TNT equivalence used
- Geometry of the charge including any fragmentation
- Stand-off distances
- Atmospheric conditions including temperature and humidity requirements or limits of conditions within which the trial should be conducted
- Measurement and recording system including type of pressure transducers to be used and how they are mounted
- Assessment of output data

1.3 Why Do Sensitivities Matter?

If all of the above elements of a blast test are not understood or carefully considered, it is possible to produce a poor-quality trial which may have further serious ramifications if, for example, a poorly tested target ends up in commercial use. Likewise, if data produced from a blast test is subsequently used for calculations or model validation, they are required to be relevant and accurate to the scenario in which they are being used. This highlights the importance of accuracy over precision, where accuracy is how close data and measurements are to the true or accepted value while precision is simply a measure of the frequency or number of significant figures recorded of the measurements. In order to know what a true or accepted value is, there must be validation and confirmed precision of the sensitive blast test elements along with a thorough understanding of how the blast test has been conducted. Attempts to statistically quantify variability on model predictions when compared to experimental data have been attempted by Netherton and Stewart [108, 109]. Bogosian et al. [21] compared an extensive database of experimental blast data with the Kingery-Bulmash experimental database [44] and used the comparisons to assess the variability in experimental data. The Kingery-Bulmash database has been extensively cited both directly and through model comparisons with ConWep and Autodyn.

There is a clear need to better understand the inherent variability and sensitivity of blast parameters that are produced in experimental trials. Smith et al. in 1999 [143] suggested that, due to the inherent variability in experimental trials, repeats should always be conducted, although this has been disputed by other test facilities that state a high level of repeatability of like-for-like testing [121, 155]. The DNV Spadeadam Research and Testing has been conducting repeat tests with identical set ups for more than 15 years - this thesis will produce new understanding in the repeatability shown for the data produced in trials conducted by the author during their period of study for this PhD by analysing for the first time the uncertainty and coefficient of variation of the collected data. Borenstein showed in their thesis [22] that some blast parameter's uncertainties can have greater effects than others when considering a blast load on a target. Understanding the uncertainties of the different parameters in a blast can assist in measurement processes but mostly offers value in aiding the choice of parameters when using the data for further studies [61].

These sensitivities need to be relevant for the application too. For example, when building a computer program to model a scenario, stand-off and charge positioning may be accurate to ±1 mm. When trying to position a 100 kg spherical charge within a 100 metre by 100 metre arena outdoors, one may struggle to achieve an accuracy of even ± 10 cm, especially when heavy machinery is being used to position targets such as gauge blocks. This lack of accuracy can reflect directly upon the pressure loading experienced by the targets. Blast test standards usually take into account sensitivities in a broad sense, such as ISO 16933 [1] which provide values of pressure loading and require that the actual values are not less than 15% of required values. However, the better understood the sensitivities, the more they can be taken into account and, as such, allow test houses to produce an increased level of accuracy, reliability and therefore re-usability of experimental measurements and data.

1.4 Thesis Aim and Objectives

This aim of this thesis is to produce a substantial experimental data sat that will allow for the critical analysis and understanding of the fundamentals of free-air experimental blast tests. Using the experimental data, the energy flux will be calculated and a new methodology utilising the energy flux calculations used to produce a single factor for equivalence independent of scale. This will be done through the following objectives:

1. To review current literature with regards to blast test parameters, TNT equivalence and incident investigation.

2. To critically assess the way in which experimental tests are designed and conducted and suggest improvements through analysis of variation and uncertainty in experimental trials conducted by the author, as well as from application of existing literature.

3. To newly validate computational models against experimental data.

4. To determine whether sensitivities change with scale and scaled distance using experimental data.

5. To calculate energy flux for TNT and other explosives using computational data and experimental data.

6. Utilise the calculated energy flux to determine if a single TNT equivalence factor can be used for explosives and also hydrogen

1.5 Thesis Structure

This thesis is broken down into seven further chapters. Section 2 is a literature review that summarises previous research and knowledge on the parameters produced or calculated in a blast test. The literature review also includes considerations for designing and conducting blast tests including values of TNT equivalence and blast scaling. The chapter considers computer models for use as both a validation and prediction tool for blast parameters. The literature review includes examples of common problems when blast sensitivities are not considered or are misinterpreted. Finally the chapter concludes with consideration of blast parameters in the investigation of incidents including Buncefield and the Beirut explosions.

Section 3 involves an in-depth review of historical data that has been collected over four years at DNV Spadeadam from forty-eight 100 kg TNT equivalent tests. The review includes statistical analysis of pressure and impulse data taken from pressure-time histories. The data is compared with those from the blast prediction models ConWep and Air3D.

Section 4 discusses complex blast test issues that should be considered to improve test data and take into account the sensitivities that were discussed in Section 2 and displayed in Section 3 historical data. This includes considerations for experimental set-up, clearing and explosive choice and design.

Section 5 displays data produced from twenty nine further 100 kg TNT equivalent explosive tests that used the considerations from Section 4. Similar analysis to that in Section 3 is conducted and comparisons drawn showing that, when sensitivities are considered, a more accurate data set can be produced. A review between the historical data and the more recent data is conducted including reviewing the coefficient of variability for the data.

Section 6 and Section 7 discusses what further analyses and investigations can be done with a reliable set of data. This includes validation of the Hopkinson-Cranz scaling law and evaluation of TNT equivalence using the energy flux method including a consideration for vapour cloud explosions.

The discussions and observations from the thesis are all drawn together in Section 8 where the sensitivities and variability of blast parameters are discussed and conclusions drawn as to the importance of the basis of reliable and accurate data for onward use from experimental trials. This chapter also provides suggestions for future research.

2 Literature Review

2.1 Introduction

When an explosive material is ignited, the energy is released in one of two ways - through burning or by detonation - with the majority of explosives capable of both under certain conditions. Most low explosives and secondary high explosives will burn when ignited in a dry and unconfined state. Due to their chemical make-up, these explosives do not require an external supply of oxygen or air for their combustion, unlike a fuel such as coal, wood, hydrogen or natural gas [92]. When the material burns, the chemical reactions take place either on the surface or just above the surface of the explosive. Layer by layer, the solid material is converted into hot gases as the material burns. If a material is confined, the gases from the combustion have nowhere to go and can build up creating a higher pressure, causing an increased burning rate [69]. When the combustion of a low explosive or propellant is self-sustaining and is subsonic, the material can be classified as a deflagrating explosive. Deflagration is when a small amount of explosive ignites suddenly due to a flame, spark, shock, friction or high explosive. Deflagrating explosives burn quickly and in a more violent manner than ordinary combustible materials. The propagation of the deflagration reaction is dependent upon thermal reactions and, as such, is based on external conditions such as ambient pressure and temperature. The speed of this process is subsonic, as opposed to a detonation which is supersonic.

When an explosive material detonates upon ignition, the reaction is through a passage of a shock wave. The velocity at which this shock wave can move through the explosive material is between 1500 and 9000 ms^{-1}. This is an order of magnitude higher than the burning velocity of the deflagration process. Detonation can be achieved either through an initial shock to detonation, such as that provided by a detonator, or through burning to detonation. Burning to detonation is when the gases generated from the deflagration reaction become trapped, resulting in an increased pressure at the burning surface and therefore an increased burning rate. This rate can increase to a point where the burning rate exceeds the velocity of sound, resulting in a detonation [3].

As air is a compressible fluid, when an explosive is detonated, the explosive gases formed cause an incandescent zone that expands rapidly, producing a shock front travelling outwards from the initiation point [12]. At any fixed distance from the explosive, the shock wave is be characterised by an instantaneous pressure rise $p_{(so,max)}$ above ambient pressure followed by a decay back to ambient pressure p_0. The time at which the pressure front arrives at a designated point is known as the time of arrival t_a. The duration in which the pressure decays to ambient is known as the positive phase duration t_d. Following this positive phase duration, a period of negative pressure is formed due to the over expansion of air that follows the shock front. This has a peak negative pressure $p_{(so,min)}$ and a negative phase duration t_{d-}. The impulse i is the integral of the positive pressure with respect to time. An ideal pressure time curve is shown in Figure 2.7. This is also known as the Friedlander Curve [64].

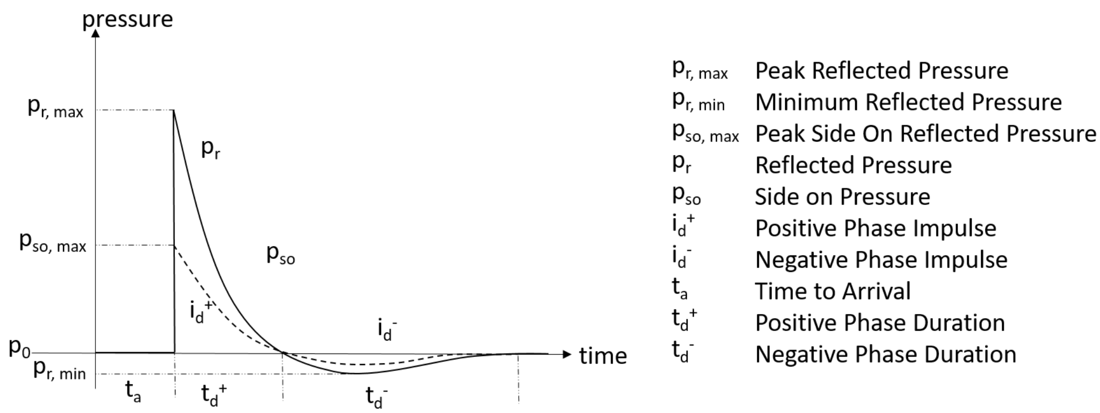

Figure 2.1: Friedlander curve

Traditionally, the positive phase of the blast was described as a simple triangle using

$$p\left(t\right) = p_{max}\left(1 - \frac{t}{t_{d,lin}}\right) \tag{2.1}$$

where $t_{d,lin}$denotes a linear positive phase decay [12]. However, this positive phase decay is more commonly described as an exponential decay, often referred to as the modified Friedlander curve using b, a waveform parameter to control the decay of the pressure-time history. Equation (2.2) displays the Modified Friedlander Equation [64]:

$$p\left(t\right) = p_{max}\left(1 - \frac{t}{t_d}\right)e^{-b\frac{t}{t_d}} \tag{2.2}$$

The reflected pressure of a shock wave refers to the pressure that is received by a rigid target such as a solid wall. The effect of reflecting the pressure wave from the target is to significantly increase the pressure, density and temperature of the shock wave above that of the incident shock wave. The incident, side-on or free field pressure is the shock wave pressure when there is no interaction with a target. Figure 2.2 displays the difference between the reflected and the incident pressure measurements with regards to the direction of the shock wave. Pressure-time curves can be further affected by interactions between many targets such as street scenarios or irregularly shaped targets causing complex reflections as the shock wave reflects off target surfaces [42] [54].

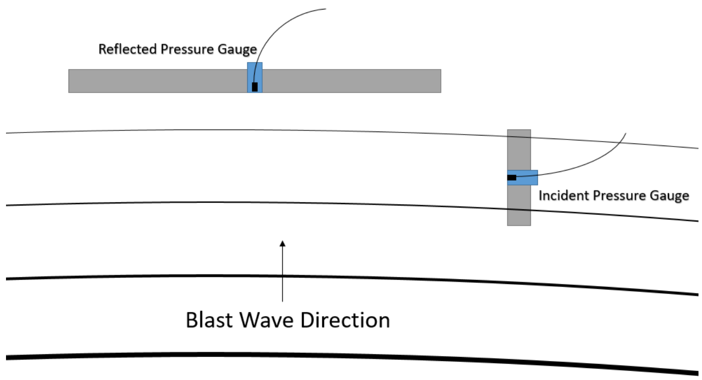

Figure 2.2: Incident pressure versus reflected pressure

2.2 Shock wave Equations

There are many equations in the literature for the determination of the shock wave parameters in a blast. The paper by Goel et al. [68] provides an abridged review of these different empirical methods. In this thesis, the author has chosen to review the response of a target or a material to a shock wave as described by the Rankine-Hugoniot relationship in which a shock wave changes the physical variables of density ρ, pressure p and velocity u of the fluid it is passing through [152]. Due to conservation laws, mass and energy can be balanced either side of the shock wave to give the density and particle velocity directly behind the shock wave.

$$p_0 + \rho_0 u_0^2 = p_{so} + \rho_{so} u_{so}^2 \tag{2.3}$$

Where quantities with suffix 0 are for pre-shock and those with suffix so are for the side on (or incident) post shock quantities. In air, the product of the density and the particle velocity (ρu) is a function of the ratio of the specific heats, γ or gamma, of the air and the shock wave. This is often called the characteristic impedance with units $kg \cdot s^{-1} m^{-2}$. Gamma is a function of the strength of the shock. The variation of gamma with shock strength is plotted in Figure 2.3 by Sadwin [136] from data of Gilmore [67].

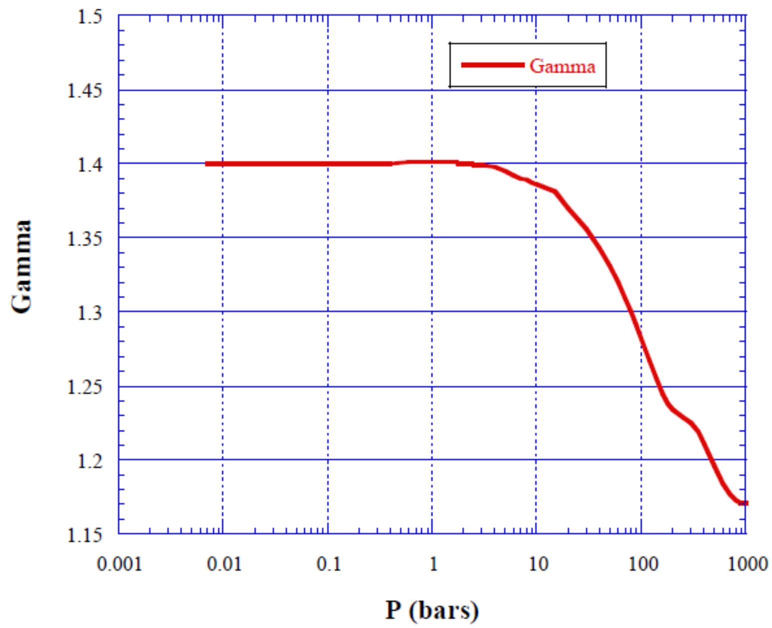

Figure 2.3: Gamma variation with shock strength (1 bar = 100kPa) [136]

The characteristic impedance (ρu) for side on targets is derived as a function of γ by combining the following two equations for density immediately behind the shock front and the particle velocity behind the shock front for incident targets:

$$\rho_{so} = \rho_0 \frac{(\gamma+1)p_{so} + 2\gamma p_0}{(\gamma-1)p_{so} + 2\gamma p_0} \tag{2.4}$$

$$u_{so} = p_{so} c_0 \sqrt{\frac{2}{\gamma \rho_0 [(\gamma+1)p_{so} + 2\gamma p_0]}} \tag{2.5}$$

to give:

$$\rho_{so} u_{so} = \rho_0 c_0 \left[\frac{2\gamma + (\gamma+1)(\frac{p_{so}}{p_0})}{2\gamma + (\gamma-1)(\frac{p_{so}}{p_0})} \right] \cdot \sqrt{1 + \left(\frac{\gamma+1}{2\gamma}\right)\left(\frac{p_{so}}{p_0}\right)} \tag{2.6}$$

This is only valid for incident pressures. The values ρ_0 and c_0 are both dependent upon ambient temperature at time of the detonation. For reflected pressures, this can be expressed and substituted in to produce the following equation:

$$p_r = 2p_{so} + (\gamma+1)q_s \tag{2.7}$$

where q_s is the dynamic pressure, calculated from:

$$q_s = \frac{1}{2}\rho_{so}u_{so}^2 \tag{2.8}$$

Substituting Equation (2.8) into Equation (2.7) gives the following equation for calculating reflected overpressure:

she

$$p_r = 2p_{so}\frac{7p_0 + 4p_{so}}{7p_0 + p_{so}} \tag{2.9}$$

This allows a value of reflected overpressure to be calculated from measurement of a side-on (or incident or freefield) pressure and vice versa as long as atmospheric pressure is known.

When the value of overpressure is known, the characteristic impedance at ambient temperature and pressure can be plotted in a graph. This assumes a constant value of the ratio of specific heats (γ) of 1.4. Using the graph shown in Figure 2.3, it can be shown that gamma only varies from 1.37 to 1.40 up to 10 bar (or 1000kPa); Sadwin [136] stated that based on this 2% variation, the value of gamma does not need adjusting for over pressures less than 20 bar (or 2000 kPa), above which the value of Gamma decreases (Figure 2.3). Using a value for gamma of 1.40, the Characteristic Impedance for incident and reflected pressures have been calculated and are shown in Figure 2.4 and Figure 2.5. The values for atmospheric temperature, pressure and humidity have been taken as the average temperature and air pressure for Spadeadam Research and Testing Site in Cumbria where much of the data from this thesis has been collected. This used an ambient temperature of 13 °C, air pressure 993.31 hPa and a humidity of 74.5 %, to calculate a value for air density of 1.204 kgm^{-3} and an acoustic velocity of 337.85 m/s.

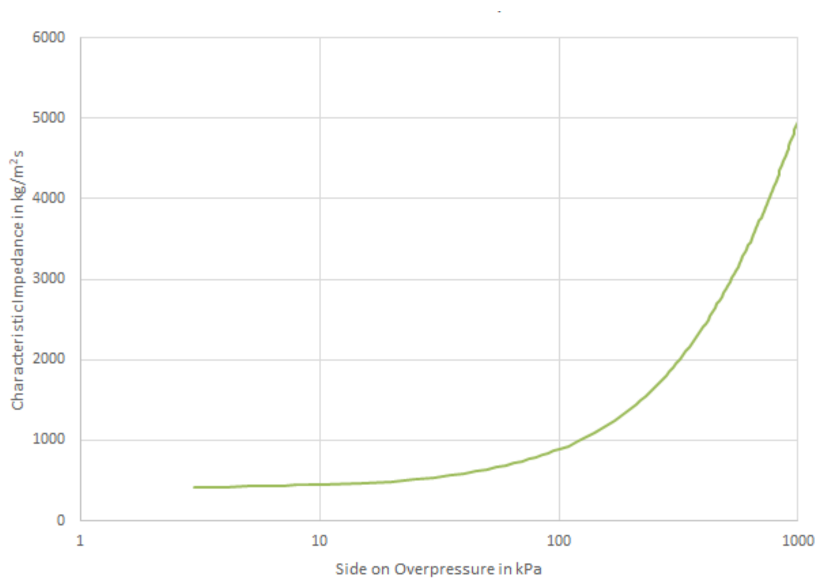

Figure 2.4: Incident characteristic impedance

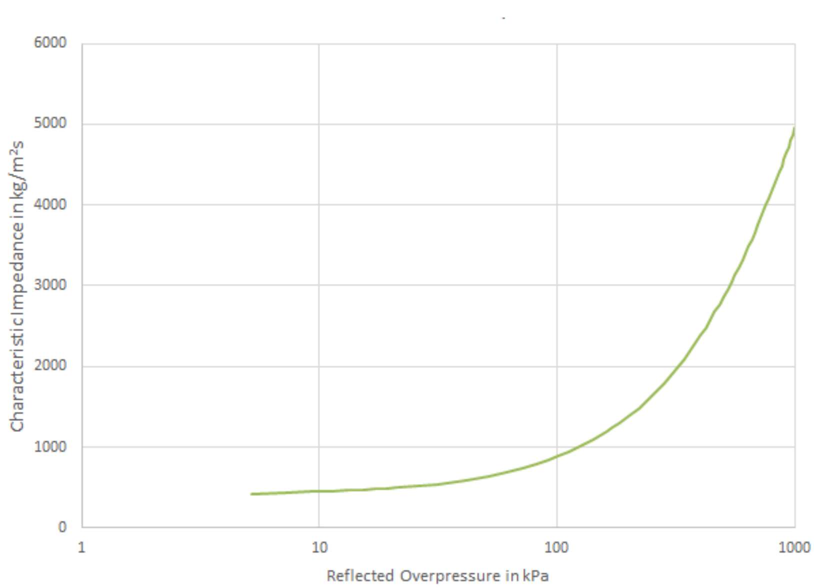

Figure 2.5: Reflected characteristic impedance

Both curves produced are complex curves and, as such, Sadwin [136] split this up into three curve fits for different regions of overpressure:

$$p_{so} \leqslant 600kPa : \rho_{so}u_{so} = 421.43 \exp^{0.918p_{so}} \tag{2.10}$$

$$600kPa < p_{sp} < 1200kPa : \rho_{so}u_{so} = 504.47 \exp^{0.6p_{so}} \tag{2.11}$$

$$p_{so} \geq 1200kPa : \rho_{so}u_{so} = 868.86p_{so}^{0.763} \tag{2.12}$$

With these equations in place, the characteristic impedance can be calculated when a value of overpressure is produced in a blast test. This allows for calculation of energy flux which will be further explained in Section 5.7. The equations mentioned in this section are to be used later in this thesis for further calculation and analysis of the shock wave parameters.

2.3 Explosive Geometries

The location, shape, orientation, and even point of initiation of an explosive can have an impact on:

- Shock wave shape
- Shock wave velocity
- Peak pressures
- Impulse
- Time of arrival

Historically, the shape and set-up of an explosive charge in a bare charge trial is rarely mentioned but, instead, assumed to be a spherical or hemispherical free-air blast. If a spherical explosive charge detonates at a sufficient distance above the ground, such that the shock wave does not interact with the ground surface, it can be considered an ideal free-air burst. If a spherical charge detonates on or near the ground surface, and the shock wave interacts with the ground surface prior to arrival at point of interest it can be considered as a hemispherical surface burst [44]. If a very large explosive charge is to be used, it cannot necessarily be located on the ground as a hemispherical ground burst due to the risk of energy being lost due to the cratering, not to mention potential damage of the ground that may not be acceptable to the test range. To counteract this issue, explosive charges can be located above ground level and spherical charges used. However, this can lead to other characteristics not experienced when a hemispherical ground based charge is used such as the impact of Mach Stem [26]. This occurs when the shock wave reaches the flat ground surface and is reflected back, travelling through the atmosphere at a higher velocity than the initial incident shock wave due to the reflected overpressure exceeding the pressure in the incident wave. When this higher velocity wave meets the incident wave, at what is known as the triple point, the shock waves merge to form a single outward travelling front known as the Mach Stem. Figure 2.6 depicts this effect. This can lead to much higher pressures than expected from a hemispherical ground burst, particularly when measured at smaller scaled distances close in to the charge. This effect of this Mach Stem reflection has been shown to be particularly important for the response of, and damage experienced by, tall structures whether in experimental or numerical blasts [48].

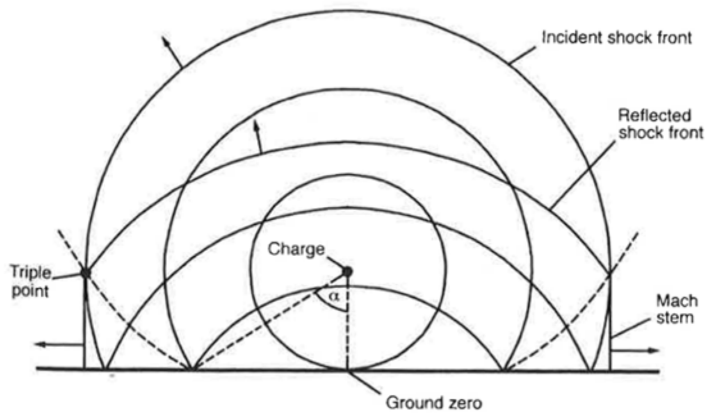

Figure 2.6 Reflection of shock waves for explosions above ground.

Figure 2.6: Mach stem [26]

For a spherical or hemispherical with a central initiation point, this produces an evenly spreading out detonation wave. If, however, the charge is not spherical, or is not initiated from the centre, the way in which the detonation wave behaves from these two cases can be very different. Yan et al. [165] showed in their paper on cylindrical charges through finite element analysis how the incident pressure varies in the axial or radial directions in a cylindrical blast. It can be seen in Figure 2.7 that in a spherical blast the incident pressure is identical in both the x and y direction. For a cylindrical charge, in the axial direction, the shock wave not only has an earlier time of arrival, it also has a much higher incident pressure compared to the radial direction. As stated by Simeons [139], the point of initiation may enhance this effect further if ignition is at one end of the cylinder rather than centrally. Further studies on how the shape of an explosive charge can influence the blast parameters can be found by Langran Wheeler et al. [98], Knock [96], Wu [162] and Ofengeim [110].

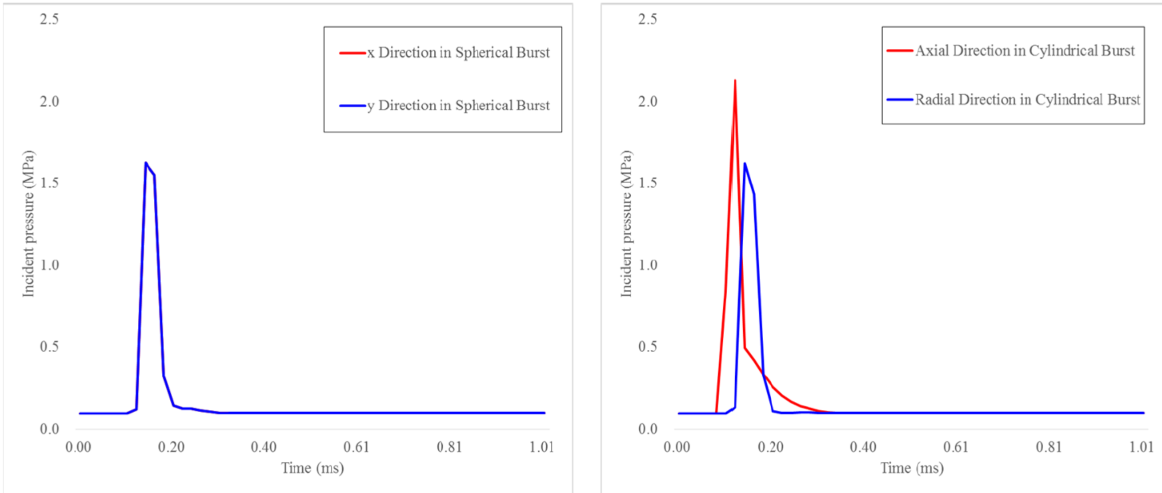

Figure 2.7: Modelled shock wave showing incident pressures in axial vs radial directions of cylindrical charges compared to spherical charges [165]

On top of the variations seen through the choice of shape, if a charge is contained in a case, the blast parameters can vary significantly. The parameters can be affected by case material, thickness and mass. Through extensive experimental work based on many weapon and cased charges trials, TM5-855-1 [44] provides equations to determine an equivalent bare explosive weight based solely on the case mass:

$$W' = \left[0.2 + \frac{0.8}{(1 + \frac{m_c}{W})}\right] W \tag{2.13}$$

where: W'= equivalent bare charge mass in kg, W= charge mass in kg and m_c= casing mass.

This is not a totally foolproof method as the values actually measured experimentally depend very much on the geometry and construction of the cased charge which influence how it detonates as well as where it is initiated from. There is debate on both how much energy is lost due to the case break up, but also whether energy is gained due to the mechanical efficiency between explosion gases and casing material. TM5-855-1 [44] provides further equations to take into account some of the different geometries of cased charges.

In summary, unless an experimental trial has an ideal set up, predictions using equations will generally be estimates that are useful for conservatively predicting effects but, when accurate values are needed, only complex computer models or experimental trials are capable of providing measurements to required standards.

2.4 TNT Equivalence

2.4.1 Introduction

As stated previously, the TNT equivalence of an explosive is a standard way of expressing the energy released by an arbitrary explosive in relation to that released by TNT. The TNT equivalence of an explosive charge is given as an equivalent mass of TNT required to produce a chosen characteristic, such as blast pressure, impulse or fireball size, of equal magnitude to that of the explosive charge. It allows for comparison of different types of explosives, both conventional and unconventional (for example home-made explosives or cased charges and munitions). TNT equivalence is widely used for regulatory issues including manufacture of explosives and munitions, explosive storage facilities limitations and for transportation. In their critical review of TNT equivalence, Fuchs et al. [65] also include TNT equivalence investigations for materials not necessarily designed for detonation such as propellants and pyrotechnics which, although they may have low TNT equivalences in terms of detonation, may actually cause larger lethal structural debris which is capable of travelling further than for similar quantities of detonating explosives.

Due to availability, the type of explosive used for trials may not be consistent, not just in the UK but in the wider world, due to considerations of availability, practicability and cost. To ensure a consistent blast trial, the required explosive charge size is usually given in TNT equivalence, with the choice of explosive to use left up to the testing facility. TNT equivalence is important for blast scaling calculations, damage predictions, theoretical modelling, and is usually the baseline explosive used for computational models, so being able to produce accurate TNT equivalences is key. However, there is no definitive method or procedure for calculating consistent and reliable values for TNT equivalence. It should be noted that in order to enable valid comparisons, like with blast scaling, the explosive in question and the original base explosive should have the same geometries and be tested under the same conditions, as variations in these properties can cause the properties of the blast to vary [148]. It is also possible to back calculate a TNT equivalence based on experimental data, or even from real-world incident data, which is then compared to TNT experimental data. Examples of this can be seen by Rigby et al. [128], Bogosian [20] and Xiao [163] who either performed experimental trials, or used existing experimental data to produce or validate values of TNT equivalence.

Table 2.1 displays the values given for TNT equivalence from the ISO Standard 16933 [1] for a range of standard explosives. These values were gathered for the ISO Standard from a number of different sources but predominantly from TM-5-855-1 [44]. It gives equivalence factors based upon pressure equivalence (k_p) and impulse equivalence (k_i). It should be noted that these are often quite different. For example, if the desired outcome was 100 kg TNT Equivalent PE4 charge, if you were to base it on pressure 81.96 kg of PE4 would be required; if the value was to be matched on impulse, 92.59 kg of PE4 would be required. If you were to take the average (k^a) equivalence, 86.95 kg of PE4 would be required, but then the measured target pressure would be expected to be high, and the target impulse to be low.

Explosive	k_p	k_i	k^a	Pressure range kPa
ANFO (94/6 Am N/fuel oil)	0,82	—	(0,82)	0 to 690
Composition A-3	1,09	1,07	1,08	35 to 350
Composition B	1,11	0,98	1,05	35 to 350
Composition C-4	1,37	1,19	1,28	70 to 690
Cyclotol 70/30 (RDX/TNT)	1,14	1,09	1,12	35 to 350
HBX-1	1,17	1,16	1,17	35 to 140
HBX-3	1,14	0,97	1,06	35 to 170
H6	1,38	1,10	1,24	35 to 690
Minol II 70/30 (HMX/TNT)	1,20	1,11	1,16	20 to 140
Octol 75/25 (HMX/TNT)	1,06	—	(1,06)	—
PE 4	1,22	1,08	1,15	10 to 1 000
PETN	1,27	—	(1,27)	35 to 690
Pentolite	1,42	1,00	1,21	35 to 690
	1,38	1,14	1,26	35 to 4 100
TNETB	1,36	1,10	1,23	35 to 690
TNT	1	1	1	standard for pressure ranges shown
Tritonal	1,07	0,96	1,02	35 to 690

[a] The average k factor for an explosive: $k = (k_p + k_i)/2$.
The equivalent mass of that explosive equals the mass of TNT divided by average k factor.
EXAMPLE The mass, m_{PE4}, of PE 4 that is equivalent to 100 kg TNT is calculated as follows:
$m_{PE4} = 100/[(1,22 + 1,08)/2] = 100/1,15 = 87$ kg

Table 2.1: TNT equivalence values taken from ISO 16933:2007 [1]

2.4.2 Current Methods

As previously mentioned, there is no single definitive, commonly-used method for determining the TNT equivalence of an explosive. There are both experimental and theoretical methodologies for TNT equivalence, each with different pros and cons. In-depth studies on these methodologies have already been conducted and can be found by numerous researchers: [39, 102, 65]. Below is a list of practical methodologies that can be used to determine the equivalency of an explosive [39]:

- **Ballistic Mortar -** This process determines the amount of explosive sample that is required to raise a ballistic mortar to the same height to which it is raised by 10 grams of TNT.

- **Sand Crush -** This process crushes a 0.4 gram of explosive in 200 grams of sand pressed at 3000 psi into a No. 6 cap as a sand test bomb using a primary explosive. The amount of primary explosive that is required to ensure that the explosive sample crushes the maximum net weight of sand is designated as its 'Sensitivity to Initiation' and the net weight of sand crushed finer than a certain size mesh is termed the 'Sand Crush Value'. Since the the amount of sand crushed is dependent upon the shock provided by the explosive, it is expected that the Sand Crush Value is related to the peak pressure of the explosive.
- **Trauzl (Lead Block) -** In this test, a sample of explosive is exploded in a 25mm diameter, 125mm deep borehole in a lead block. A blasting cap is used to initiate an explosive in a glass container inside the borehole. The mass of sample explosive is varied to give a total expansion of 250 to 300 cubic centimetres. The expansions for equivalent weights of TNT were calculated and the test value expressed in percent of the expansion of an equivalent weight of TNT.
- **Plate Dent -** The preferred plate dent test (also known as Method B) involves firing an uncased charge on a $1\frac{3}{4}$inch thick, 5 square inch cold rolled steel plate with one or more plates as backing. The depth of the dent formed in the plate is measured and then given either as just a depth or as a relative brisance which is defined as 100 times the ratio of the depth of dent for the sample divided by that produced by a TNT charge.
- **Cylinder -** This method uses high speed photography to measure the radial shock wave velocity of an explosive filled metal cylinder and then compares it with that of the same mass of TNT.
- **Air Blast -** This process uses charges fired in an open arena with pressure gauges deployed at various locations that record the pressure and impulse vs time data. The data is then compared to that of an equivalent TNT charge at the same distance and then an equivalence is determined based on one of the peak blast pressure, the peak impulse, time of arrival or other blast parameters.

On top of this, there are also theoretical methods that can be used to calculate the TNT equivalence:

- **UFC-3-340-2** [158] **-** The document from the US Department of Defence acknowledges that only a limited amount of experimental work has been conducted on explosives and suggests that the below equation is suitable for use in calculating a TNT equivalence. The document claims this is also suitable for confined explosives if there is no better alternative. It is acknowledged that shape, quantity, confinement and pressure range considered may affect the values and therefore is far from an ideal method.

$$W_E = \frac{H^d_{EXP}}{H^d_{TNT}} W_{EXP} \tag{2.14}$$

where W_E =effective charge weight, W_{Exp} =weight of explosion in question, H^d_{EXP} =heat of detonation of explosive in question and H^d_{TNT} =heat of detonation of TNT.

- **Berthelot Method** [16] - Berthelot determined an equation based on the chemical composition of the explosive:

$$TNTequivalence = 840 \cdot \Delta n \cdot (-\Delta H^o_R)/Molwt^2_{exp} \tag{2.15}$$

where Δn= number of moles of gas released/number of moles of the explosive, ΔH^o_R= heat of detonation and $Molwt_{exp}$= Molecular weight of the explosive.

- **Cooper Method** [40]- This theoretical method is based upon the ratio of squares of the detonation velocities of explosives:

$$TNTequivalence = D^2_{exp}/D^2_{TNT} \tag{2.16}$$

where D= detonation velocity in m/s.

Regardless of this list of both practical and theoretical methodologies, many will return to the TM5-855-1 data (table 2.1) and use these values regardless of the purpose of the test being conducted.

- **Computational Simulations -** Computer models can be used to simulate any of the experimental methods mentioned above and the data produced from the simulation can be compared to reference values. An example of this is Ackland et al [2] who used Ansys AUTODYN (a high-fidelity, physics based solver) to simulate the air blast method mentioned above. Ansys AUTODYN uses a Lagrangian finite element solver to model structural components subjected to shock loading [6]. The values for pressure and impulse numerically simulated were then compared to values presented in the Handbook for Blast Resistant Design of Buildings [54].

- **Numerical Simulations -** There are numerous examples of papers producing equations for blast parameters and comparing these to equivalent values of TNT from literature [25, 9]. Bajic et al. [10, 84] propose an equation that is claimed to compare well to experimental data based on the calculated detonation pressure of an explosive calculated through the Sadovskiy equations [135] modified and in conjunction with the Kingery Bulmash equations [44].

2.4.3 Variations with Existing Methods

As put by Locking [102] in his "Trouble with TNT equivalence" paper in 2011, "there are no definitive methods" and "variability is found to be so significant that errors can be up to 50%, with 20% and 30% being typical".

Cheesman [32] collated TNT equivalence values from numerous sources for RDX, HMX and TATB and plotted them together (reproduced by Locking [102] and shown in Figure 2.8). This suggested values varying for TATB between 0.8 and 1.2, for HMX between 1.1 and 1.8, and for RDX between 1 and 1.8.

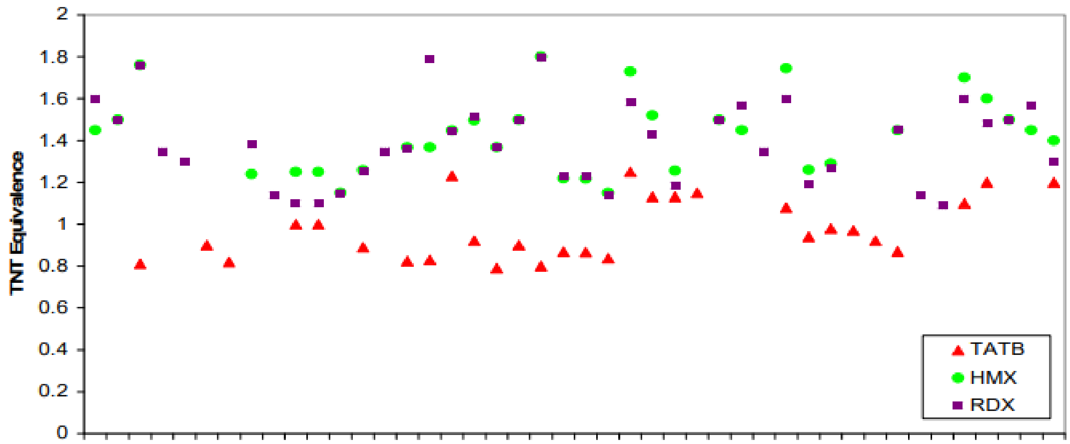

Figure 2.8: TNT Equivalences from various sources [102]

This inherent variability is clearly a problem when it comes to choosing an explosive type and charge size as, depending on the chosen value of TNT equivalence, the chosen explosive charge could end up nearly twice as large or half as large as necessary or required, meaning that when testing a structure to a set requirement, the pressure and impulses produced may be significantly over or under the expected values, producing an invalid test with both practical and cost implications through the requirement for re-tests and new structures. If attempting to back calculate the size of an explosion after it has occurred based on pressure, impulse, time of arrival or damage, the variation in TNT equivalence used could produce a significant spread of predicted values of explosive charge. This spread was explored by Chang and Yong [31] in a study of probability of protection from a terrorist threat for 'home-made' ANFO. Chang and Yong stated that, due to nature of the explosive, the TNT equivalence could vary significantly from factors such as the amount of absorbed water in the mixture, the lack of uniformity in the mixing, differences in the specific gravity and also the type of oxidiser and fuel oil used. The paper took values of equivalence for the home-made ANFO from literature of between 0.3 and 1.6.

2.4.4 Scaled Distances and TNT Equivalence

Scaling of shock wave properties is a common practice that is used to generalise blast data from different sized high explosives. One large barrier to experimental testing is the complexities and cost that comes with a large trial. Kleine et al. [95] in their paper on laboratory scale blast wave phenomena describe how, driven by the need to reduce time and cost during an explosive testing campaign on PPE, that the ability to reduce the charge size down to milligram size would remove the majority of difficulties associated with large-scale experiments. This illustrated the extent to which small scale trials can produce appropriately scaled results that would replicate a large or even full scale explosive trial.

After World War 1, Hopkinson (1915) and Cranz (1926) [92] independently produced what has now become the most commonly used scaling law (also known as the “cube root“ scaling law). This law states that the shock waves produced when two explosives of similar geometry and of the same explosive material, but of different size, are detonated in the atmosphere, will produce the same peak pressures when measured at equivalent scaled distances [12]. The scaled distance Z, in $mkg^{-\frac{1}{3}}$, is given by 2.17:

$$Z = \frac{R}{W^{\frac{1}{3}}} \tag{2.17}$$

Where R is the distance from the detonation point of the explosive and W is the explosive charge weight. This can be explained by the example in Figure 2.9 where a target at distance R from the centre of an explosive charge W is subjected to a shock wave with peak overpressure P, duration t_d and impulse i. The Hopkinson-Cranz scaling law states that a target positioned at distance kR from an explosive charge with mass k^3W will be exposed to the same peak overpressure P and then duration kt_d and impulse ki.

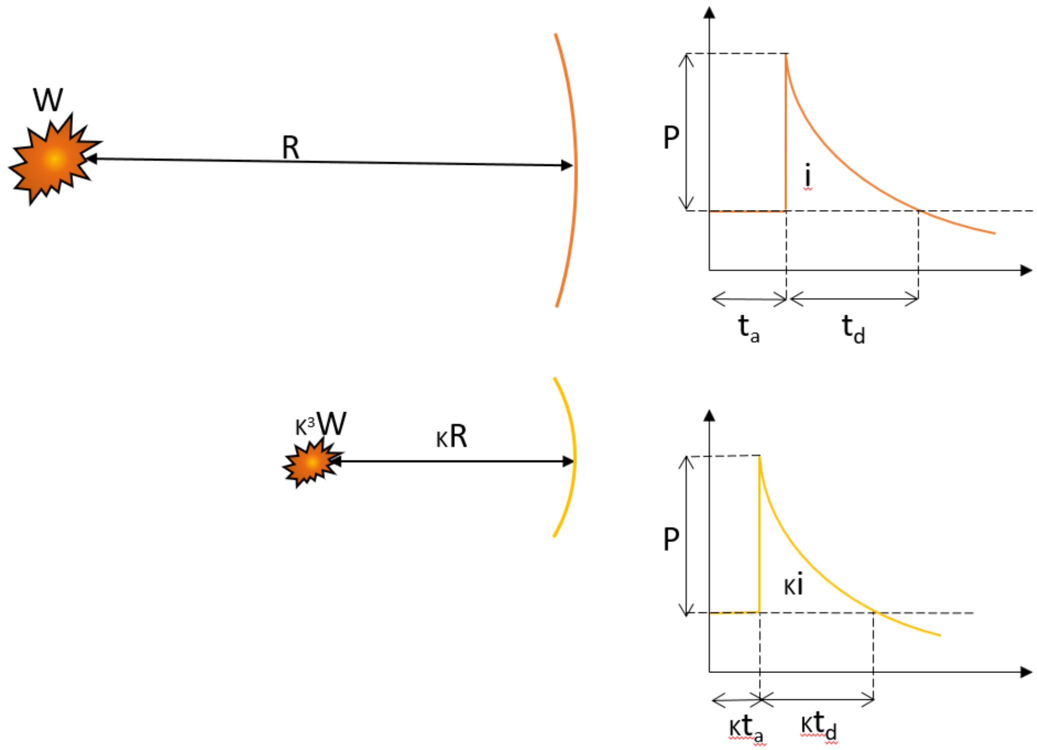

Figure 2.9: Hopkinson-Cranz shock wave scaling [12]

The ability to accurately scale the blast characteristics allows smaller, and therefore usually cheaper and easier to conduct, trials to be carried out instead of full-scale trials for every scenario, although it is important to note that the scaling laws are only applicable for identical conditions with regards to ambient temperature and charge shape [148]. This rule assumes that, if the same explosive and shape is used and only the mass changes, than the TNT equivalence also is identical. Many studies have been conducted to prove the scaling law through both numerical [9, 37, 104] and experimental studies [34, 35, 49, 138] and [5]. The Hopkinson - Cranz law is also investigated further in this thesis.

Despite this scaling law, it has been theorised by many, including Swisdak, that the equivalent weight of an explosive for any given blast parameter may vary as a function of distance from the charge. This would suggest that the TNT equivalence would vary over distance, therefore, a single value would not be suitable for TNT equivalence when targeting two different distances for a particular parameter. Cooper [39] from the data provided by Swisdak [148] plotted out how the TNT equivalence of five explosive types varies with scaled distance in Figure 2.10. He showed that when the initial expansion wave of an explosive has an expansion wave that is not identical to that of TNT, the peak pressure of the shock wave will decay at a different rate to that of TNT. However Cooper [39] noted that there were large errors in the experimental determination of the TNT equivalence for this graph, suggesting further work was needed. This work used the Hopkinson-Cranz scaling law quoted previously and relies on the assumption that this law is valid for all distances and all explosive types used. Cooper along with Locking and many others claim that for the purposes of predicting blast effects on structures, TNT equivalence is usable as the only common tool available. It should however be noted that the purpose of the test and the target outcome, should assist in determining which method of TNT equivalence identification is used.

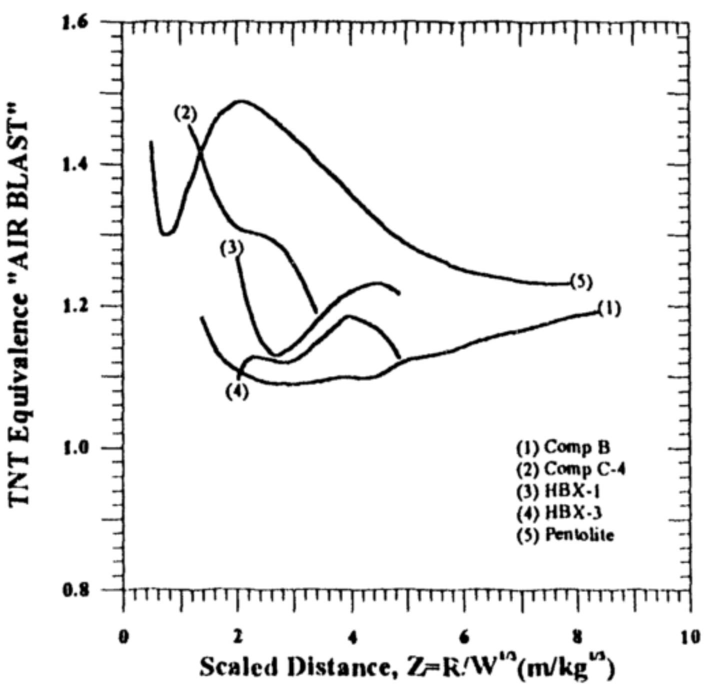

Figure 2.10: Variation of TNT equivalence with scaled distance for overpressure 5 explosive types [39]

Plotting the same data for C4 for pressure and impulse from Swisdak that was used to produce Figure 2.10, produces Figure 2.11 which shows how extreme some of the variation in values can be as the scaled distance changes. For example, for C4, producing an overpressure of 120 kPa, a TNT equivalence of 1.3 should be used, yet the corresponding impulse produced at this pressure is at a TNT equivalence of 1.5. At 275 kPa, the values are quite opposite with the overpressure TNT equivalence at a value of approximately 1.35 and the corresponding impulse at 0.96 TNT equivalence.

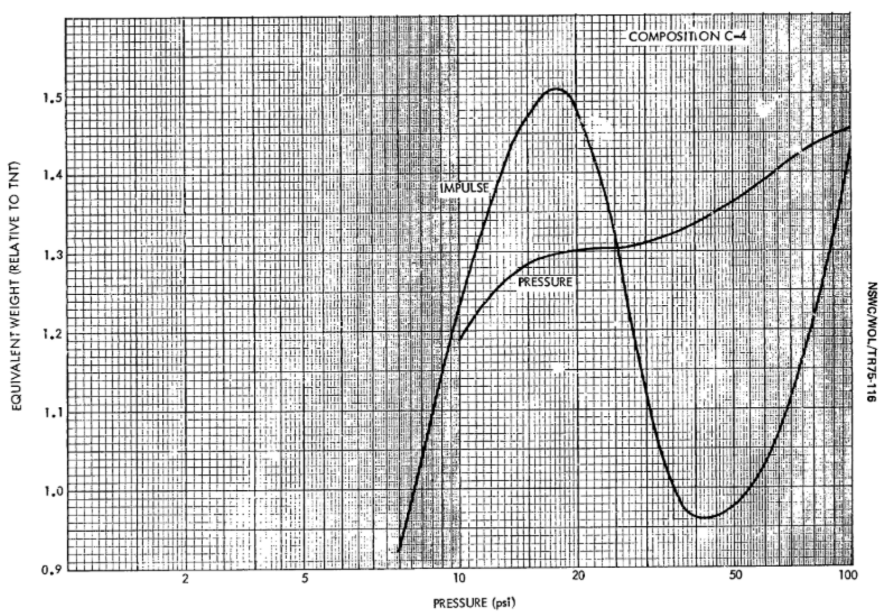

Figure 2.11: Variation of TNT equivalence with overpressure for C4 [148]

Figure 2.11 highlights how important it is to take into account the TNT equivalence based upon the scaled distance being targeted in an experimental blast test, especially if a specific pressure and/or impulse is required to be met. This could be difficult if there are multiple targets at varying distances in a blast test. It also suggests that, without a full set of data of TNT equivalences for the explosive being used, it may not be possible to chose an exact TNT equivalent to use satisfying both pressure and/or impulse and as such an average value should instead be used. Where an average value is used, it should be expected to see variation in the blast parameters measured at different stand-offs.

2.5 Blast Test Parameters Measurable from Pressure-Time Curves

Aside from analysing how a target responds to a blast, it is important to analyse the blast itself to ensure firstly that the explosive itself detonated fully; and secondly that the desired loads exerted upon the target were achieved. The majority of analysis of the blast can be achieved from pressure-time curves (Figure 2.1) from a pressure gauge, but high-speed video may also be used. Properties of the shock wave that can be analysed from pressure-time curves and from video footage include:

- Peak overpressure
- Positive phase impulse

- Negative phase impulse
- Time of arrival
- Positive phase duration,
- Negative phase duration

As shown in Figure 2.1, the production of a pressure-time curve from a blast test allows measurement of many of the parameters mentioned above.

Figure 2.12 gives an example of a pressure-time curve from a detonated explosive charge.

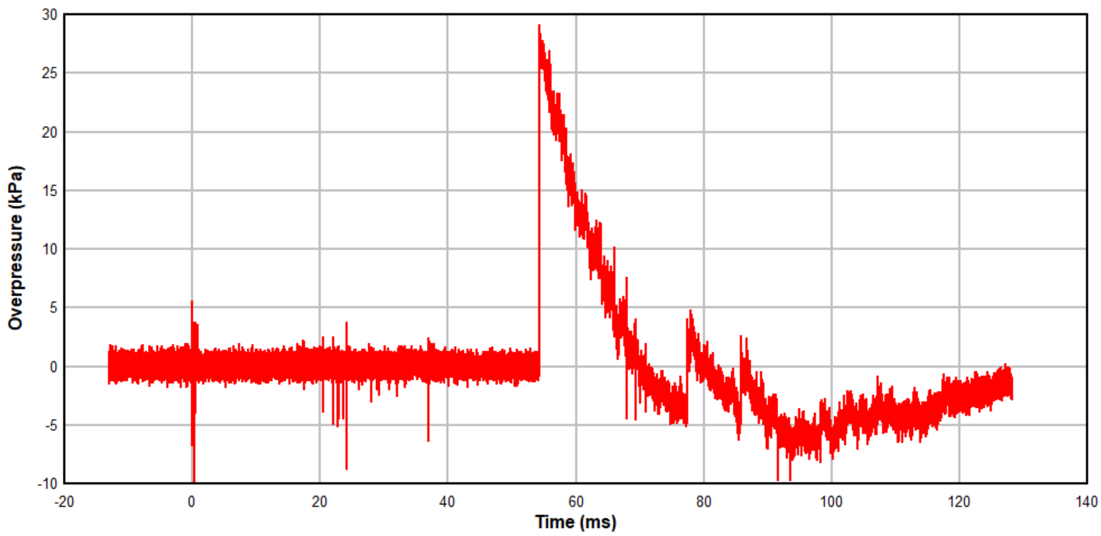

Figure 2.12: Example pressure-time curve

Pressure-time curves produced from blast tests can be very noisy (especially those close to the explosive charge) and can be affected by ground shock, external noise (for example generators running equipment) and heat effects. There are numerous studies that describe in detail difficulties faced when they were measuring pressure loadings from experimental trials, particularly in the near field where pressures can exceed 1000 MPa, including noise, poor signals and damaged gauges [53], [56], [57]. The experimental trials covered in this thesis are in the far field, with scaled distances greater than 2 $mkg^{-\frac{1}{3}}$ and, as such, near field measurements are not covered further in this thesis. Even once a pressure-time curve is produced, in either the near or far-field, it can be difficult to determine the true values for the previous mentioned properties of a shock wave, especially to provide consistency when analysing hundreds of pressure-time curves. For this reason, to aid analysis of the pressure-time curve, the modified Friedlander curve equation is fitted to the pressure/time histories using

DPlot [81] based on the time of arrival and positive phase duration which can be accurately interpreted from the plots. Farrimond et al. [61] proposed another method for curve fitting the Friedlander curve to pressure-time curves through identification of reliable parameters of the time of arrival and the positive duration using the positive impulse - a step by step method and example can be found in the reference. Figure 2.13 shows the pressure-time curve with the modified Friedlander curve overlaid on top using the DPlot function.

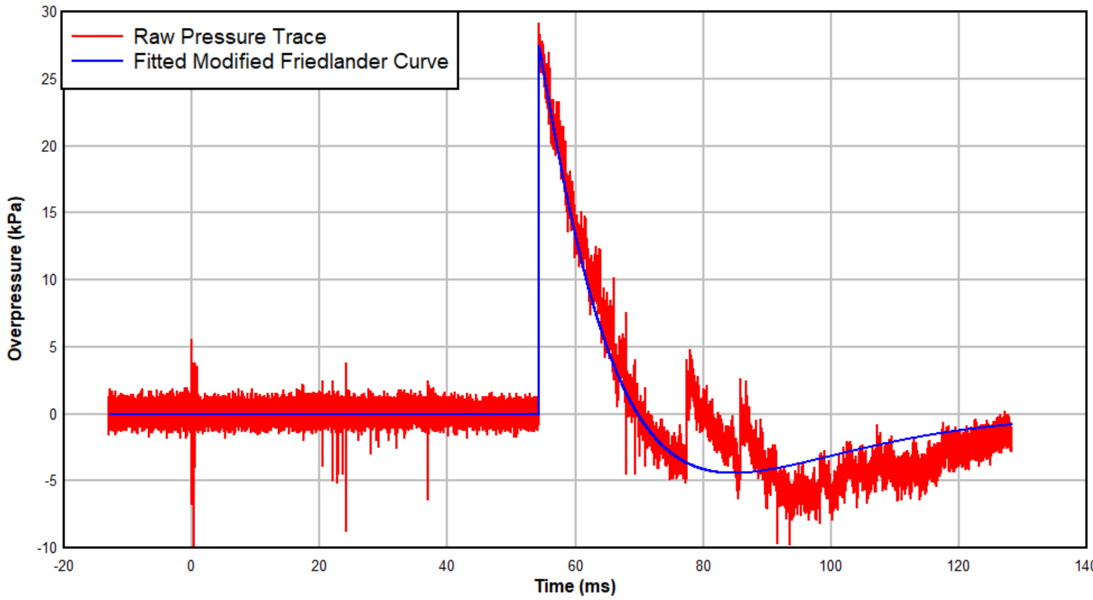

Figure 2.13: Example pressure-time curve with fitted modified Friedlander curve

From the fitted modified Friedlander curve graph and the integral we can deduce the following properties:

- Peak pressure = 27.50 kPa
- Positive phase impulse = 187.09 kPa.ms
- Negative phase impulse = -160 kPa.ms
- Time of arrival = 54.28 ms
- Positive phase duration = 15.49 ms
- Negative phase duration = 73.95 ms

As seen from the above curve fit, the modified Friedlander curve does not account for the secondary shock evident in the raw pressure-time curve. When an explosive is detonated, the expansion of the detonation products results in an additional shock wave that moves back towards the detonation point and subsequently reflects outwards following the primary shock wave [107]. Rigby [125] stated that the secondary shock delay parameter could be used to estimate explosive properties based on the delay between the arrival of the primary shock wave and the arrival of the secondary shock wave, although this was not yet easily predictable by numerical analysis. Most computer models and empirical equations do not account for the secondary shock.

Pressure-time curves can be affected by external factors as well as a result of the explosive geometries. Interactions with structures is discussed in Section 2.10 with the results of multiple reflections of the shock wave off structures causing peaks and troughs in pressure-time curves making identifying key blast parameters difficult. The atmosphere in which the explosive has detonated can also affect the pressure-time curve. Weather conditions that may involve particularly warm, cold or damp air can affect the air density, resulting in small adjustments in the shock wave velocity, although this has been shown to be negligible unless considering explosions at altitudes such as 30,000 metres above sea level [148]. The larger effect of atmosphere conditions involve the amount of available oxygen. Many explosives have a negative oxygen balance in their composition, meaning there is not enough oxygen in their chemical make up to fully react [55]. This is particularly the case with TNT which is 74% oxygen negative. In their paper about effects of afterburn, Tyas et al. [157] demonstrated lower reflected pressure and impulse from PE4 detonated in Nitrogen when compared to an air atmosphere, suggesting that pressure loading is enhanced when explosives detonate in air due to the rapid afterburn. To take this to the extreme, explosives that detonate underwater have, as expected, a different shaped pressure-loading curve to that of free-air blasts that typically include a instantaneous rise of pressure with a very rapidly decaying pressure, much faster than that in air [149].

The angle at which the measurement target is positioned with respect to the explosive charge can also affect the pressure-time curve. This is displayed in graphs in the US Army Handbook [51]. There have since been have been several studies [94, 141, 142, 124] investigating angles of incidence on shock wave parameters and how sensitive the parameters can be when the angle of the target moves from a truly freefield position towards a reflected position. Rigby et al. [124] state in their study that the pressure can be seen to decrease gradually relative to the normal reflected pressure for increasing angles of incidence.

2.6 Blast Test Parameters Measurable from Video Footage

High speed video cameras have been used since at least 1957 when Deal [43] used them to measure plate velocity and air shock velocity in a blast. Since then, camera technology has advanced substantially and has been used in many experimental trials [45, 59]. From the test that produced the pressure-time curve in figure 2.12, high speed video footage was also recorded. Figure 2.14 shows a still taken from the high speed video showing the fireball at its largest expansion. When it is at its largest, an approximate measurement can be made. This is aided through the use of distance markers set out at 1 metre intervals from the location of the charge. From these stills the estimated fireball radius is 6.5 metres. This is a very inaccurate parameter to measure due to the irregular shape of a fire ball and the blurring of the edge making it difficult to accurately determine diameters.

Figure 2.14: Diameter measurement of fireball

In their 2020 paper on near-field blast pressure using high speed video, Rigby et al. [126] used computation algorithms with high speed video to define the outer edge of the fireball, which was then used to calculate the velocity-radius of the shock wave using the Rankine-Hugoniot jump conditions. This was shown to be an accurate way to calculate blast parameters in the near to mid field of a blast where it is often difficult to measure blast pressures due to the proximity to the explosive charge and the high pressures instruments can be exposed to. Fireball analysis was also used by Díaz [50] for estimate of blast sizes in accidental explosions, this is discussed further in Section section 2.12.

Using thermal high speed video of tests, it is possible to measure the temperature of fireballs from explosive tests. Xiao et al. [164] used a thermal camera to investigate if any degradation had occurred within an explosive due to storage. This was done by examining the temperature distribution between four tests (Figure 2.15) eventually determining that the storage conditions could reduce fireball temperature by more than 6% in this particular case.

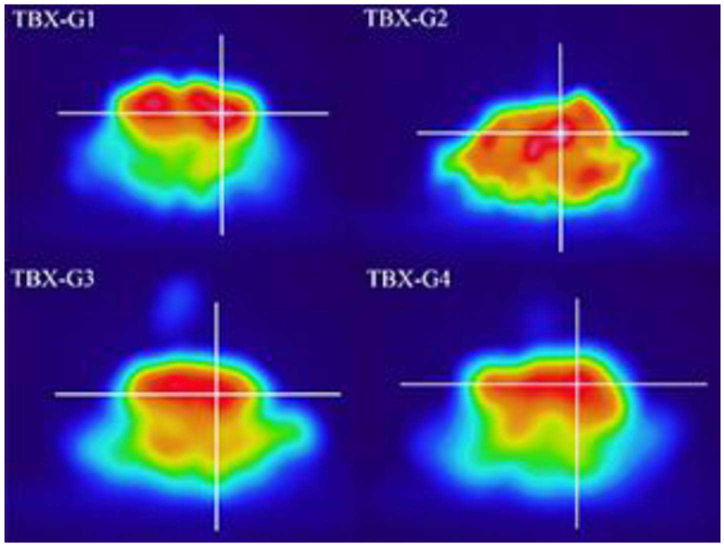

Figure 2.15: Comparison of fireball temperatures using high speed thermal camera [164]

2.7 Blast Test Parameters - Calculable

2.7.1 Energy Flux

Approximately one third of the total chemical energy available in a high explosive material is released in the detonation process [158]; some of this energy will be given off as sound and light as well as the pressure wave. The remaining two thirds is released more slowly as the detonation products mix with air and burn and has limited effect upon the shock wave.

Generally the energy in a shock wave is not a calculated or reported property in an explosive, except perhaps in underwater explosives. In an underwater explosion this is simpler as the particle velocities in water are typically very constant except close to the explosion point [137]. For explosions in free air, the particle velocity can have a larger impact upon the energy flux measured. In literature, the energy flux in air has been calculated in different ways by both Swisdak [137] and Grisaro [70]. Swisdak calculated it using the characteristic impedance and a pressure-time curve as defined in the following equation [137]:

$$E_f = \int_{t_a}^{t_a+t_{d+}} (\frac{1}{\rho_{so}u_{so}}) \left[p(t) - p_0\right]^2 dt \tag{2.18}$$

Where $p_{so}u_{so}$ is the varying characteristic impedance along the pressure-time curve. The integral of the characteristic impedance multiplied by the pressure-time history of the measurement gives the energy flux at that particular distance. Calculating this value allows the total shock wave energy in a blast to be calculated by multiplying it by the surface area of the shock wave [137]. Figure 2.16 shows how Sadwin [136] used the energy flux to calculate the total air blast energy in a surface burst of 42 grams of PETN detonating cord. Sadwin states that the shape of the curve is due to the initial energy build up and its subsequent decay with range.

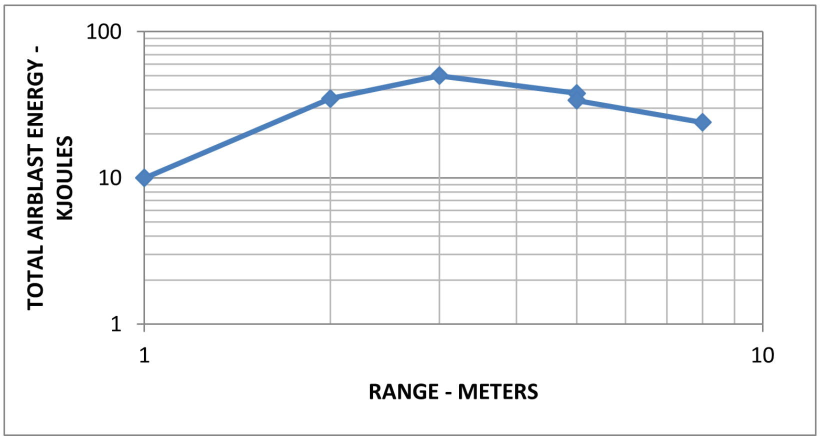

Figure 2.16: Total air blast energy vs range for surface burst of 42 grams PETN det cord [137]

By dividing the total air blast energy per the charge mass, an energy by kilogram value can be determined. If this is divided by the value of total available energy of one kilogram of explosive, it provides the relative efficiency of the explosive. Sadwin did this for PETN and produced a value of between 8.9 % and 18.9 % depending on the stand-off.

Grisaro used a similar methodology but based on the particle velocity instead of the characteristic impedance using the below equation:

$$E_f = \int_{t_a}^{t_a+t_{d+}} [p(t) \cdot u_p(t)] \, dt \tag{2.19}$$

The particle velocity was shown by the Rankine-Hugoniot equations to be a function of the peak overpressure as below:

$$u_p = \frac{p_{so}}{\gamma p_a} \cdot \sqrt{\frac{\frac{\gamma p_a}{\rho_0}}{1 + \frac{\gamma+1}{2\gamma} \cdot \frac{p_{so}}{p_a}}} \tag{2.20}$$

Grisaro [70] used this method to perform calculations on numerical data for TNT, C4 and ANFO and compared the values to determine a TNT equivalence. The two methods will be considered in this thesis as methodologies for the calculation of TNT equivalence using experimental data.

There have been only a small number of studies calculating energy flux, mostly using just numerical data in the case of Grisaro [70] or a couple of pressure-time curves from small experimental trials in the case of

Sadwin and Swisdak ([136, 137, 147]. There are questionable limitations with the experimental trials carried out for the studies as some are are based upon lengths of PETN based Detonating Cord [136]. Detonating cord (also known as det cord) is a flexible plastic wrapped tubing usually filled with PETN. It is frequently used for joining explosive charges together in demolitions and quarrying. Due to the det cord make up, it is difficult to determine the shape of the shock wave that would be produced from the detonation of the det cord. Borgers and Vantomme [23] examines methods and computer models for analysing the shock wave from a length of detonating cord with the eventual aim of creating a parametric model of planar blast waves that would be suitable for the prediction of blast parameters from det cord. Section 2.3 discusses further the pressure-time curve differences that can occur from none spherical explosive charges. No information is provided in the study on the set up of this explosive trial. Likewise another experimental trial from the same authors utilises a two kilogram cast TNT explosive charge with a measurement at 7 metres from the charge [136]. This trial produced the pressure-time curve shown in Figure 2.17.

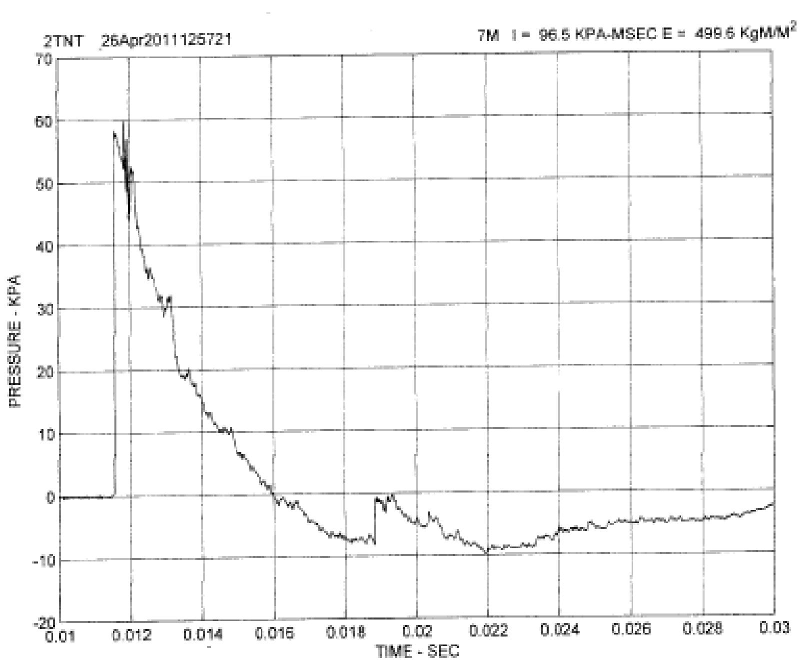

Figure 2.17: Pressure-time curve produced at 7 m from a 2 kg cast TNT explosive charge [136].

Similar to the PETN based Det Cord trial, no information is provided on explosive charge and instrument measurement set-up. When a 2 kilogram TNT explosive charge is modelled in quick-to-run computer model ConWep (Section 2.8.1) at a 7 metre stand-off ConWep produces the values for peak pressure, impulse, time of arrival and positive duration. The table below compares the ConWep estimations (based upon a hemispherical surface burst) with the measurements estimated from the graph in Figure 2.17.

Blast Parameter	Experimental Data	ConWep model
Pressure (kPa)	58	36.05
Impulse (kPa.ms)	96.5	67.90
Time of Arrival (s)	0.0116	0.0122
Positive Duration (s)	0.0045	0.0049

Table 2.2: Experimental values [136] versus ConWep values

There is significant variation between the experimental values and the computer predicted models with higher values for pressure and impulse. It is difficult to make further comments on why this may be due to the lack of information provided on the experimental setup, measurement processes or explosive charge build. It is likely that the blast sensitivities discussed in this thesis have an effect upon these parameters measured in Figure 2.17. Energy flux and calculations from experimental data will be considered further in this thesis along with comparisons of experimental data with computer models.

2.8 Blast Prediction Models

Computer programs can be used for both the prediction of shock waves from different sizes and types of explosives and also for the validation of data post-trial. Modelling approaches can vary from highly sophisticated programs such as LS Dyna [103] or Viper Blast [146] to the simpler quick-to-run semi-empirical codes such as ConWep. It is imperative that reliable and repeatable experimental data is used for the setup of these models to ensure that when they are used to model trials and blast scenarios to ensure that these are appropriate when they accurately predict the characteristics expected. In this thesis, ConWep and Air3D will be investigated further for their use as validation tools for experimental data.

2.8.1 ConWep

ConWep is a simple to use software developed by the US Army Corps that uses weapons effects calculations based on the empirical equations in TM5-855 (Now UFC3-340-01) 'Design and analysis of Hardened Structures to Conventional Weapons Effects' originally Kingery and Bulmash [44]. This database was derived from a large database of existing experimental trials. ConWep is a semi-empirical software that involves look-up tables and is therefore quick to run providing instant estimates for reflected and incident pressures for specified distances and charge type and sizes. The lookup tables were formed by Kingery and Bulmash using a curve fit to a mix of data from both computer analysis and measurements on medium to large scale experimental blast tests. They are valid for scaled distances between 0.067 and 39.67 $mkg^{-\frac{1}{3}}$. Figure 2.18 displays two of the screens on the basic run through of the ConWep programme when determining a peak pressure and impulse from a chosen explosive at a set distance. The data produced from ConWep can be exported to produce full pressure-time curves. ConWep has a number of inputs and scenarios and is suitable for predefined weapons as well as bare charges. It can also take in to account structures and internal explosions. ConWep has since been renewed by the Energetics Materials Blast Information Group (EMBIG) [144] to package the legacy software in to a new product now named EMBlast, available by becoming a contributing member of EMBIG.

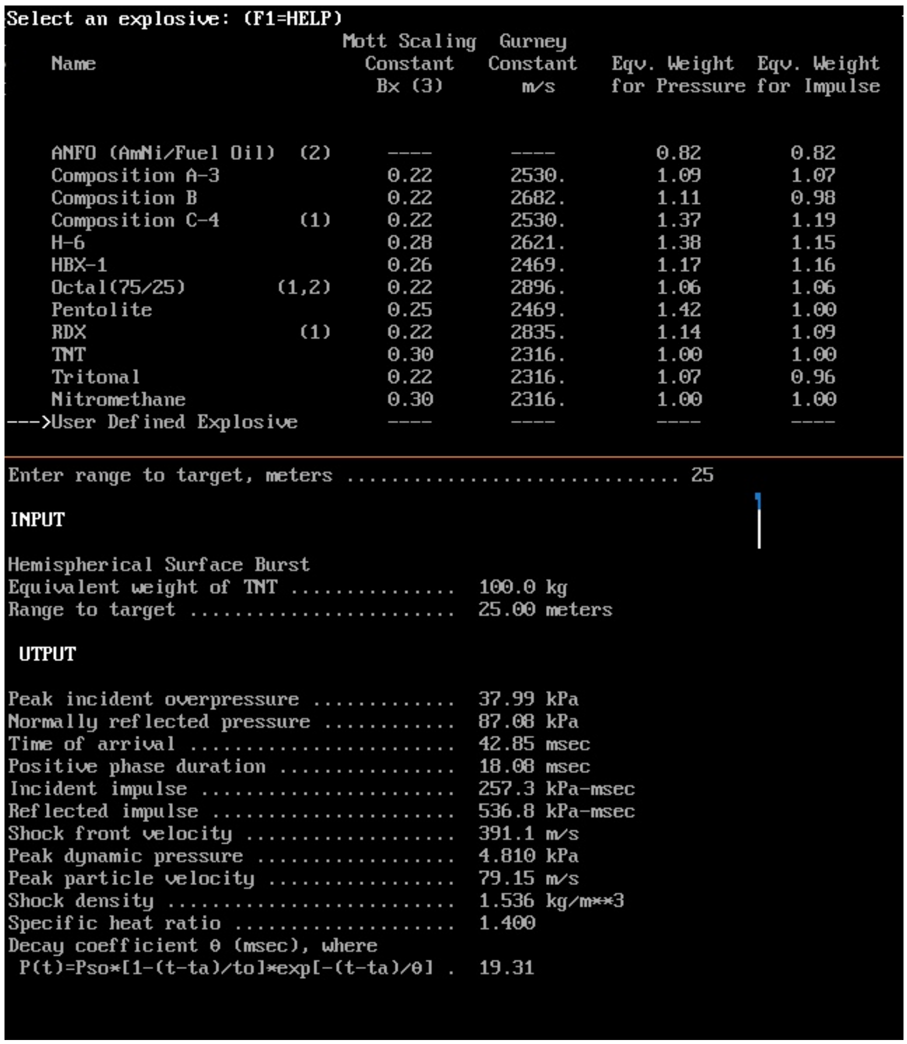

Figure 2.18: ConWep Screenshot

2.8.2 Air3D

Air3D is a hydro-code that models the propagation of a shock wave and its interaction with structures. Air3D was developed at Cranfield University [131] and is a more complex programme than ConWep which, depending on the complexity of the problem and the cell size used, can take a significant run time. The code solves differential Euler equations of fluid mechanics in space and time for 1-dimensional, then 2-dimensional and finally 3-dimensional models using fundamental physical principles as opposed to empirical formulae derived from experiments. Air3D is relatively easy to set-up and run using a text file, and generates solutions that generally compare well with ConWep and test data, particularly for incident pressure. Figure 2.19 gives an example of an input file for Air3D. The Spherical Input involves specifying the explosive input, including shape, size, density and detonation velocity. The Main Input is the arena in which obstacles and target points are plotted for recording the pressures. Figure 2.20 shows a screenshot during an active run of an Air3D, showing the shock wave moving across the plotted arena - any target points that have been specified within the arena will record pressure readings as the wave moves over them. Air3D can be used for free air models such as shown in this thesis, but is also extensively used for more complex scenarios such as by Ballantyne et al. [13] who modelled blast loadings on structural components. Air3D has since been repackaged and is now sold by Cranfield University as ProSAir with both academic and commercial licenses available [41, 101].

```
SPHERICAL_INPUT---------------------------------------------------------------
!
!___explosive input
!
1.60e+3                     density             (kg/m^3)
4.52e+6                     energy              (J/kg)
6.73e+3                     detonation velocity (m/s)
!
! Reference:
! Baker WE, Cox PA, Westine PS, Kulesz JJ & Strehlow RA
! "Explosion Hazards and Evaluation."
! Elsevier Scientific Publishing Company,
! ISBN 0-444-42094-0 (Vol 5), 1983.
!
!___output remap file
!
589_t175_s.tnt              output file
!
!___charge mass and domain
!
100                        charge mass     (kg)
1.2                        radius          (m)
2.0e-3                      delta r         (m)
!
!___program control
!
1.0                         problem time    (sec)
0.75                        CFL
true                        execution flag
!
!___plotting parameters
!
0.0  100                    display increment (sec) or cycles
1                           plot variable
false                       bitmaps
!
!___target points
!
0 1 noformat static true    no. points, start, reformat, stat/dy, temp_flag
MAIN_INPUT-------------------------------------------------------------
!
!___input remap file
!
spherical                      file type
0.0     0.0     1.2      origin of remap x,y,z (m)
!
!___domain definition
!
!
0.5                            cell size  (m)
0.0   60.0                    xmin, xmax (m)
0.0   60.0                    ymin, ymax (m)
0.0   10.0                    zmin, zmax (m)
-1 +1 -1 +1 -1 +1             bxl,bxu, byl,byu, bzl,bzu

!___program control
!
0.5     true                problem time (sec), persist
5                          switching factor
5.0e-1                       CFL
!
!___plotting parameters
!
2                            plot option
1                            plot variable
false                        white background
0.0       5                 display increment (sec) or cycles
40.0  0.0                     scale factor, exponent (shock indicator)
3       0.001   0.001   0.001           ixyz, plotlevx, plotlevy, plotlevz
true                        right hand rule
true                         bitmaps
true                         vrml_flag
true                         vrml_windows
true                         vrml_average_pressure
true                         vrml_gauges
!
!___obstacle definition
!
begin_obstacles
end_obstacles
!
!___windows and average pressure regions
!
0                            no. of window types
!
0 1 0 noformat               no. of windows, start, cells contained, format flag
!
0 1 0 noformat               no. of ave pressure zones, start, cells, format flag
!
!___target points
!
3  1 reformat static false    no. points, start, reformat, stat/dy, temp_flag
!
! Target points
! Free field gauges
!10
7.1 7.1 1.2
!11.28
8.0 8.0 1.2
!12.02
8.5 8.5 1.2
Stop
```

Figure 2.19: Air3D example input file

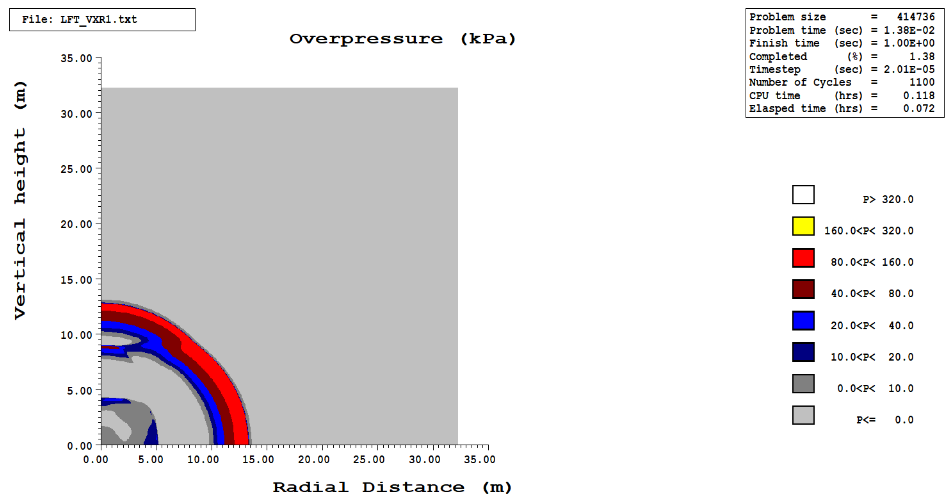

Figure 2.20: Active Air3D run

2.9 Complex Computer Models

There are many commercial software packages available for prediction of blast effects on top of the quick-to-run model ConWep and Air3D that have already been discussed. One of the most important aspects of all computational models (excluding those like ConWep that use empirical look-up tables), is the mesh size, also called cell size. A smaller or finer mesh size will give more accurate results, but causes the computing time to increase significantly [140]. A larger or coarser mesh size will provide less accurate results, but the computing time is reduced. Figure 2.21 shows the difference between a cell size of 0.05 and a cell size of 0.5 in Air3D for a 0.35 kg explosive charge. The pressure-time curve produced by the smaller cell size shows a definitive time of arrival and peak pressure but took in excess of 14 hours to run. The larger cell size used to produce the pressure-time curve, modelling completed in just under 5 minutes, results in the omission of the peak of the curve leading to inaccurate predictions for peak pressure and impulse. Many studies can be found on the influence of mesh size in blast modelling including from Chester [33] and Powell [116]. Powell proposed guidelines for selecting the appropriate mesh size for modelling of explosive detonations on LS Dyna (discussed in the later in this section) that theoretically could be carried across to other blast modelling software including recommendations of scaled element sizes as a function of scaled stand-off and accuracy. Later in this thesis, Air3D is used as a validation tool for experimental data, with the mesh size adjusted based on these recommendations, i.e. smaller mesh size for the smaller scaled stand-offs.

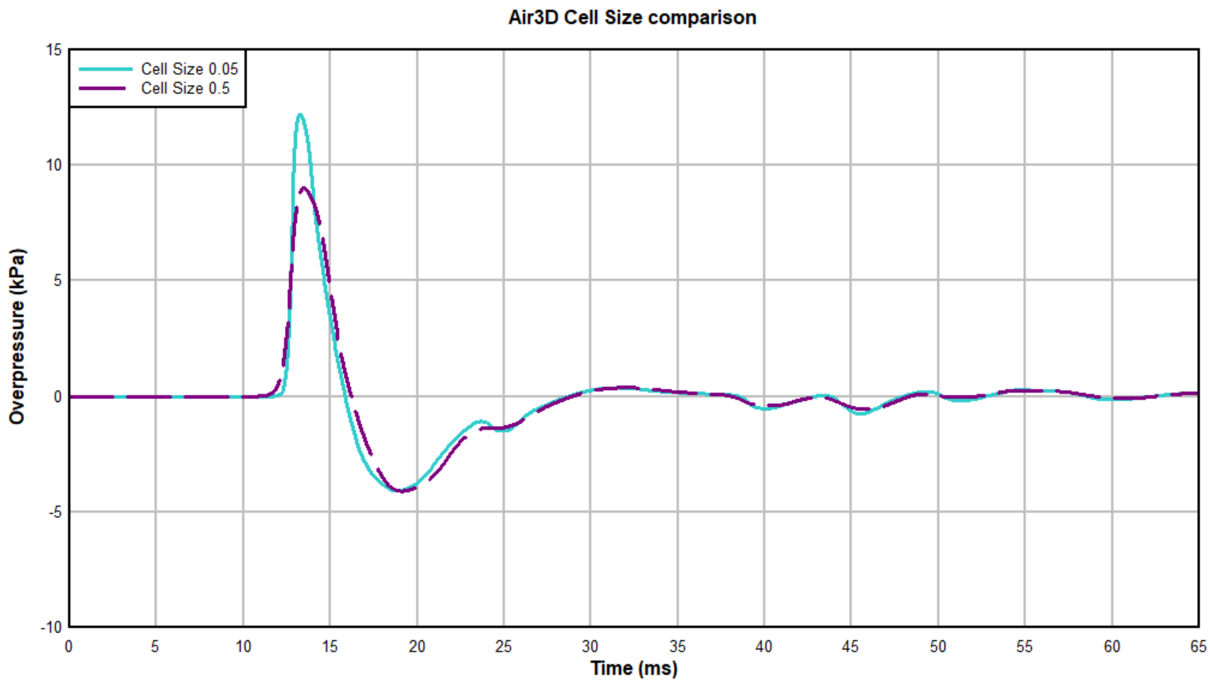

Figure 2.21: Comparison of mesh size in Air3D

Although not being investigated further in this thesis, this section provides a brief overview of four solver packages: Autodyn, LS-Dyna, blastFoam and Abaqus/Explicit. Further information on each programme can be found on the associated websites and in the references quoted.

Ansys Inc. Autodyn is a model designed for the response of materials to mechanical loadings, high pressures and explosive events and the interactions between liquids, solids and gases in these events [7]. There are studies that describe in depth the mathematical and computation principles behind Autodyn and then compare its effectiveness to experimental data [60, 120, 138, 23]. Figure 2.22 shows an example of the model produced by Autodyn from a paper produced by the Global Technology Development where Autodyn was used to optimise timing of delayed detonations [117].

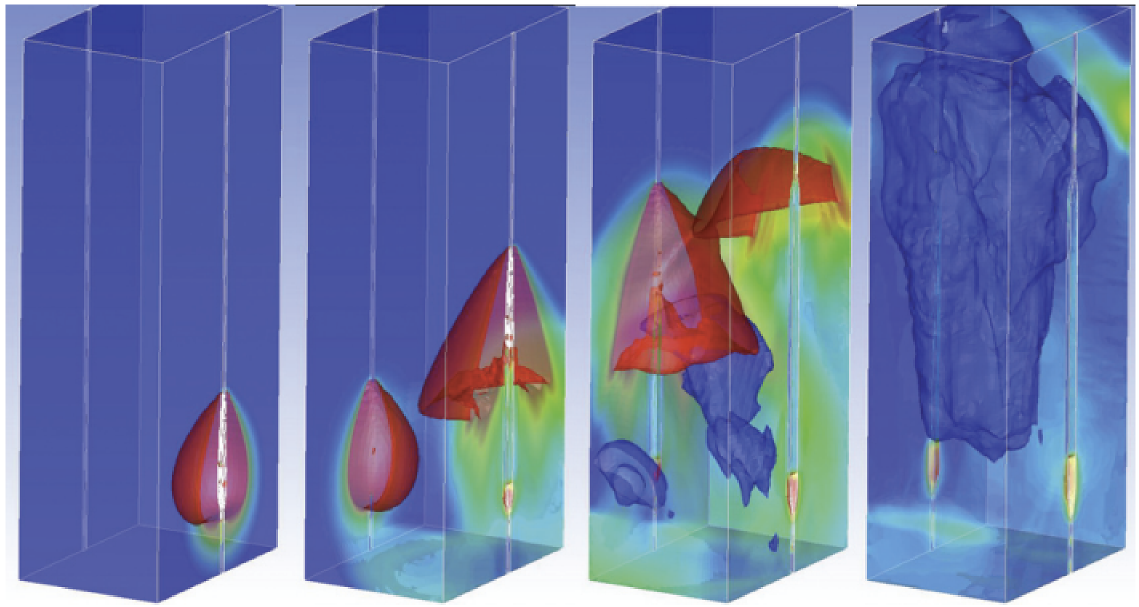

Figure 2.22: Example of Autodyn model showing shock wave and pressure distributions in a blast field [117]

Also produced by Ansys Inc. in collaboration with Livermore Software Technology is LS Dyna. This is quoted on their website as a 'general purpose finite element program capable of simulating 'real world problems' [103]. The program allows for changing boundary conditions, deformations, non linear materials and includes explosives: both bare and cased charges along with a number of pre-determined weapons such as mines and shaped charges [73]. It is heavily used in the blast industry and is well respected for it's accuracy in predicting blast parameters [99, 90, 108, 77].

blastFoam [19] is a relatively new solver for multi-component compressible flow predominantly designed for use for high explosive detonations. It is an open-source programme that uses OpenFoam technology. The blastFoam website provides extensive detail and guidance as to how it can be used. There is very little published literature comparing the modelling of blastFoam to experimental data for validation, although the blastFoam website does provide examples - but these are obviously not independent studies [19, 18]. Chester [33] has presented a comparison of available software and included blastFoam in their analysis of a single 100 kg TNT equivalence explosive blast at 25 metres - the model can be seen in Figure 2.23.

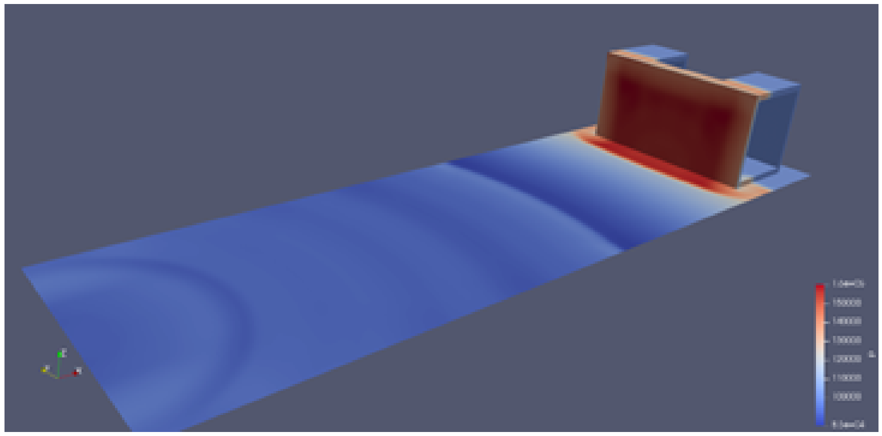

Figure 2.23: blastFoam model of the response of concrete structure to explosive blast [33]

Abaqus/Explicit is a finite element analysis product that can be used for simulations of quasi-static events and is widely used in the blast industry. It has been used to replicate experimental data and has proved a suitable and appropriate tool for model validation [128, 62, 97]. Figure 2.24 shows an example from Langdon et al. [97] where Abaqus/Explicit was used to model blast loading on stiffened plates. The Abaqus/Explicit model showed favourable comparisons to the experimental results.

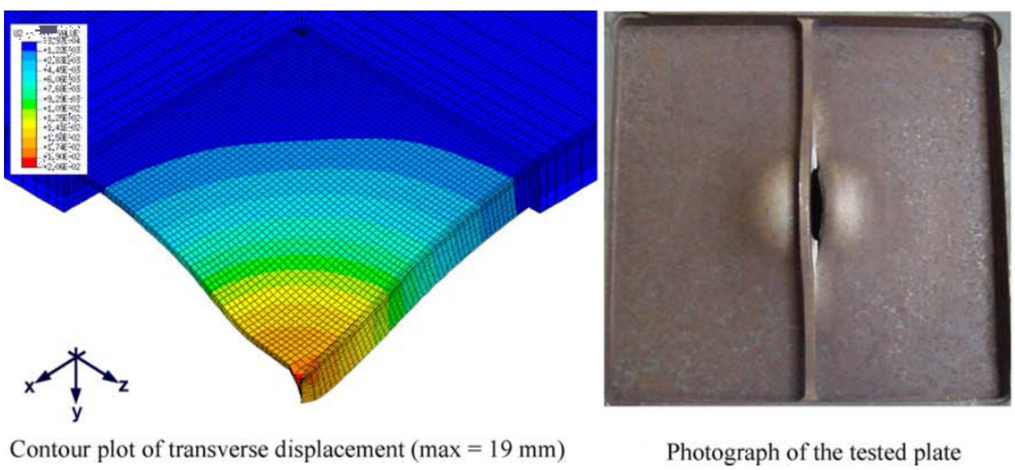

Figure 2.24: Example of Abaqus/Explicit model compared to experimental results [97]

2.10 When Sensitivities Are Not Considered

If the sensitivities of blast parameters are not considered, it can result in a poor quality trial which may have further serious ramifications if, for example, a poorly tested target ends up in commercial use; or if data produced from a blast test is subsequently used for further calculations or model validation. As already discussed in Section 2.7.1, when experimental trials are conducted with no details provided about experimental setup including charge shape, instrument and measurement details, it can be difficult to accept the data as true and valid without taking the paper's author's word that the data has been gathered using an accurate and reliable method.

In other trials, details are given of the setup that can give rise to concerns about the data quality. An example of this is a trial that was conducted by the Health and Safety Executive in 1995 [63] at Spadeadam when it was part of British Gas. During these trials, gauges were positioned flush with the ground at 25, 50, 75, 100 and 150 metres from the charge location. The concern arises because some of the gauges were not in a direct line of sight, or at the same ground height as the charge with embankments in the way and a fall of land to one side as seen in Figure 2.25. Formby and Wharton state in the paper that the pressure time recordings from the gauges did not exhibit the typical shock wave characteristics as expected from the explosives. Formby attributes this non ideal nature of the profiles to the topography of the site. Despite this, the data from these trials has been cited in excess of fifty times in further studies.

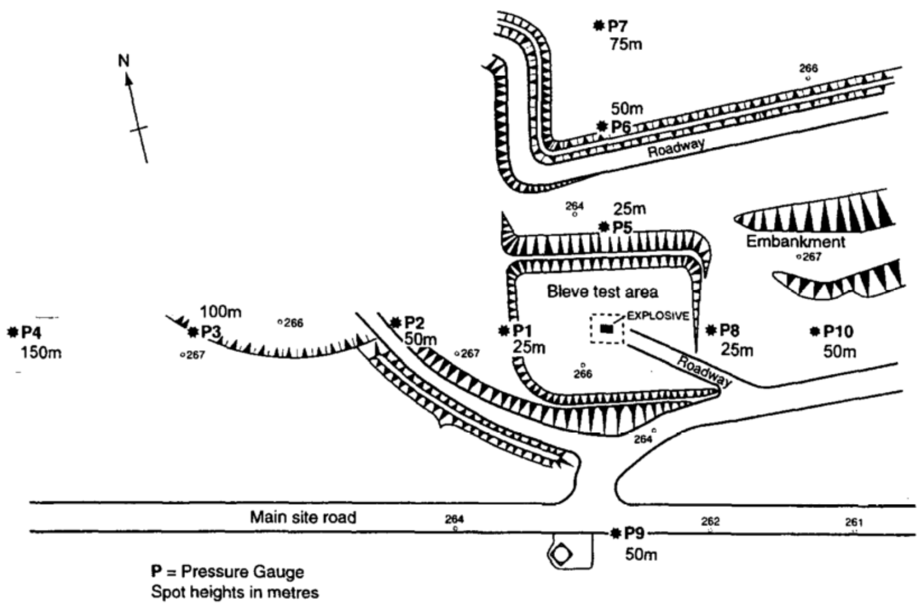

Figure 2.25: HSE trials site layout [63]

This study only hints at issues of interaction of structures or influence of the area in a blast. As a shock wave passes through complex scenarios such as streets, congested areas (process areas or even wooded areas) or even just areas with changes in the lay of the land, reflections can occur causing unexpected and noisy pressure peaks when measurements are taken. Due to the cost and effort of conducting these complex trials, the number of experimental tests that replicate these scenarios are limited and, fairly obviously, done at a small scale. An example of this is the study by Benselama et al. [15] in which explosive trials were conducted and then matched to a computer simulation. Figure 2.26 presents one of the pressure-time curves from the experimental test with the overlaid model. This shows excellent fit of the model to the experimental data, but highlights the difficulties if the parameters were to be used in anything other than the exact same built-up scenario. Further studies on the interactions of shock wave propagation between buildings, structures and shapes for both experimental and numerical models can be found from Li [100], Ofengeim [110], Riedel [122], Rose [134, 133], Smith [141, 142] and Thompson [151],

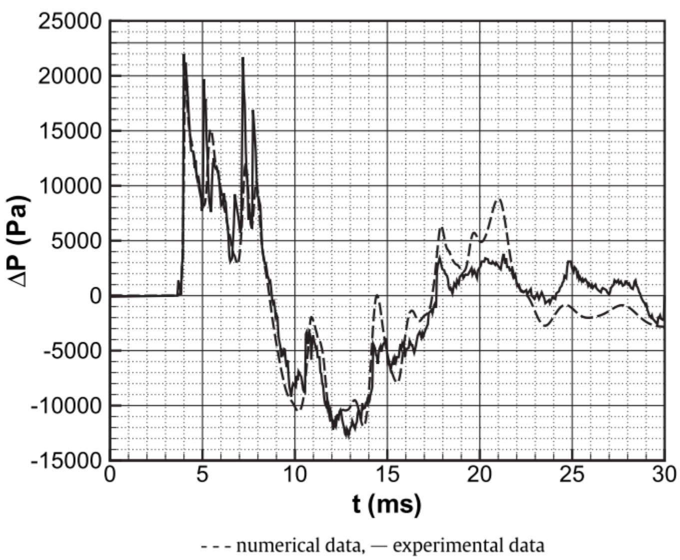

Figure 2.26: Example of complex scenario overpressure-time curve [15]

In the aforementioned trial by Formby, it was stated that there was significant difficulty in the building of the explosive charges [63]. Formby experienced cracking in built explosive charges during movement which then required additional pressure to remove air pockets. This additional pressure produced distortion of the container, which was not sufficient to prevent movement, suggesting that the explosive charges were not homogeneous charges of uniform density. The type of explosive used can hinder or help with the build of explosive charge. ANFO comes in prills, and much like the liquid Nitromethane, as long as the container used is spherical, it is simple to build a uniformly dense and appropriately shaped explosive charge. Where solid explosives are used such as PE4, Semtex or flaked TNT, it is much more difficult to ensure that the desired shape is met and that the density of the explosive is uniform. It depends on the person who is building the charge, the tools they are using and the explosive type in question, which may be affected by atmospheric conditions. From the author's experience, Semtex in warm weather is much stickier and pliable than when it is cold, in which it is very rigid and tears easily instead of stretching or moulding. Likewise, PE4 is a very crumbly material and when shaping from its raw storage in 50 kg drums into a spherical charge by hand, particularly at larger charge sizes, there is risk of variation in how tightly the explosive is packed and how spherical it is possible to make the charge. If packing a cased charge with explosives, air gaps between explosives or between the casing wall and the explosives can result in irregular casing breakup, resulting in larger, often heavier fragments that may impact differently upon a target. This has been found from the author's experience. Even if a cased charge is well packed, the complexities involved with case expansion, case fragmentation, blast wave diffraction through the case and fragment impact on the air blast all influence the parameters that may be measured in a blast [14].

A trial conducted to investigate response of glass panels to an explosive blast measured blast overpressures from charge sizes between 600 gram and 1600 gram [66]. The images below have been lifted direct from the paper and show two of the pressure-time curves produced. As discussed in 2.5, it can be difficult to determine blast parameters from noisy pressure-time curves. The examples in Figure 2.17 display how difficult it can be to determine values for peak overpressure, impulse and positive duration.

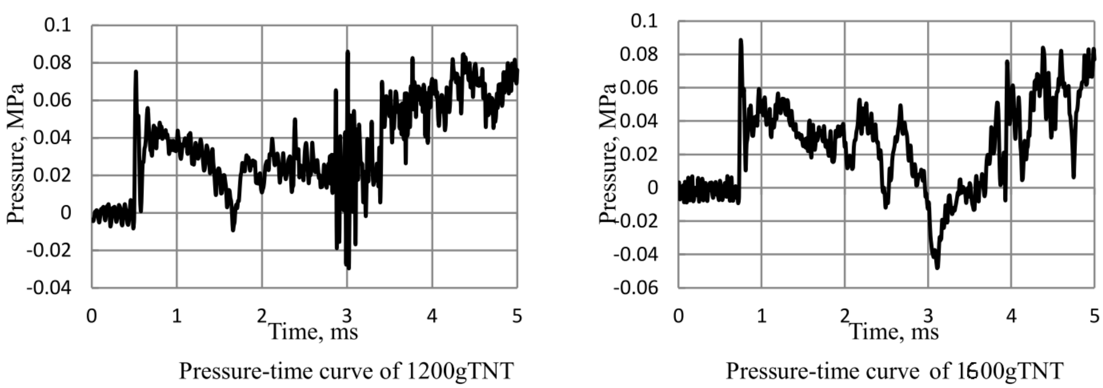

Figure 2.27: Pressure-time curves from experimental glazing trial [66]

The only clear and definitive parameter shown from these pressure-time curves is the time of arrival. In this set of trials, the focus was not on the overpressure produced in the blast, instead relating the projection velocity of glazing directly to the charge size, regardless of the overpressure measurement. The issue of poor quality pressure-time curves is a similar issue faced by Hudson [79] when identifying blast parameters from the Coyote Canyon trial [78]. Here he states that individual pressure-time curves were 'difficult to interpret'. Hudson put this down to evidence of circuitry malfunction, arrival of the flame front at the same time as the shock front, and the complex nature of the target causing local disturbances. Instead of individual readings which independently were not usable, the data were then used collectively to provide average values for the blast parameters. Later in this thesis, the difficulties in producing usable pressure-time curves are discussed further.

In trials carried out on an explosive to determine TNT equivalence [Reference Redacted], a value was produced and issued to test houses for use in UK government trials. When investigations to confirm this value were carried out at Spadeadam in 2001, the value of TNT equivalence was found to be wildly different [Reference Redacted]. On further investigation, it was found that the original trials had been carried out in sand and had not accounted for the energy lost to cratering, compared with the Spadeadam trials which were carried out on a flat concrete 100m x 100m pad with a 75mm thick steel blast mat directly under the charge. If the background of a trial is not known, values may be incorrectly used or cited if the conditions do not match up.

The paper by Gruss in the Journal of Trauma [71] details what Gruss refers to as a 'significant systematic error' in accepted primary blast injury criteria in literature produced by the use of low-quality experimental data, particularly to do with the impulse values. As described in the paper, the implication of the use of poor quality or inappropriate impulse values that were used by Bowen et al. [24] to produce time curves for lethality for an number of scenarios is significant. These lethality curves based upon this data lead to the prediction of a more severe blast injury than may occur in reality. The Bowen criteria is still the standard for many primary blast injury criteria [71].

Inconsistencies can occur not just from the setup of an explosive test, but also in the data analysis of any measurements gathered. In TM5-855-1 [44], it is stated that there were issues with the Conventional High Explosive Blast and Shock (CHEBS) test series. These tests were used as the main source of data for peak free-field pressure and impulse models. The measurements were obtained from 16 general purpose 500 and 1000 lb bombs tests with air blast data. Where the bomb size was different this was scaled based on their TNT equivalence. Many of the gauge readings were discounted due to peak pressures and impulses decreasing when at angles closer to the nose or tail of the cylindrical cased explosives. Other values were discounted when there was excessive noise in the pressure plot, or if the pressure region was unusually wide or narrow compared to the other readings, likewise if it was too smooth compared to the others it was also discounted. The document does not state how many pressure and impulses were discounted and how many were used. Much of this data was used to feed into computer models such as ConWep [44] and have been cited hundreds of times in further research.

When the data from multiple sources in multiple set ups are viewed together, the variations become obvious. Karlos et al. [91] plotted various blast wave parameters versus scaled distance for spherical blast waves from up to 10 different data sources some of which have already been discussed in this thesis. Figure 2.28 displays the peak incident overpressure from 10 sources. There is a clear split on the data below a scaled distance of 1 $mkg^{-\frac{1}{3}}$ and, although above this distance there appears good agreement in values, the log scale still suggests a significant spread of data. Later in the same paper, Karlos et al. [91] notes that from literature, the peak overpressure can differ by more than 40% from the proposed values by Kingery and Bulmash. If one was to validate a model or predict blast parameters using data from literature, the choice of data source could significantly skew the predictions or model validity.

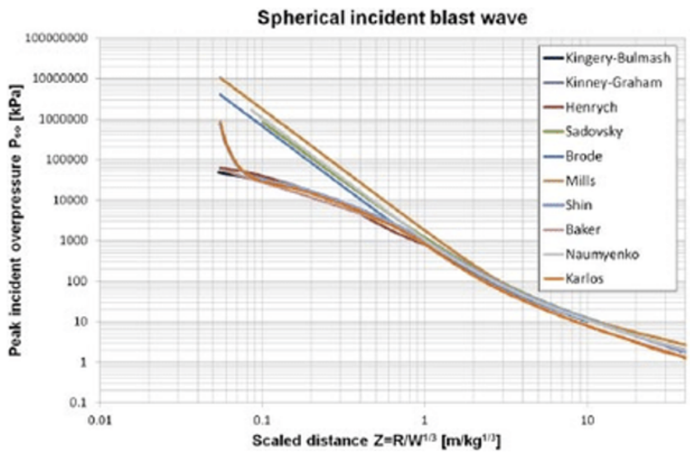

Figure 2.28: Karlos et al. [91] review of incident pressure values versus scaled distance from literature

2.11 Understanding Blast Parameters for Incident Investigation

In incident investigations and terrorist attacks, one of the key tasks is to identify and characterise the cause of the blast. This includes establishing the size of the blast in TNT equivalence in order to provide a quantification for the size and effects of the blast and for comparison of between incidents. Figure 2.29 below from Baker [11] is one such method that can be used to estimate overpressure based on distance in an incident by the damage seen, although this is considered a very rough guide. As mentioned in the previous sections, in a real life scenario blast pressures will be influenced by interactions between structures, reflections, absorption of energy due to collapsing and distorting structures all of which can increase or decrease the pressure exerted upon targets [93].

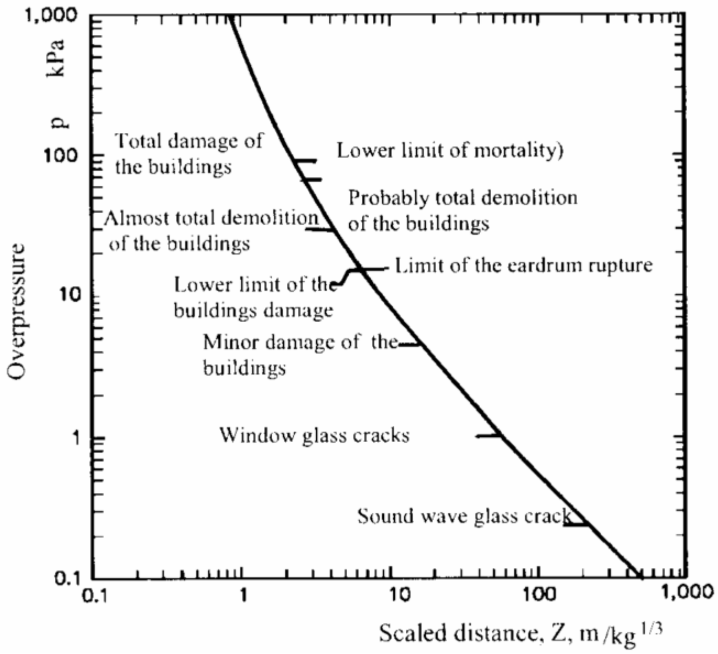

Figure 2.29: Damage and injury consequences from overpressure based on scaled distance [11]

Overpressure damage can also occur from events that do not involve explosives, but instead pyrotechnics or even flammable vapours or gases, such as the Buncefield Incident in 2005 in which 300 tonnes of petrol was released, forming a flammable cloud that was subsequently ignited and, due to congestion within the vapour cloud, the flame accelerated to detonation [86]. Difficulty comes when assessing the TNT equivalence of gases and vapours using comparisons that involve parameters that are usually only produced in a detonation, as fuel-air mixtures may only detonate if the cloud is partially confined, congested, obstructed or has a sufficiently energetic initiator [159]. These complex sensitivities are augmented by the concentration of fuel in air, which will affect the ability of the mixture to detonate, as well as the blast parameters.

The TNO Multi-Energy method is traditionally used for estimating gas explosion sizes. This model is based on curves which display relationships between overpressure and distance based on the estimated congestion and confinement of a vapour cloud where 10 is very heavily congestion or confined and 1 is almost open air (Figure 2.30) [106]. Once the overpressure and the stand-off is known, an estimation of charge size and an TNT equivalence can be calculated using blast overpressures of TNT at the same distance and stand-off. The paper by Mercx et al. [106] describes in detail how this method is used in estimating vapour cloud explosion blasts.

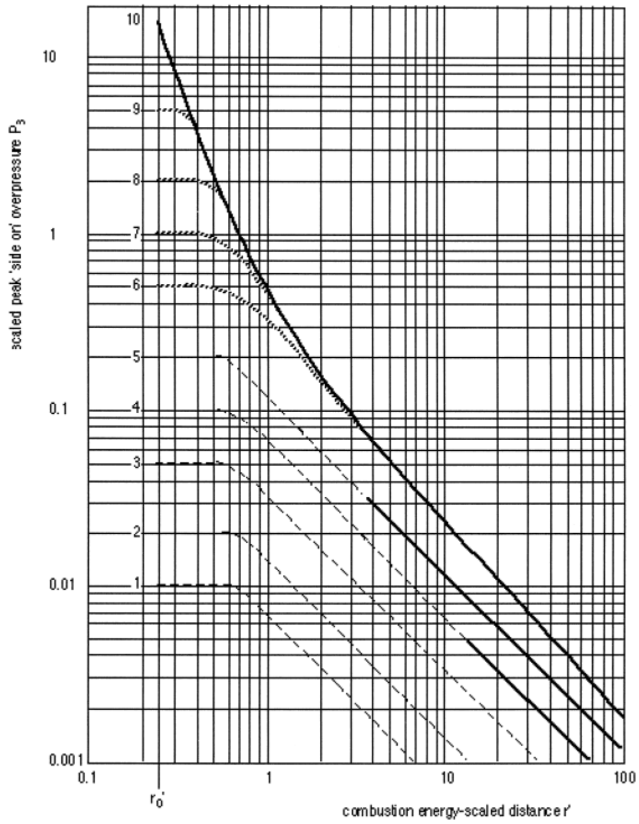

Figure 2.30: Overpressure estimation curves for the Multi-Energy Method [106]

In an incident, estimation of the overpressure can be reliant on evidence gathering such as window breakage distance and vehicle damage. Experimental trials can be used to collect empirical data for assessment of damage under overpressure loading. Following the Buncefield incident, as part of a much larger joint industry programme of investigation into explosion characteristics of large vapour clouds [28], tests were conducted placing vehicles, oil drums, ISO containers and instrument enclosures at various distances from vapour cloud explosions and recording the damage (Figure 2.31) [4]. Direct comparisons were made between the damaged items from the Buncefield Incident, as well as from a similarly occurring incident at Jaipur in 2009 [85]. This enabled an estimation of the pressure loadings on the items in the incidents to be estimated. In the same report, Allason and Johnson investigated whether far field pressure-time curves could be used to estimate the pressure loadings and therefore TNT equivalence of the vapour cloud, finding some success using both the Multi-Energy method and the method proposed by the Center for Chemical Process Safety [30], which involves assuming an efficiency of 40 % in terms of energy conversion to the shock wave and multiplying by the ratio of heat of detonations of the fuel and TNT [4].

Figure 2.31: Comparison of damage of 50% oil drums from experimental trials (left) to those seen at Jaipur (right) [4]

A similar methodology of comparing incident damage to that observed in trials was used to estimate the mass of explosives used in the vehicle bourne explosive charge that was detonated in the 2011 attack on Oslo. Christensen [36] assessed window breakage in the buildings around the detonation point to estimate the pressure exerted upon the glass. Since the distance to the vehicle was known, a charge size could be estimated. This correlated well with the actual amount quoted by the person responsible for the bombing.

2.12 Estimating Blast Parameters from the 2020 Beirut Explosion

On the 4th August 2020, a large explosion occurred from Ammonium Nitrate stored at a warehouse at the Port of Beirut in Lebanon. There were at least 218 fatalities and 7,000 injuries, as well as extensive property damage. Due to the sheer size of the explosion, it naturally made headlines around the world. As such there was a flurry of activity to predict the amount of explosives detonated in the explosion. This section discusses some of the techniques used to estimate the blast parameters in the incident.

Prior to the explosion at the Port of Beirut, there was a large fire. Due to the nature of accidents and incidents, there was significant public interest in the large fire, meaning that many videos were taken capturing the moment of detonation on camera. Johnson and Cronin [87] conducted analysis of video recordings to predict a TNT equivalence of the Ammonium Nitrate stored. They were able to do this as when a shock wave is generated in a humid atmosphere, the rarefaction can result in the water vapour condensing out of the atmosphere to cause a mist. As the detonation occurred at the port, in very close proximity to the surface of the sea, the shock wave was clearly visible as it moved across the water, along with the rarefaction following it (Figure 2.32[87]). Using buildings in the foreground of the explosion as a method to calculate scale, it was possible to calculate the velocity of the shock wave and the leading edge of the mist. The speed of the shock wave and the rarefaction was plotted against time using the video footage to produce an average speed of 335 m/s. The distance between the rarefaction and the shock wave from this graph can be used to produce the positive phase of the pressure wave as rarefaction occurs when the air pressure drops below ambient and the air temperature drops. When temperature drops to below the dew point, condensation will occur and a mist form. Using weather data available from the day, Johnson calculated an 80 mbar drop would be required to cause the rarefaction to occur. Using the positive phase duration and shock wave speed, Johnson determined that the Ammonium Nitrate detonated with a TNT efficiency of between 30 and 42%, equalling a TNT equivalent charge weight of between 825 and 1150 tonnes.

Figure 2.32: Stills from video footage showing the shock wave and rarefaction moments after the detonation [87]

Rigby et al. also used video footage in the determination of blast parameters to estimate the yield of the explosion [127]. As previously mentioned, many residents of Beirut were filming the fire at the time that it detonated and those recordings were very quickly uploaded on to public available social media. Rigby et al. [127] used 16 videos and quantified the time of arrival of the blast at 38 locations across the city. The time of arrival was determined by measuring the delay between the moment of detonation, seen as bright flash, and the visual disturbances or audio spike of the shock wave arriving at the locations. Using Kingery and Bulmash semi-empirical predictions, they best estimated the explosive yield to be 500 tonnes TNT Equivalent, with an upper limit of 1120 tonnes. Stennett et al. [145] used the same method using public videos and Google Street View to determine the position of the observer's camera to produce values for the time of arrival from 6 videos. This produced a best estimate of 637 tonnes TNT Equivalent with an upper limit of 960 tonnes - comparable with that calculated by Rigby.

Aouad et al. [8] also utilised video footage of the blast, but concentrated on the fireball evolution, tracking the shock from in the first 170 milliseconds of the explosion. This produced a much lower value for TNT Equivalent charge than Johnson and Rigby of approximately 200 ± 80 tonnes. This was however in agreement with the lower limit of Dewey's predictions, whom, using the data from Rigby et al. [127], calculated shock Mach number and peak hydrostatic overpressure behind the shock front to produce a TNT Equivalent charge of between 150 and 700 tonnes [46]. Pasman et al. [111] utilises three different methods of estimating the TNT equivalence of the blast: crater size, damage to nearby structures and, like previous papers, the time of arrival. The results of these three analyses provide a best estimate of 650 tonnes with an uncertainty range of 300 to 700 tonnes. Díaz [50] conducted fireball analysis from four videos to estimate the radius size of the fireball to produce a best estimate of 600 tonnes with an uncertainty of ± 300 tonnes.

This section has shown that there are many methods available to provide estimations for TNT equivalence from a blast, which, post-incident, is one of the key questions to be answered. The results have shown that there is no one single methodology that is best suited for estimating the equivalence, showing that even when working from the same data (such as with Rigby and Dewey), differing values can be produced based upon the methodology utilised and the parameters compared to, highlighting the importance of accurate experimental data where the constants are known and well tested and validated models.

2.13 Summary

This chapter has reviewed the basis of experimental blast trials and the outputs produced. It has considered the way in which blast measurements are produced and reviewed literature and equations for the basis of these measurements. This chapter also discussed the influences in a blast test such as geometries, explosive choice and TNT equivalence.

The deficiencies in blast testing have also been discussed and ways to avoid or mitigate these have been the basis of this thesis. Whilst studies of experimental data are numerous, many are based on a single or a small number of experimental trials and often produce data values that are presented without the necessary detail as to the data gathering process or the setup. The consequence of using poorly gathered or unsuitable data can lead to inaccurate conclusions for both blast mechanics assessments and, more critically, for real-life threat assessments. For example, Benselama et al. [15] used experimental data from a small scale experiment conducted by the UK HSE [29] to validate a numerical simulation of a PE4 explosive charge detonating in a real world full size congested site.

This chapter also discussed how understanding of blast parameters can be used to calculate TNT Equivalence in incidents such as Buncefield, Beirut and the Oslo terrorist attack. Using known parameters against computer models and trusted equations allow for assumptions to be made on charge size and type in an incident.

This literature review highlights a few important assumptions: validation of the scaling law, validation of the numerical simulation and assumption of valid experimental data. As emphasised by Bowles et al. [25], computer models predicting blast loads used to design buildings, develop blast mitigation, restrict traffic and plan for evacuations require 'voluminous, high-quality, experimental data' which if not accurate and reliable, can result in poor quality studies that may have disastrous consequences.

3 Spadeadam Historical Data Review

The author has been conducting explosive trials since 2015 and collecting pressure and impulse data from a variety of target distances (or stand-offs). These tests have ranged in purpose and size from small 1 kg tests to 640 kg tests with a variety of explosive types and set-up. By far the most common charge size for an explosive test is a 100 kg TNT equivalence blast and, as such, the author has chosen to review the data from these tests as part of a historical data review.

3.1 Test Setup

The trials considered in this data review all consisted of the same basic setup. This involved a single 100 kg TNT Equivalent charge at the centre of an arena. The explosive type, mass and geometry remained identical for each test. The charge was initiated with a non-electric detonator initiated by shocktube. The value of TNT equivalence used for all these explosives was the same, based upon tests carried out in 2001 at Spadeadam [Reference redacted]. The centre of the charge was located at 1.2 metres above ground by supporting it on top of styrofoam blocks. The styrofoam blocks were placed on a 75 mm thick steel charge plate (also called a blast mat) on top of a 100 m $\times$ 100 m concrete test pad. The blast mat aims to reduce energy loss through crater prevention, this also assists with preventing damage to the test pad. This test setup matches the requirements of ISO 16933 [1] and the Protected Spaces Test Standard [redacted] and can be seen in Figure 3.1. Test Pad C, where these tests were conducted, is located at DNV Spadeadam Research and Development in Cumbria, UK at an altitude of 258 metres above sea level.

Figure 3.1: Typical explosive setup of a 100 kg TNT equivalent arena trial

The pressure-time curves were produced through reflected and incident gauges fielded in the blast arena. These were typically alongside targets under test for specific purposes such as those mentioned in Section 1.1. Reflected gauges were mounted in nylon discs fixed to the front face of reinforced concrete blocks that could be stacked to produce a large reflected surface. The gauge block final size varied for these trials between 2 m × 2.5 m and 3 m × 3.5 m depending on whether the 'large' gauge block or the 'medium' gauge block was used. In trials where it was necessary to measure reflected pressure at more than one distance, both gauge blocks were fielded. In trials requiring just one reflected stand-off distance, just the large gauge block was used. Gauge blocks are instrumented with a minimum of 3 pressure gauges to a maximum of 9. These are installed in nylon mounts as per Figure 3.2. Nylon mounts are used to prevent movement of the gauge when subjected to the shock wave. The desired position for the gauge block is measured from the centre of the charge plate using a long tape, with the blocks then positioned using a telehandler.

Figure 3.2: Gauge setup of the 'medium' gauge block

Incident measurements are recorded in the same format as reflected pressures but, instead of a gauge installed in the gauge block, the gauge is installed into a nylon mount on a large streamlined disc. These are known as pancake gauges. The streamlined 'pancake' is to produce a laminar flow of the shock wave as it passes the gauge, producing a smooth pressure-time curve. These large discs are housed on heavy metal stands that can be positioned around the test arena. Guidance on setting up gauges can be found directly from the gauge manufacturer PCB [160, 161]. The distance from the centre of the charge plate to the required incident gauge stand-off is measured using a long tape and marked on the ground. The gauge at the centre of the disc is lined up with this mark, with the face of the disc side-on to the direction of blast propagation. Where there are multiple measurements to be made, gauge stands are lined up facing the blast radially around the charge as seen in Figure 3.3.

Figure 3.3: Incident pressure gauges fielded radially for an arena blast

Both the gauges installed in the pancake stands and those installed in the gauge block are PCB 113B26 gauges. These gauges are specifically designed for use in blast wave measurements. Further specific information on the gauge can be found in the product specification and user manuals supplied by PCB [160, 161]. These are connected with microdots and the signals fed back to amplifiers through coaxial cable. Amplifiers are kept as close as possible to the gauges, usually in protected sangars where they will be unaffected by the blast. The amplifiers connect back to HBM high-speed loggers, connected via Ethernet links to a laptop running the logging software Perception. The loggers were either triggered manually upon exit of the area prior to the blast or by remote desk-top from a remote control room and triggered prior to ignition of the charge. Also fed back to the loggers is a trigger cable, which is a length of coaxial cable connected to a 24 volt trigger box. The cable is twisted and the ends separated and taped directly onto the explosive charge. When the charge detonates, it melts the insulation surround causing the cable to make a circuit and presenting a 24 volt signal on the logger. This produces a very accurate time at which the detonation wave reaches the edge of the explosive charge, against which the data from the pressure gauges can be zeroed during processing. This may produce very small delays in the true time zero due to the time taken for the shock wave to pass through the explosive charge.

There are other methodologies for collecting pressure data that are not currently utilised at Spadeadam, many of which are reviewed in depth by Draganic et al. in his overview of methods for pressure measurement in blast loading for field tests as well as laboratory style tests such as use of a Shocktube [52]:

- Hopkinson Pressures Bars - this was a technique originally developed by Hopkinson and presented in 1913 [76]. It has since seen a resurgence in use, particularly for the measurement of near field pressure measurements [153, 56]. Tyas presents a comprehensive study of the use of Hopkinson Pressure Bars in work conducted on the University of Sheffield Characterisation of Blast Loading (COBL) test facility [153, 154].
- Optical fibre based sensor - MacPherson et al. [105] utilised the hydrophone optical fibre based pressure sensor that operates from the change in optical path length caused by pressure via the strain optical effect and the dimensional changes in the optical fibre sensing element. The initial test programme showed a 'high degree of correspondence' between tests but stated that there were still some technical issues that remain to be addressed.
- Held [75] describes a set up of momentum rods to measure the blast impulse. This is similar to the ballistic pendulums (also described in Held's paper and also by Dragnaic [52]) which have been used since the mid 1700s as way to measure the velocity of bullets from a gun [130]. The pendulum system measures the momentum from a blast by how far the shock wave moves the pendulum and can be used to determine the impulse loading upon a structure. This system has also been used by Cloete and Nurick [38] in conjunction with a centrally mounted Hopkinson Bar.

3.2 2015-2018 Data Review

Between October 2015 and October 2018, forty-eight 100 kg TNT Equivalent experimental tests of the arrangement described in Section 3.1 were carried out at DNV Spadeadam. Pressure and impulse values were recorded from a variety of different gauge types at varying distances equating to 333 reflected pressure readings from reflected gauge blocks and 277 incident pressure readings.

Figure 3.4 to Figure 3.7 display the reflected and incident pressures and impulses collected during these forty-eight trials.

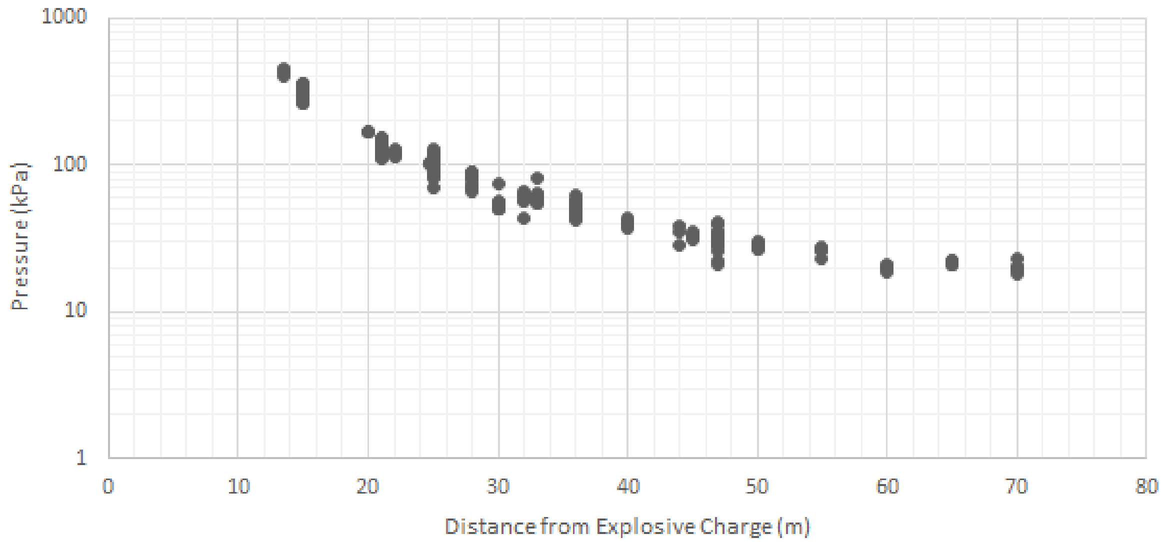

Figure 3.4: 2015-2018 reflected pressure values

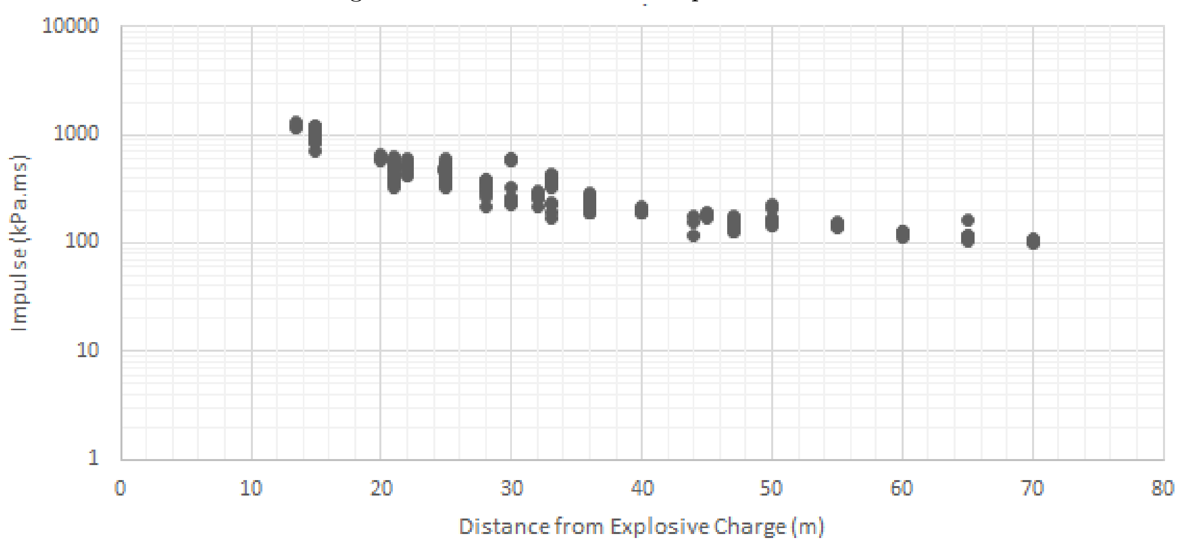

Figure 3.5: 2015-2018 reflected impulse values

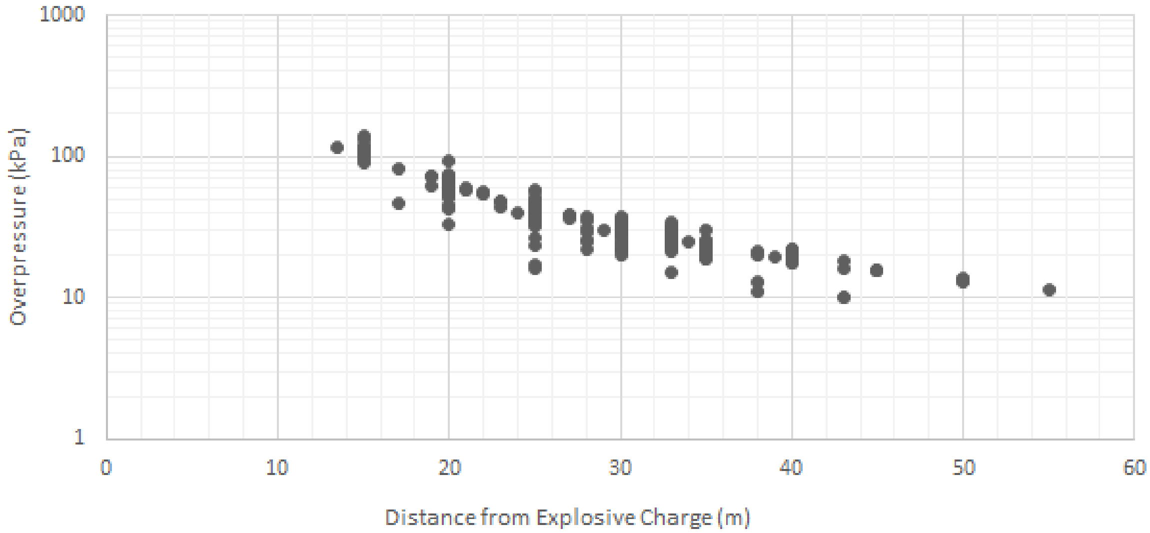

Figure 3.6: 2015-2018 incident pressure values

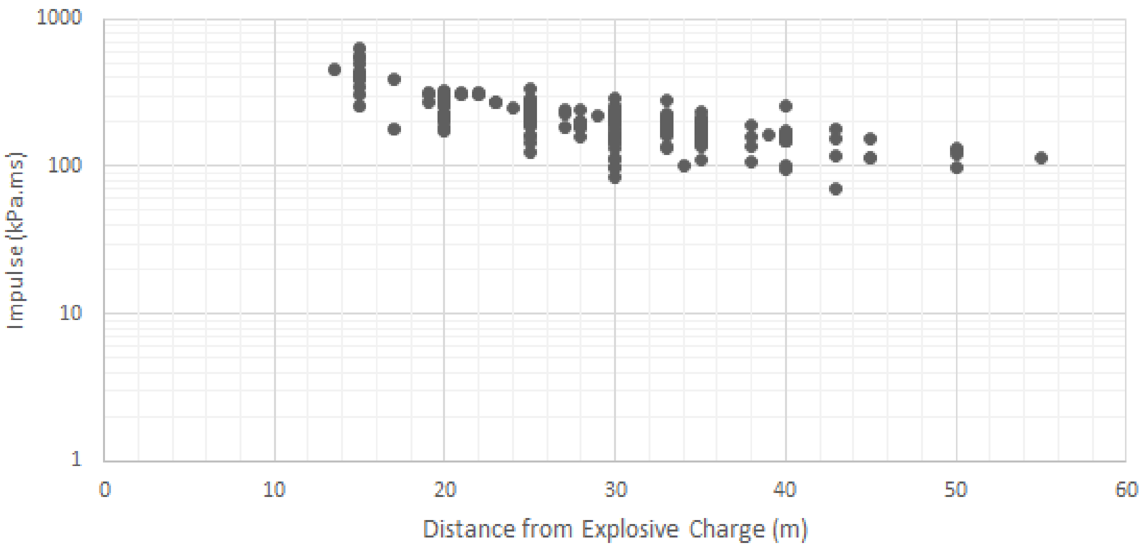

Figure 3.7: 2015-2018 incident impulse values

3.3 Statistical Variations

To allow assessment of the data, the tables below give the Mean and Standard Deviation at stepped distances from the experimental data. The distance 33 m has been chosen instead of 35 m as this is a distance commonly used for compatibility with the Explosion Resistance of Curtain Walling Test Standard [redacted].

Distance from Explosive Charge (m)		15	20	25	30	33	40	45	50	65	70
Pressure (kPa)	Mean	306.32	167.33	99.99	54.38	57.75	40.05	32.57	28.04	21.40	20.07
	Standard Deviation	24.15	1.70	10.62	6.36	0.35	1.51	1.24	0.88	0.51	1.53
Impulse (kPa.ms)	Mean	991.48	604.33	447.91	354.92	227.45	199.71	180.60	170.53	120.07	104.70
	Standard Deviation	80.38	27.01	57.01	159.07	5.05	8.24	7.15	24.74	18.85	3.48

Table 3.1: Mean and standard deviation from historical reflected pressure and impulse

Distance from Explosive Charge (m)		15	20	25	30	33	40	45	50
Pressure (kPa)	Mean	108.73	60.38	40.48	29.18	26.23	19.44	15.63	13.33
	Standard Deviation	12.47	12.11	6.67	4.00	3.82	1.36	0.09	0.42
Impulse (kPa.ms)	Mean	428.79	252.83	239.25	189.26	192.19	159.57	127.67	119.99
	Standard Deviation	90.91	43.48	34.73	45.56	29.90	29.63	18.98	13.50

Table 3.2: Mean and standard deviation from historical incident pressure and impulse

Table 3.1 and Table 3.2 both suggest similar findings in that as the stand-off distance approaches the near field with a scaled distance of less than 4 $mkg^{\frac{1}{3}}$, the standard deviation increases significantly compared with the far field where the standard deviation is much lower.

The impulse for both reflected and incident data show a greater spread than that of the pressure data. The reflected data are marginally better than the incident data. This could be due to the difficulties in recording the incident pressure data, this is covered further in Section 4.1. Due to the nature of standard deviation, where the value of the standard deviation scales with the values themselves, the Coefficient of Variation has been calculated in Table 3.3 and shown graphically in Figure 3.8. The Coefficient of Variation (or CoV) is calculated as the standard deviation divided by the mean [58]. The values are dimensionless and therefore can be used to compare between the pressure and impulse.

Distance from Explosive Charge (m)	15	20	25	30	33	40	45	50	65	70
Reflected Pressure	0.08	0.01	0.11	0.12	0.01	0.04	0.04	0.03	0.02	0.08
Incident Pressure	0.11	0.20	0.16	0.14	0.15	0.07	0.01	0.03	-	-
Reflected Impulse	0.05	0.04	0.13	0.45	0.02	0.04	0.04	0.15	0.16	0.03
Incident Impulse	0.21	0.17	0.15	0.24	0.15	0.18	0.15	0.11	-	-

Table 3.3: Coefficient of Variation for historical pressure and impulse data

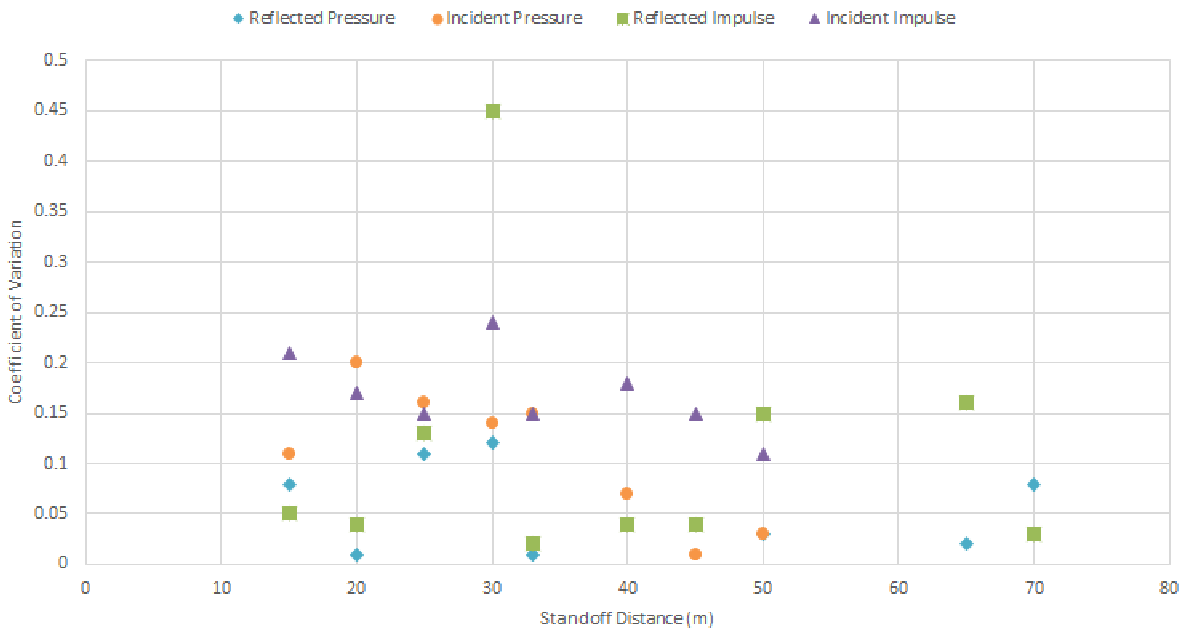

Figure 3.8: Graph of Coefficient of Variation for historical pressure and impulse data

The Coefficient of Variations show a great deal of spread for all the measured parameters, but a consistently high Coefficient of Variation for the incident impulse. Further critical review of this data can be found in Section 5.7 where it is compared to recent data and conclusions drawn.

3.4 Comparison with ConWep

It has already been mentioned in Section 2.8 that ConWep is a commonly used tool in blast parameter assessment and predictions. ConWep was used to produce pressure and impulse values from a stand-off distance of 10 metres up to 80 and 70 metres respectively for reflected and incident scenarios. The results were plotted against the historical data and can be seen in Figure 3.9 and Figure 3.10.

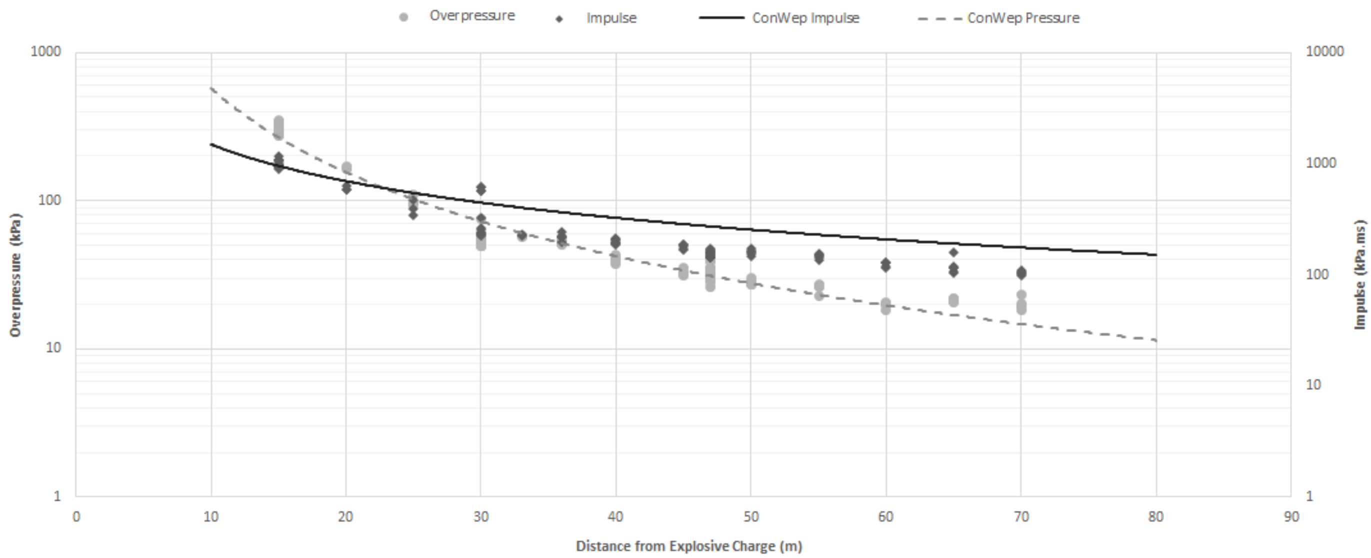

Figure 3.9: Comparison of historical reflected data with ConWep

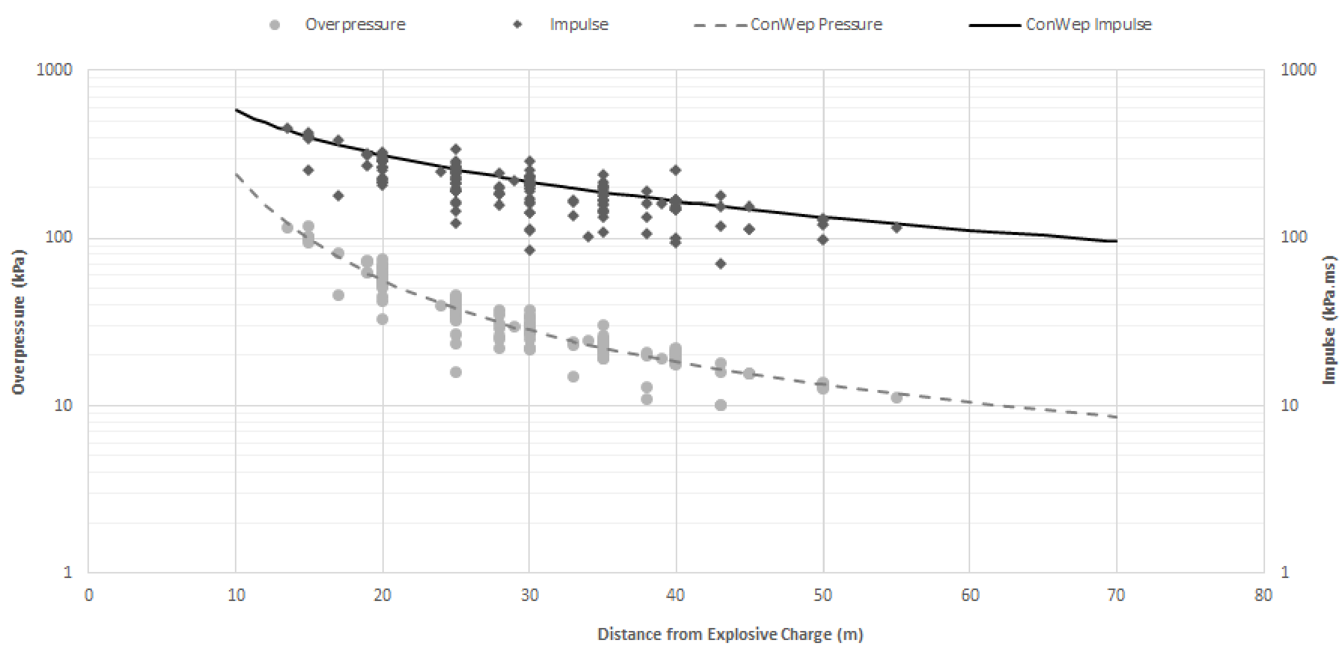

Figure 3.10: Comparison of historical incident data with ConWep

These graphs show that in general ConWep is a suitable tool for the prediction of pressure data for both reflected and incident data. A large variation of real data was shown at some of the common measurement, distances falling both above and below the ConWep values, but most frequently below the calculated prediction. For the reflected impulse data, the experimental values were consistently below the calculated ConWep value.

This is very likely due to the clearing effect that was not considered during the measurement of the pressure data, nor during the ConWep model, which involves an infinite reflected surface compared to the limited reflected surface in the experimental trials. This is discussed further in Section 4.2. Another reason for the lower impulse values may be due to the explosive type used. The explosive type used in this trial is not present in ConWep data, which instead uses values of TNT for predicting the values. It has been shown in studies [Redacted] that the impulse for this explosive is often up to 10% lower than predicted when the pressure value is matched with that of TNT in ConWep.

3.5 Comparisons with Air3D

As discussed in Section 2.8, Air3D is one of the simpler computational methods for predicting blast parameters. The trial set up was modelled in Air3D at stand-off distances matching those of the data set and equivalent values produced. Unlike the ConWep method used in the previous section which modelled a fully reflected face for the reflected measurements, the model created in Air3D included a 3 metre wide by 3.5 metre high gauge block that replicated that used in the trial, and as such it is expected that the reflected impulse data may show a better fit than that of ConWep. The results of the models have been plotted against the historical data and can be seen in Figure 3.11 and Figure 3.12.

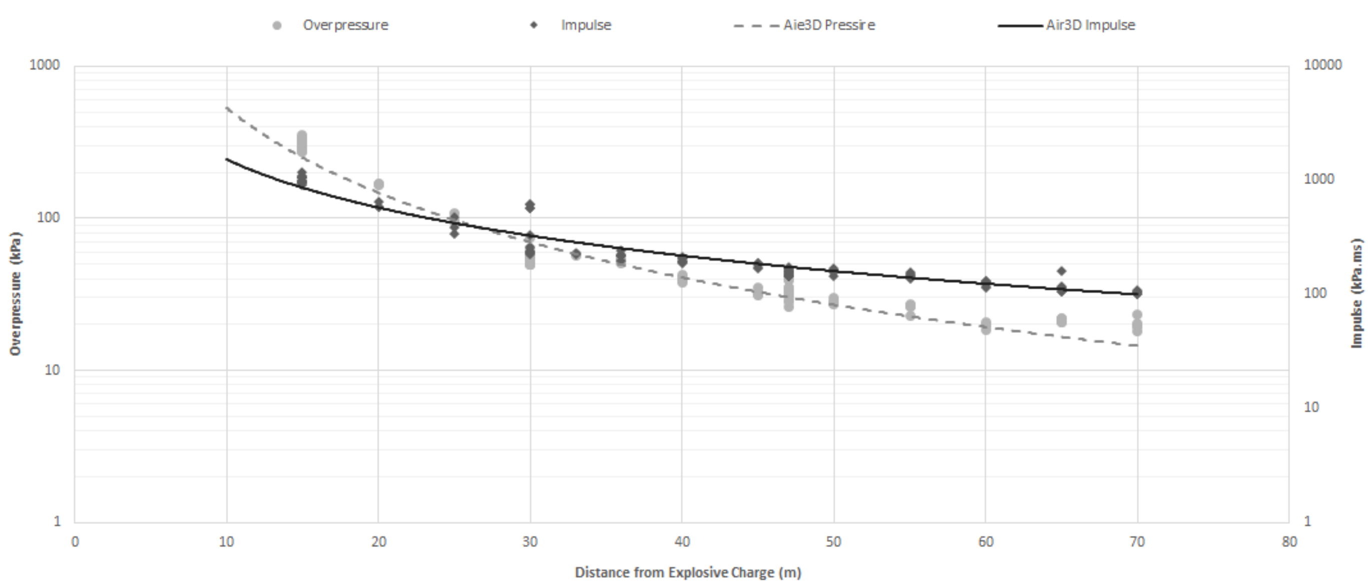

Figure 3.11: Comparison of historical reflected data with Air3D

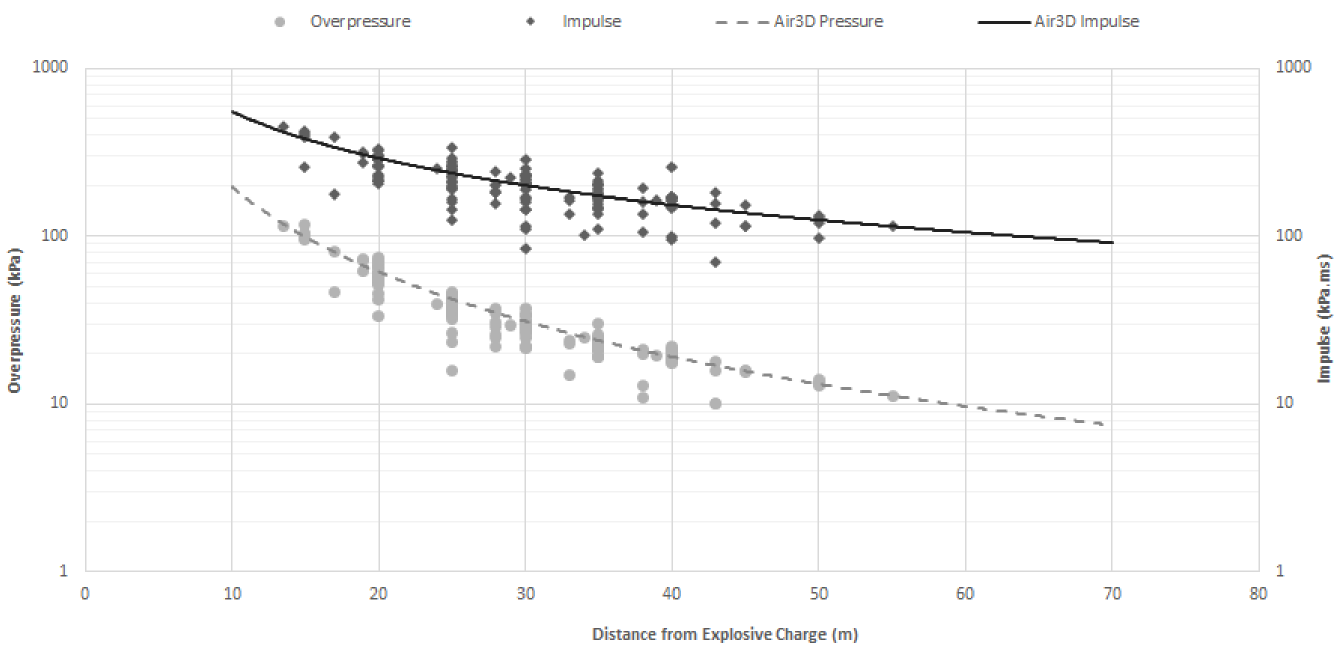

Figure 3.12: Comparison of historical incident data with Air3D

Much like ConWep, Air3D can be seen to be a suitable tool for the prediction of both reflected and incident data. As expected, the impulse values that were below the ConWep prediction for reflected pressures fit more closely with the Air3D prediction, almost certainly due to the model within Air3D that takes in to account the effect of clearing around the gauge block. From the review of both of these models, it can be suggested that both tools are adequate for simple predictions, with Air3D providing a more relevant prediction based upon building the arena set up within the model that more closely matches the experimental setup, although with the counter issue that the model can take a significant amount of time to produce results, especially if a small cell size is used.

3.6 Conclusion

This chapter has identified significant variation in the blast test data that has been measured. In particular, the poor accuracy of measurements taken close to the explosive charge have been discussed with the standard deviation reducing for both pressure and impulse as the distance from the charge increases. The data review has found a good comparison on blast pressure with that of ConWep for both reflected and incident data; however the values for impulse were found to be under estimated for reflected impulse although this may be an effect of the explosive used. The statistical variation seen in this chapter fits with the study from Bogosian et al. [21] in which data from 11 experimental trials is discussed and compared to the significant data set gathered by

Ohrt and Dailey from over 180 explosive trials consisting of both bare and cased explosive charges performed at the Air Force Research Laboratory. In their analysis, Bogosian provided findings of higher uncertainty for peak pressure over impulse, comparable uncertainty for reflected and incident measurements and decreased uncertainty with increased stand-off. Much like the data seen in this chapter, Bogosian also noted that even gauges placed very close together or at the same stand-offs did not produce true repeat measurements. No detail has been provided by Bogosian for reasons for the uncertainties seen in their study.

Farrimond et al. in a review of variability of blast wave parameters [61] described findings by Tyas [154], Rae and McAfree [119] and Rigby et al [126]. These findings described three ranges of scaled distances where the shock wave front behaved differently. The data reviewed in this chapter all falls within what they classified as the far field: a scaled distance of more than 2 $mkg^{-\frac{1}{3}}$. The researchers hypothesise that in this area, the instabilities at the shock front experience large growths giving rise to more chaotic behaviour which in itself can lead to variability in measurements. Farrimond explains that these instabilities occur when the detonation products expand and compress the surrounding medium until the medium's pressure exceeds that in the fireball, but where the air density is still significantly lower [150].

The following chapter considers many of the factors that can impact the blast loadings and makes recommendations for adjustments that can be made to provide more accurate and reliable data.

4 Complex Considerations

In the historical data review in Section 3, it is suggested that there are many blast parameter sensitivities that need to be considered with the aim of reducing the variability and improving the accuracy of the data produced in an experimental trial. In this chapter, topics are discussed that strongly impact upon these parameters with the aim of improving best practice for data gathering in experimental tests. This includes gathering pressure data to assess the type of gauge and position that is used to measure incident pressure data and the way in which the reflected pressure can be affected by target size. Through understanding of the sensitivities, it is hoped to mitigate the variation of the blast parameters in measurements taken in arena blast trials seen in Section 3.

4.1 Incident Gauge Type Analysis

Historically at Spadeadam, incident pressure loading has been measured using pancake gauges as seen in Figure 4.1. In the late 2000s, a commercial client requested the use of bullnose gauges (Figure 4.2) for trials. More recently pencil gauges (Figure 4.3) have become common place in test arenas. The pancake gauge and bullnose gauges are positioned perpendicular to the shock wave so that the streamlined housing lines up with the direction of travel of the shock wave with the aim to measure a distortion free pressure. The pencil gauges are aligned with the direction of the shock wave propagation. Description of how the gauges are set up and measurements taken can be found in Section 3.1, used in conjunction with information on the gauges direct from PCB [114, 113].

Figure 4.1: Pancake gauge

Figure 4.2: Bullnose gauge

Figure 4.3: Pencil gauge

A single 100 kg trial was carried out to compare the responses of these three gauges at up to four different stand-offs from the trial. The charge was set-up at 1.2 m above ground level on a polystyrene block resting on a steel plate to prevent damage to the concrete pad. The pad is a stable consistent base to ensure minimal loss due to absorption of the shock wave from the ground. Nine pancake gauges, three pencil gauges and three bullnose gauges were laid out radially at distances of 10, 15, 20 and 25 metres from the charge centre as seen in Figure 4.4.

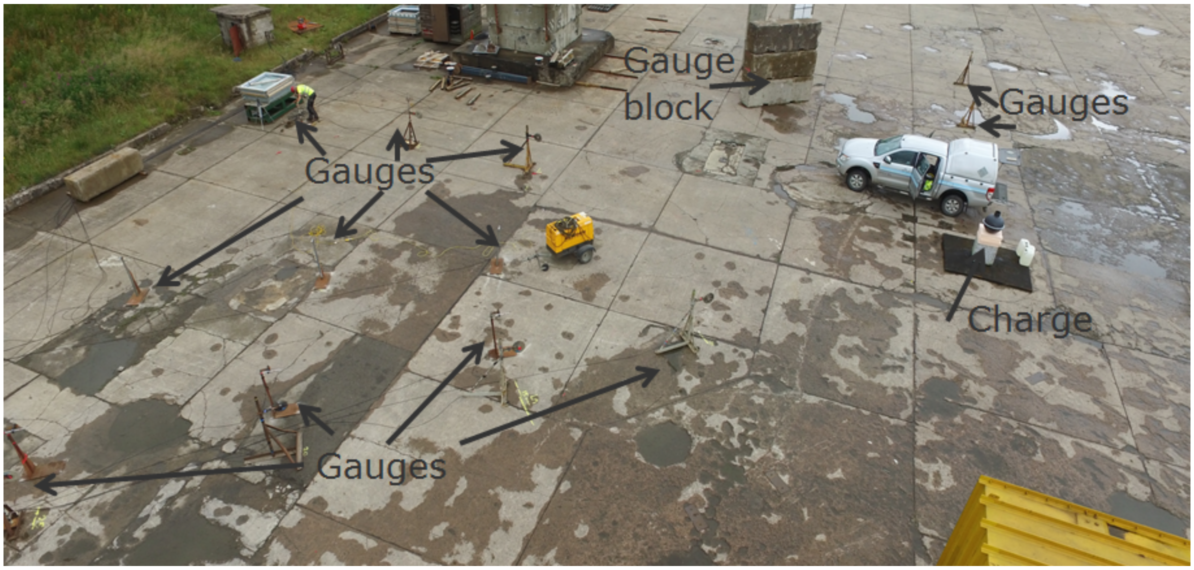

Figure 4.4: Arena layout for gauge type assessment

A single trial was carried out to ensure that the data collected had identical atmospheric, logging and cabling conditions in order to minimise variables that may affect the data recorded. The data was logged at a sampling frequency of 200 kHz. Each gauge was calibrated prior to the trial. Table 4.1 displays the gauges that were positioned in the trial, the type of gauge and the distance placed from the charge in metres.

Gauge Number	Gauge Type	Distance from Charge (m)
1	Pancake	10
2	Pancake	15
3	Pancake	20
4	Pancake	25
5	Pencil	15
6	Pencil	20
7	Pencil	25
8	Bullnose	15
9	Bullnose	20
10	Bullnose	25
11	Pancake	15
12	Pancake	20
13	Pancake	25
14	Pancake	10

Table 4.1: Gauge type and distances for trial

Figure 4.5 displays the results from the trial. Apart from an outlier (P3 at 20m) from one of the pancake gauges, the different gauge type did not produce significantly different peak pressures when the exponential curve fitting method was used to determine the peak pressure. However, when studying the individual curves

(Figure 4.6 - Figure 4.8), the bullnose gauges tend to produce much noisier curves and the pancake gauges appear to overshoot the initial peak. It is for both of these reasons that the exponential curve fit method is used to find the peak overpressure from the blast.

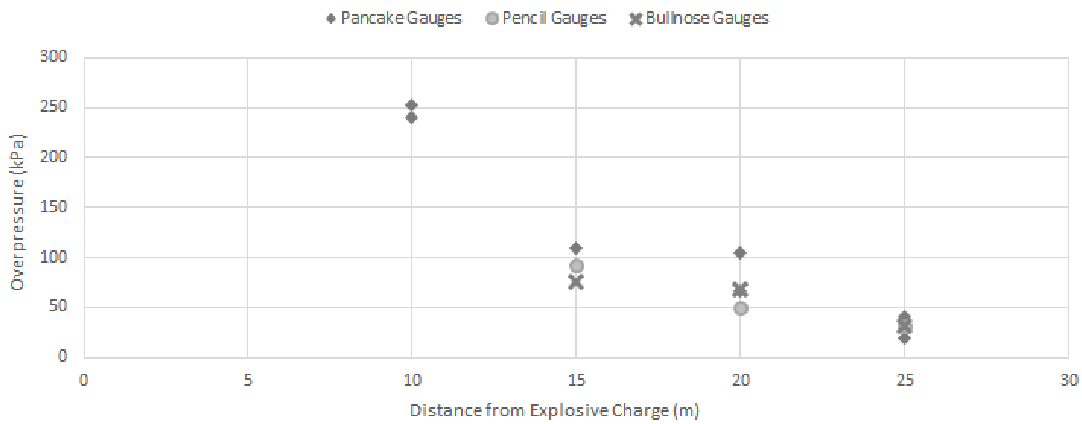

Figure 4.5: Gauge type overpressure vs distance

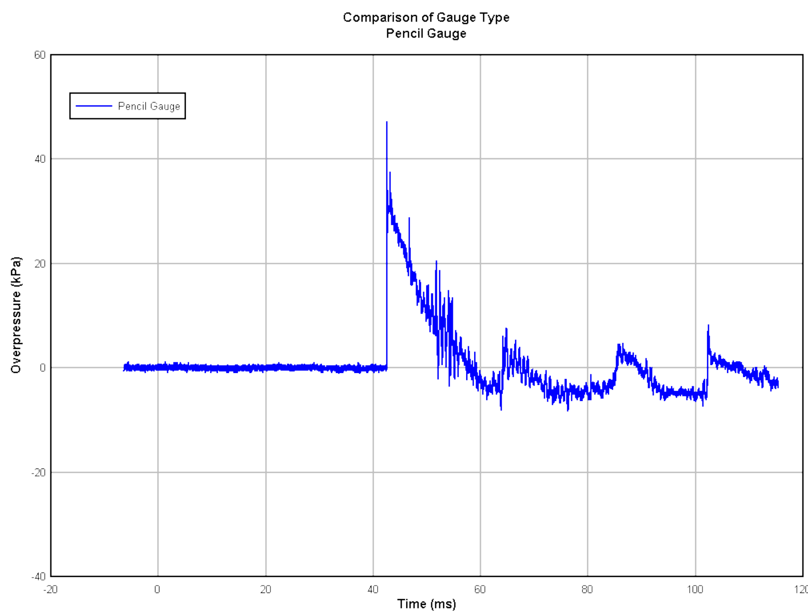

Figure 4.6: Pencil gauge pressure-time curve from P7 at 25m

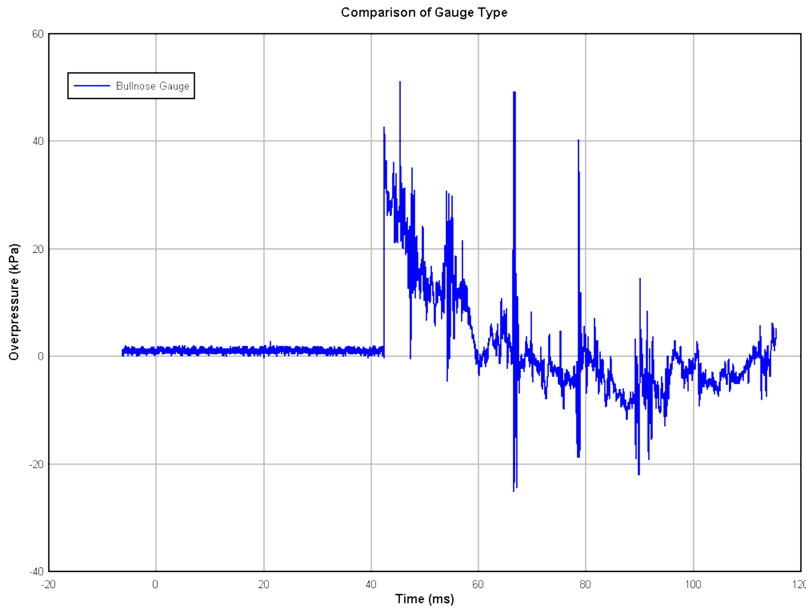

Figure 4.7: Bullnose gauge pressure-time curve from P10 at 25m

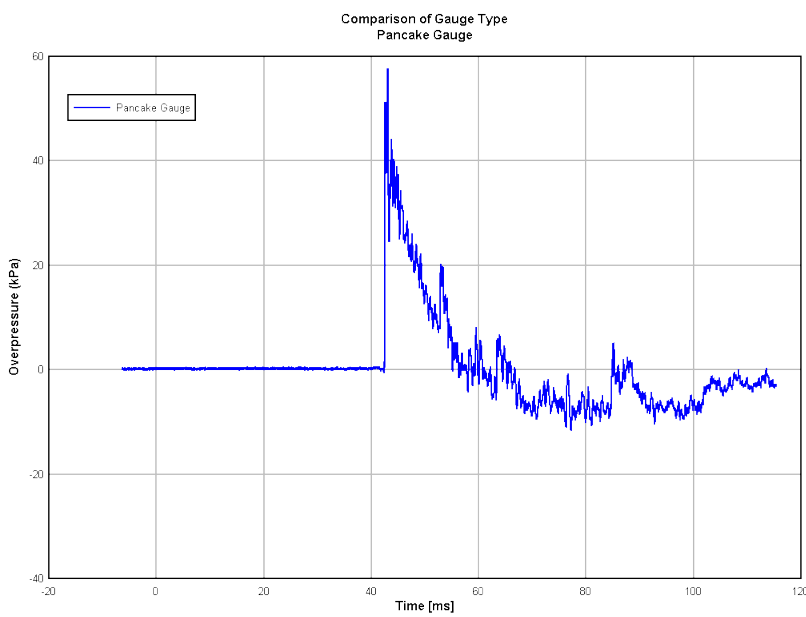

Figure 4.8: Pancake gauge pressure-time curve from P13 at 25m

Overall, it was concluded that the pencil gauges produced slightly better pressure curves and because of this will be predominantly used in the future trials at Spadeadam. Bullnose gauges will not be used in future trials. What is noticeable on all of these curves is the presence of an initial sharp peak at the time of arrival, before the trace settles down in to a curve.

The shock wave from an explosive charge can result in a temperature rise which has been shown by PCB, the makers of the piezoelectric pencil gauges, to cause false negative pressure drift even when the temperature rise is only approximately 10ºC [161] as seen in Figure 4.9 where the pressure does not return to ambient.

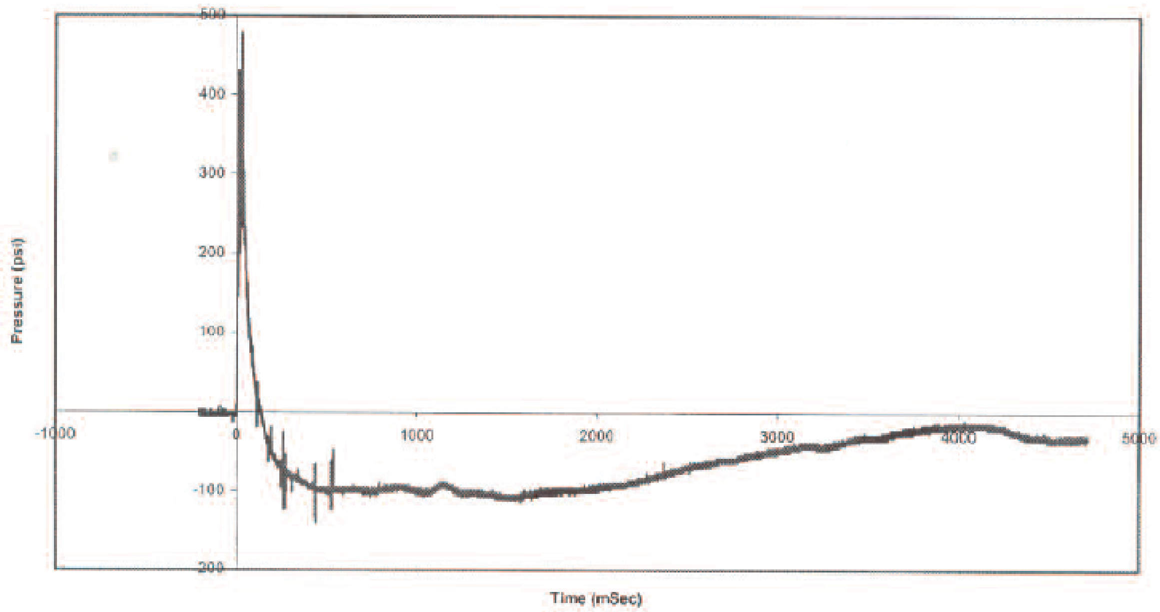

Figure 4.9: Negative pressure drift on a pressure-time curve [160]

Walter [160] noted that through the use of a tight wrap of black electrical tape around the sensor, the heat transfer into the sensor is delayed until the shock wave passage is complete, which helps to reduce this false negative drift. This was investigated further by DNV [80] after there was evidence of issues with gauges measuring high magnitude shock waves. This study of work compared the ability of PCB transducers and Kulite transducers mounted in close proximity to measure the shock wave produced from a 0.5 kg PE4 explosive charge. Since these gauges were frequently used for longer duration gas explosions as well as high explosive tests, further thermal protection was investigated using silicon grease and aluminium foil over the gauge face. It was concluded from the thirteen tests carried out that the Kulite gauges are not necessarily suitable for the short duration high explosive tests due to their response time. It was also found that the noise levels were excessive compared to the pressure magnitudes being measured and that, although this could be filtered out, this would further affect the response time. From the data, the author concludes that for short duration high explosive tests, the use of silicon grease and foil is unnecessary if the gauge was outside the fireball region, but tightly wrapped black tape has the potential to aid the effectiveness of the reading through reducing thermal load onto the gauge and preventing the negative pressure drift seen by Walter [160] in Figure 4.9.

This conclusion was also carried over onto the reflected pressure gauges.

4.2 Reflected Pressure Loading and Shock wave Clearing

For reflected pressure predictions, Kingery and Bulmash [44] assumes an infinite reflecting surface perpendicular to the shock wave. In an experimental blast test, it is clearly impossible for an infinite structure to exist and, as such, shock wave clearing will occur. Clearing occurs when a shock wave reaches the edges of a structure and rarefaction waves are moved along its free edges and propagate back towards the centre of the front face, with the effect of reducing the overpressure loading and thereby reducing the total positive phase impulse on the structure. The closer the edge of the structure to the point of measurement, the larger the impact is of clearing [123].

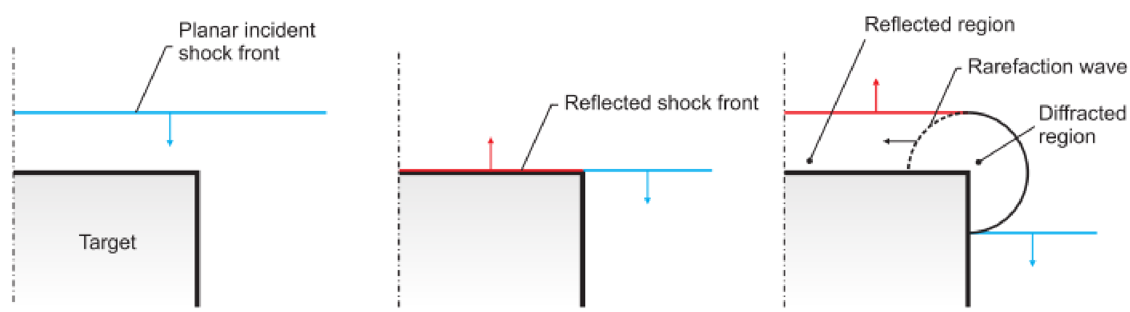

Figure 4.10: Diffraction of a shock wave around a finite structure [123]

The impact of this reduced impulse can be seen in Figure 4.11 where the cleared pressure drops away after matching the initial peak reflected pressure while duration remains the same.

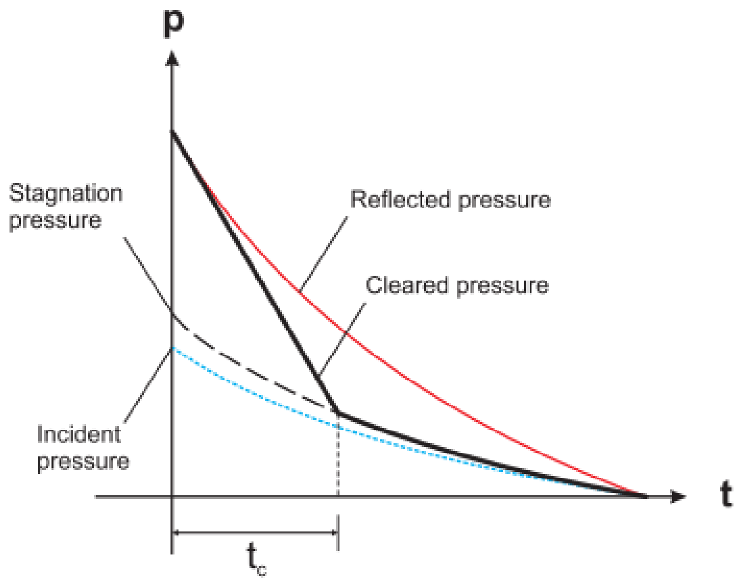

Figure 4.11: Example pressure-time curve for a cleared structure [123]

Figure 4.12 shows the peak pressure to be the same as the ConWep prediction, but the impulse is drastically below the prediction. This result was produced from a pressure gauge mounted at the centre of a 3 metre wide by 3.5 metre high concrete block structure (Figure 4.13) exposed at a set distance from a 100 kg TNT equivalent blast; with the ConWep prediction calculated from the same charge size and stand-off, but upon an infinitely reflecting structure. It can be seen that, although the time of arrival and peak pressure are consistent with the ConWep prediction, and that the pressure-time trace follows the prediction for approximately the first 3 ms, after this time the clearing wave arrives causing the pressure to drop off, resulting in the impulse almost half that of the prediction due to the effect shown in Figure 4.10. This estimate of the magnitude of the impact relies on the assumption that ConWep is accurately predicting the blast pressure and impulse correctly.

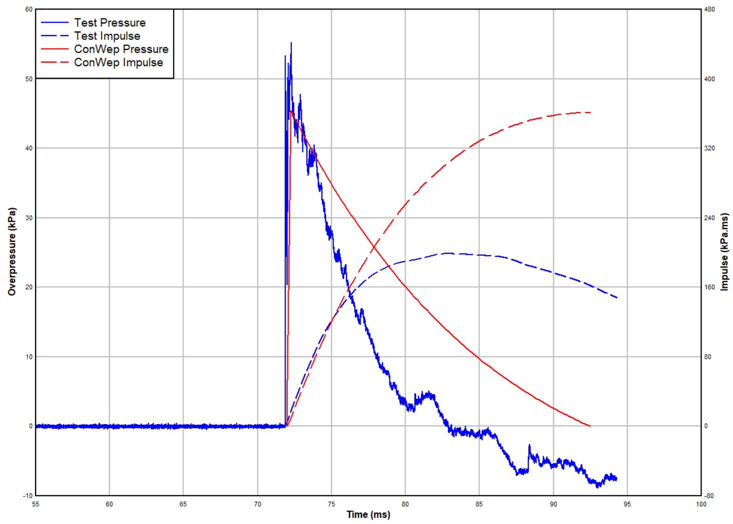

Figure 4.12: Effect of shock wave clearing on a finite structure compared to ConWep predictions

In full scale arena trials, the clearing effect is usually mitigated by enlarging the reflected target (Figure 4.14) so that the shock wave behaves more as though it is interacting with an infinite target.

Figure 4.13: Gauge block with no clearing mitigation

Figure 4.14: Enlarged gauge block to mitigate the clearing effect

The time to clearing (t_c) is given in UFC-3-340-2 [158] as:

$$t_c = \frac{4S}{(1+R)C_r} \tag{4.1}$$

where S = clearing distance, equal to H or W/2, which ever is the smallest, H = height of the structure, W = width of the structure, R = ratio of S/G where G is equal to H or W/2 which ever is larger and Cr = sound velocity in the reflected region. This equation produces an average clearing time by modelling the clearing across the whole target face. This is just one possible equation for clearing, an extensive study of clearing can be found by Rigby [123] and includes experimental studies conducted by the University of Sheffield on clearing effects [155, 156]. Further discussions can be found by Smith et al. [143, 132] and Johnson [89]. Based on 4.1, where possible the gauge block was installed and built to be of a size that matched the target size or, if the target was too large, constructed as large as was practical to build.

4.3 Positioning of Targets in an Arena

When deciding to conduct a blast test, cost is a huge factor, leading to the temptation to place as many targets as possible around a single explosive blast in order to produce as much data as possible. This itself can have a detrimental effect upon the testing that is conducted as interactions between targets can affect blast loading so that the results may not be realistic or relevant. A study conducted over a number of trials at Spadeadam by Payne et al. [112] on behalf of what was at the time the Home Office for Centre of Applied Science and Technology (now part of DSTL) involved both experimental measurements and comparable computer models to identify the effects on blast pressure and impulse of targets that may be placed too close together, whether at the same distance from the charge or a staggered distances from the charge. The output of this study was a series of tables showing recommended angular separation distances for between targets in an arena blast at 0% (Figure 4.15), 2% or 5% interference between targets, along with the conclusion that, as a general estimation, a 45° separation angle corresponds well to the limit of interference between targets. For any further testing conducted at Spadeadam, this rule was taken in to account to ensure that pressure gauges (both free field and reflected installed in a gauge block) and targets were placed at an appropriate distance from each other to ensure no interference on pressure and impulse.

0% Threshold (Recommended Separation Distances)

Fixed Target Location \ Variable Target Location	15 m	20 m	25 m	30 m	35 m	40 m	45 m	50 m
15 m	3.88	3.30	5.55	6.88	7.96	8.70	9.21	9.64
20 m		4.58	4.03	6.49	8.08	9.50	10.1	10.7
25 m			5.03	4.51	7.18	8.97	10.5	10.9
30 m				5.26	4.72	7.87	9.87	11.2
35 m					5.58	5.42	8.32	10.3
40 m						5.99	5.48	12.1
45 m							6.87	5.83
50 m								6.92

Figure 4.15: 0% Threshold - Recommended separation distances from Payne [112]

4.4 Weather Impacts

UFC 3-340-02 states that 'the pressure varies as a function of sound velocity with altitude above the ground surface' [158]. Although it does emphasise that this is more of an issue with significantly larger scaled distances upwards of $60mkg^{-\frac{1}{3}}$, Swisdak [148] noted that air blast pressures should be corrected based upon altitude above sea level, but these calculations generally consider altitudes of up to 100,000 feet (30,480 metres).

Spadeadam is located at approximately 258 metres above sea level and therefore it has been decided not to adjust the data measured based on the UFC or Swisdak suggestions as they would generally be considered more appropriate for free air explosions at high altitude. If comparison is needed between data from multiple tests performed in significantly different environments such as sea level or altitude, tropical or arctic style conditions, this may become more relevant and further investigations should be conducted.

When conducting blast testing at Spadeadam, the author recorded the weather conditions at the time of firing. Particularly for commercial testing, and when testing to a standard, it is part of the requirement to record altitude and the weather conditions at the time of firing. It is also important to consider the weather conditions effect upon the target under test, especially in the case of glass, where for example even the same pane of glass may respond differently depending on the air temperature due to the PVB interlayers, to ensure that it is being tested in the appropriate operating conditions and not conducted in unrealistic conditions. When calculating Energy Flux (Section 2.7.1), this involves calculating the characteristic impedance or particle velocity (Section 2.7.1), both of which take in to account the air temperature, humidity and pressure at the time of firing and as such accounts for the variations in firing conditions. Generally these are calculated using equations as shown in the previous section, although there have been recent research in experimental methods of determining particle velocity. Jenkins et al. [83] used Particle Image Velocimetry to obtain high resolution images of particles in explosive trials, although noted it was of more use for identifying particle phenomena rather than determining fluid velocities in the surrounding gas.

4.5 Conclusion

This section has investigated the sensitivities that impact the outputs of explosive blast testing. A gauge type analysis was conducted using three different types of incident pressure gauges - pancake, bullnose and pencil. The recommendation from this analysis is to use blast pencils where possible as they were easier to position and provided less noisy curves that fitted well with the predicted Friedlander Curve. A study was also conducted to investigate how best to protect gauges from the temperature rise caused by the blast and recommendations made to provide heat insulation on both reflected and incident pressure gauges in arena trials.

The impact of the clearing effect on reflected pressure gauge readings was investigated further through the use of an enlarged gauge block, after the smaller, previously used, gauge block was showing obvious impact from the clearing wave. Recommendations for reflected pressure measurements going forward are to use the largest gauge block possible unless the gauge block is mirroring a specific target for matching pressure gauges.

Where this is the case, it should be anticipated that the impulse measurement will be affected by clearing effects.

The arrangement of an arena was discussed to note that the positioning of targets in an arena can have an effect on the pressures exerted upon them. It was noted from trials conducted at Spadeadam that, as a general rule, a 45° separation angle corresponds well to the limit of interference between targets. This recommendation will be implemented for all arena blast testing at Spadeadam.

Through understanding of these blast sensitivities, these investigations will help to mitigate the variation of the blast parameters in measurements taken in arena blast trials. The next sections investigate the impact of implementing these considerations for limiting the sensitivities of blast parameters.

5 Recent Data Review

Section 4 discussed some of the issues that impact the sensitivities of blast loading measurement. To assess if the sensitivities can be reduced by improved practices, this chapter reviews more recent data obtained where the practices suggested in Section 4 have been implemented.

5.1 Adjusted Setup

To account for the clearing wave for the reflected pressure targets, larger structures were provided. This involved additional concrete culverts placed alongside the gauge blocks with the effect of enlarging the reflected targets, resulting in the pressure-time curves being unaffected by the clearing wave. Further care was taken in the placement of targets to ensure that there was no interaction between targets that may affect the pressure wave. For incident pressure measurements, PCB Pencil gauges were used where possible and backed up with pancake gauges if there were insufficient numbers of pencil gauges available. On top of this, the stand-off distances have been further reviewed. Traditionally the distances at which targets were set at were based upon test standards and set distances e.g. a C25 protected spaces test equated to 100 kg at 25 metres, which can fail to meet the specific pressure and impulse required by the standards. To ensure more accuracy, the targets were modelled in Air3D to provide more accurate target stand-off distances for explosive tests resulting in a greater spread of distances.

5.2 2019 - 2021 Data Review

From 2019 to 2021, a further 29 100 kg TNT equivalent tests were conducted at DNV Spadeadam. These all used the same explosive set-up in terms of explosive type, explosive mass and explosive geometry. Pressure, impulse, time of arrival and positive duration values were recorded from a variety of different gauge types at varying distances equating to 102 reflected pressure readings from reflected gauge blocks and 151 incident pressure readings. The explosive charges were all spherical and placed at a height of 1.2 metres from ground level on polystyrene foam blocks resting on a 75mm steel blast mat to prevent energy loss due to cratering. The distances were usually determined using Air3D to meet specific pressures and or impulses and as such are not always round numbers. Additionally, other tests have been conducted using ANFO and PE4, but these are not displayed in this data review and will be considered in Sections 6 and 7.

Figure 5.1 to Figure 5.8 display the reflected and incident pressures, impulses, time of arrivals and positive durations collected during these twenty-nine trials.

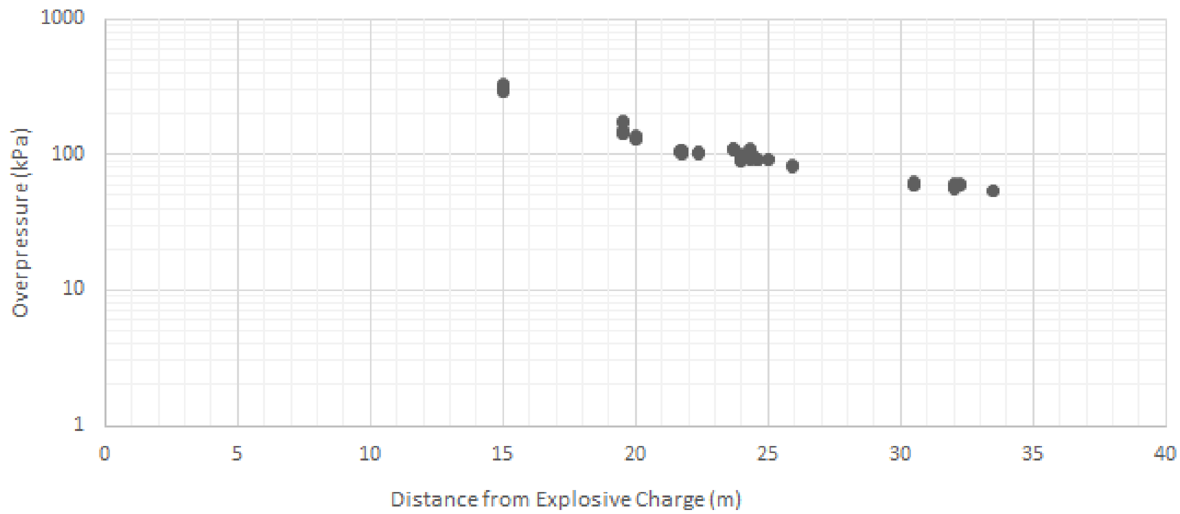

Figure 5.1: 2019 - 2021 reflected pressure values

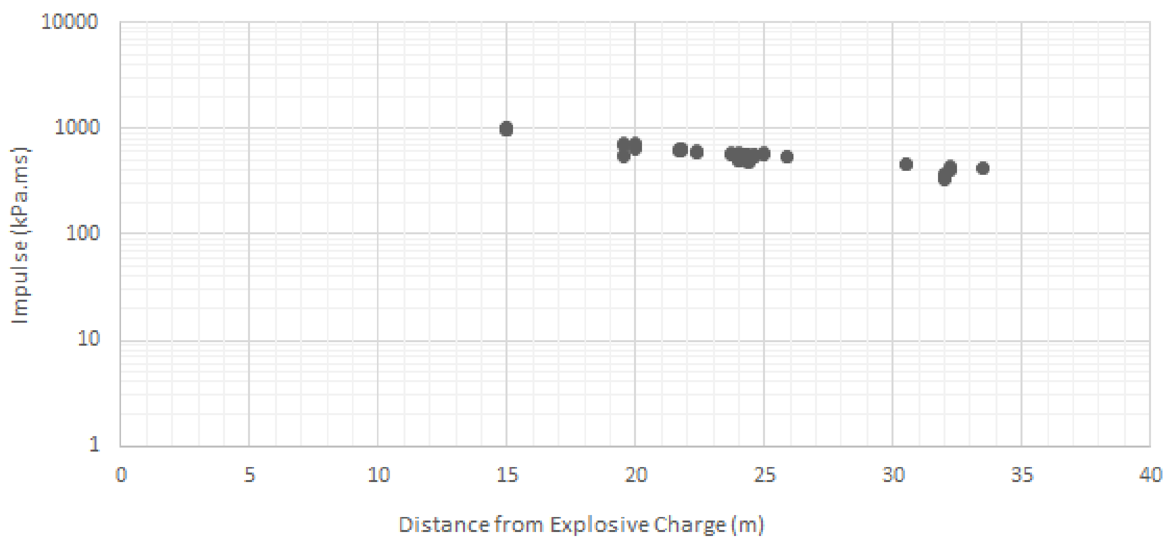

Figure 5.2: 2019 - 2021 reflected impulse values

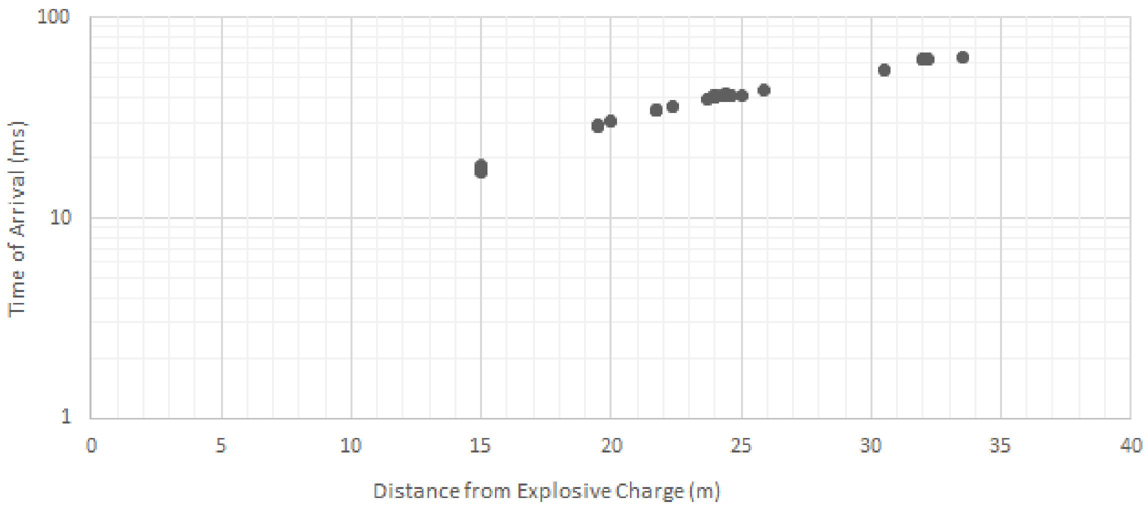

Figure 5.3: 2019 - 2021 reflected time of arrival values

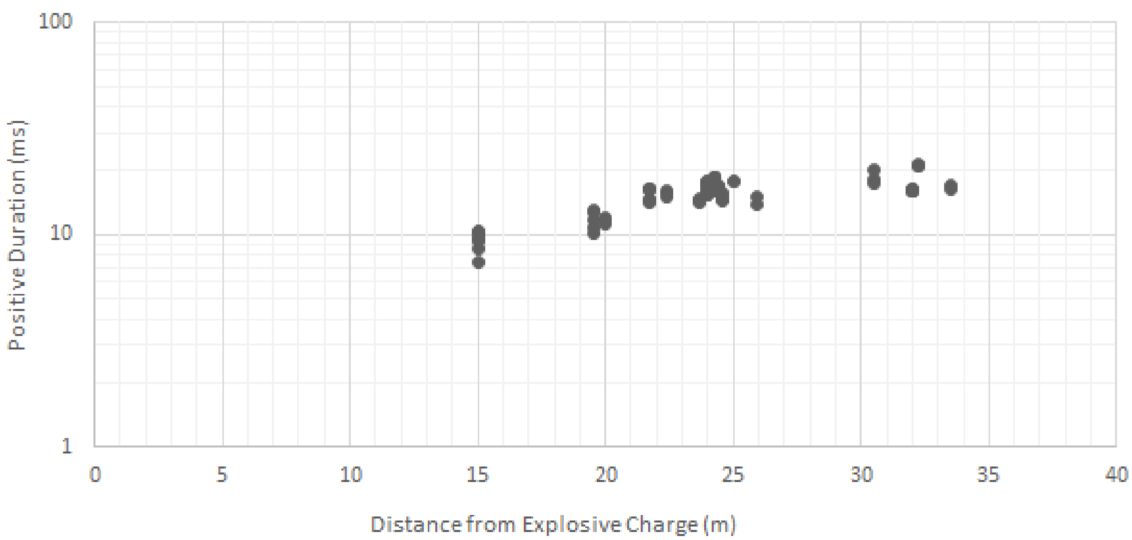

Figure 5.4: 2019 - 2021 reflected positive duration values

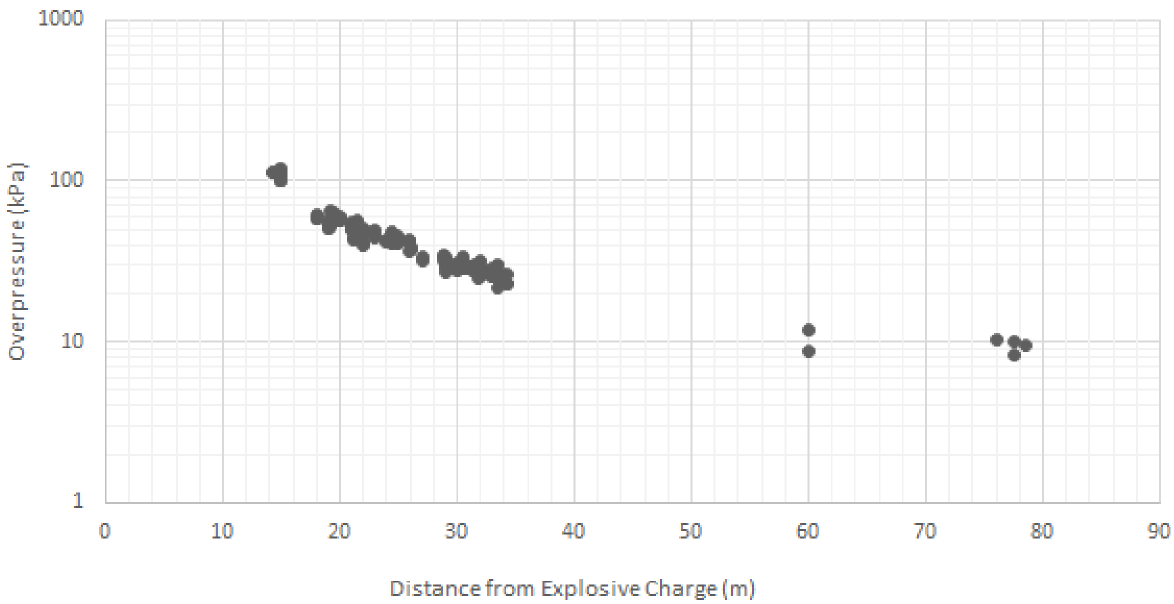

Figure 5.5: 2019 - 2021 incident pressure values

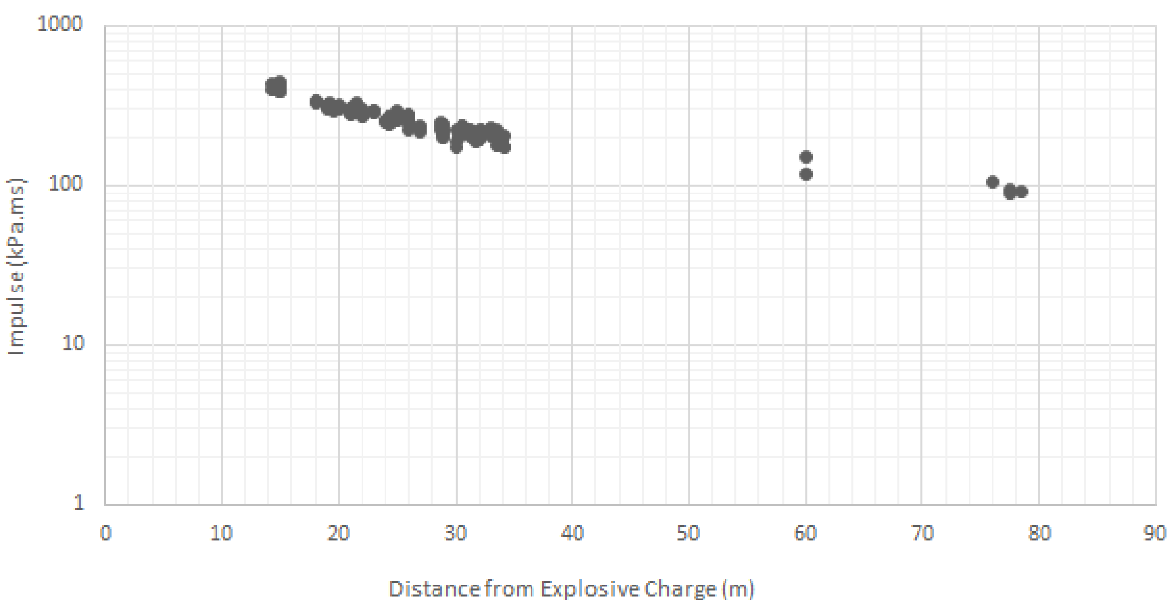

Figure 5.6: 2019 - 2021 incident impulse values

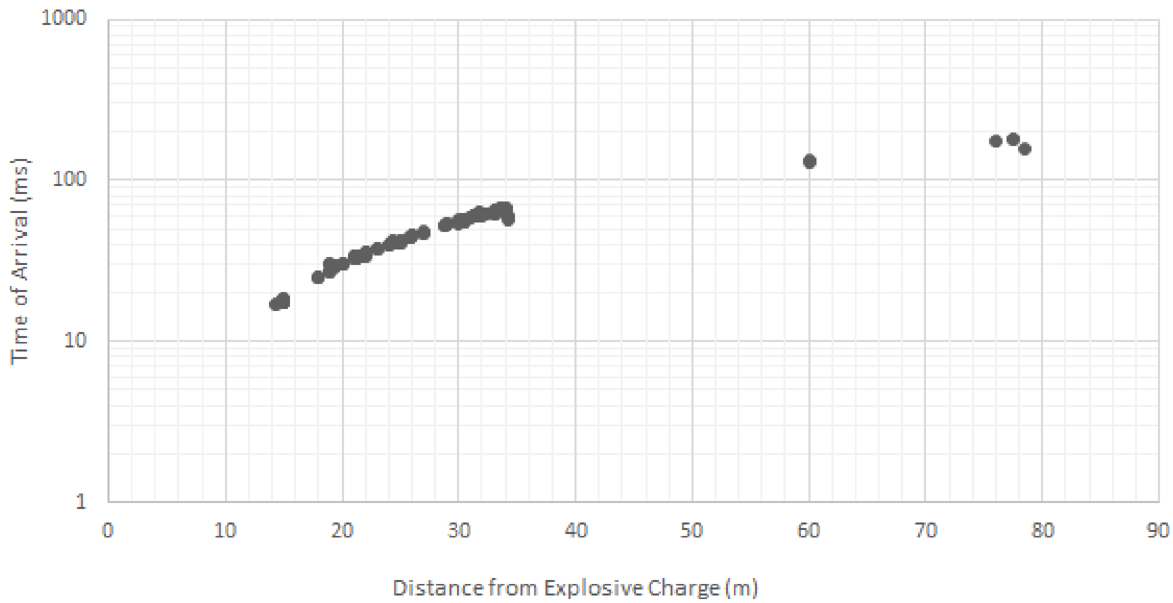

Figure 5.7: 2019 - 2021 incident time of arrival values

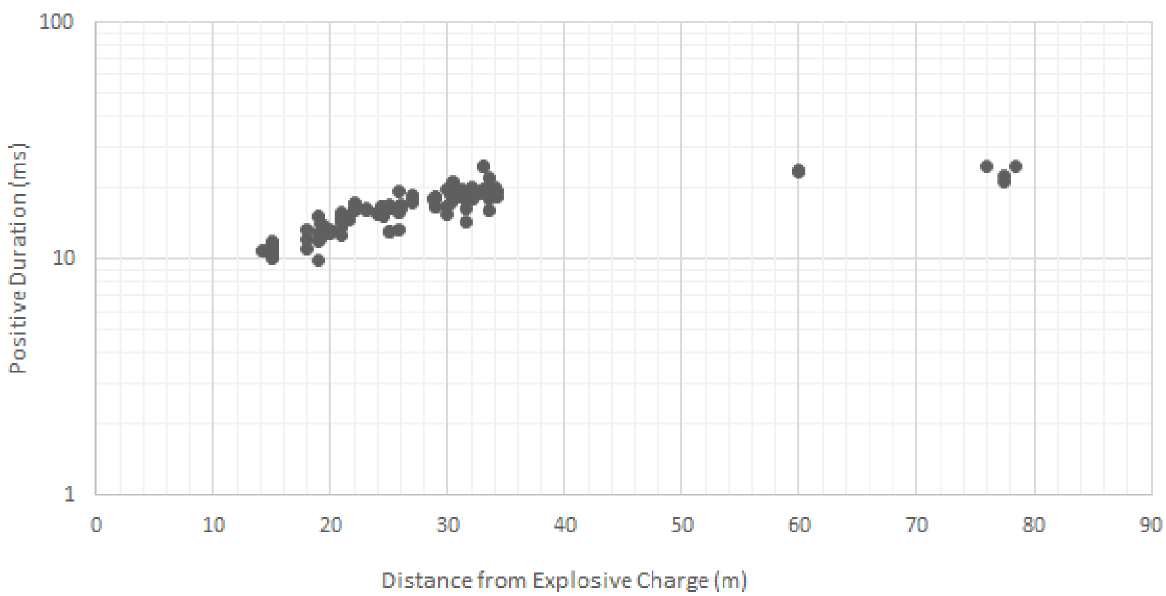

Figure 5.8: 2019 - 2021 incident positive duration values

5.3 Statistical Variations

The tables below give the mean and standard deviation at stepped distances from the experimental data. The distances chosen for these tables are based on the most commonly occurring stand-off distances from the trials.

Distance from Explosive Charge (m)		15	20	24	30.5	33.5
Pressure (kPa)	Mean	309.36	133.21	94.93	60.55	54.37
	Standard Deviation	14.97	3.58	2.81	1.19	0.21
Impulse (kPa.ms)	Mean	992.38	675.88	556.92	455.15	421.72
	Standard Deviation	19.85	24.77	12.16	4.58	5.25
Time of Arrival (ms)	Mean	17.51	30.67	40.46	54.90	63.87
	Standard Deviation	0.48	0.03	0.16	0.01	0.11
Positive Duration (ms)	Mean	9.38	11.71	16.09	18.59	16.78
	Standard Deviation	0.97	0.30	0.78	1.12	0.49

Table 5.1: Mean and standard deviation from 2019 - 2021 reflected pressure, impulse, time of arrival and positive duration

Distance from Explosive Charge (m)		15	21	25	29	33.5	60	77.5
Pressure (kPa)	Mean	108.33	50.13	42.87	30.40	26.13	10.35	9.14
	Standard Deviation	6.59	3.58	1.72	2.13	2.72	1.65	0.84
Impulse (kPa.ms)	Mean	410.36	296.06	272.63	219.32	200.99	133.70	91.08
	Standard Deviation	18.36	8.76	13.81	13.53	14.21	17.20	3.03
Time of Arrival (ms)	Mean	17.61	33.03	40.99	53.66	67.12	131.60	178.54
	Standard Deviation	0.35	0.36	0.43	0.07	0.68	2.50	0.66
Positive Duration (ms)	Mean	11.02	14.62	14.51	17.42	19.05	23.40	21.76
	Standard Deviation	0.62	0.83	1.80	0.79	1.85	0.23	0.64

Table 5.2: Mean and standard deviation from 2019 - 2021 incident pressure, impulse, time of arrival and positive duration

Much like the pre-2018 data, Table 5.1 and Table 5.2 show the spread of data for pressure and impulse is larger closer to the explosive charge than further into the far field; this is as expected as the standard deviation will naturally be larger, with larger values. For this reason the Coefficient of Variation is displayed in Table 5.3 and Table 5.4 to allow direct comparisons to be made. A comparison with the historic data can be found in Section section 5.6. For both reflected and incident data, the time of arrival and positive durations standard deviations are consistently low at all distances. The time of arrival is certainly shown to be more repeatable compared to the other parameters as was also the case in the University of Sheffield data review [61]. Although there is still a spread of data, this appears to correlate well with the analysis by Karlos et al. [91] that shows a smaller spread and standard deviation for overpressure and time of arrival, and a much wider spread for positive duration. Karlos et al. put this down to the difficulty in calculating the positive duration from the experimental data - stating it is hard to accurately define from a recorded pressure signal the point at which the blast pressure becomes equal to the ambient value. From the data set in this chapter, this difficulty was mitigated through the curve fitting of the modified Friedlander exponential decay curve which gives a definitive value at which the curve returns to ambient.

The impulse data for both the reflected and the incident measurements still show a wide spread but, utilising calculations of the Coefficient of Variation, the extent of variability in relation to the mean of the population can be shown [58]. Table 5.3 and Table 5.4 display the values of CoV for the values calculated in Table 5.1 and Table 5.2.

Distance from Explosive Charge (m)	15.0	20.0	24.0	30.5	33.5
Pressure	0.048	0.027	0.030	0.020	0.004
Impulse	0.020	0.037	0.022	0.010	0.012
Time of Arrival	0.027	0.001	0.004	0.000	0.002
Positive Duration	0.103	0.026	0.048	0.060	0.029

Table 5.3: Coefficient of Variation for reflected data

Distance from Explosive Charge (m)	15.0	21.0	25.0	29.0	33.5	60.0	77.5
Pressure	0.061	0.071	0.040	0.070	0.104	0.159	0.092
Impulse	0.045	0.030	0.051	0.062	0.071	0.129	0.033
Time of Arrival	0.020	0.011	0.010	0.001	0.010	0.019	0.004
Positive Duration	0.056	0.057	0.124	0.045	0.097	0.010	0.029

Table 5.4: Coefficient of Variation for incident data

These calculated Coefficient of Variations show that, although there was a larger spread of impulse data, the variation is not dissimilar to that of pressure or positive duration. Time of arrival was shown to be the least variable. There were no obvious trends between the values closer to the charge and those as the stand-off increased, although there is less variation for reflected data than incident data.

5.4 Comparison with ConWep

As in Section 5.4, ConWep was used to model pressure, impulse, time of arrival and positive duration values for a stand-off distance from 10 m up to 80 m for reflected and incident pressures of 100 kg TNT spherical explosive charges. The reflected model in ConWep assumed an infinitely reflected surface. The results were plotted against the experimental data and can be seen in Figure 5.9 and Figure 5.10.

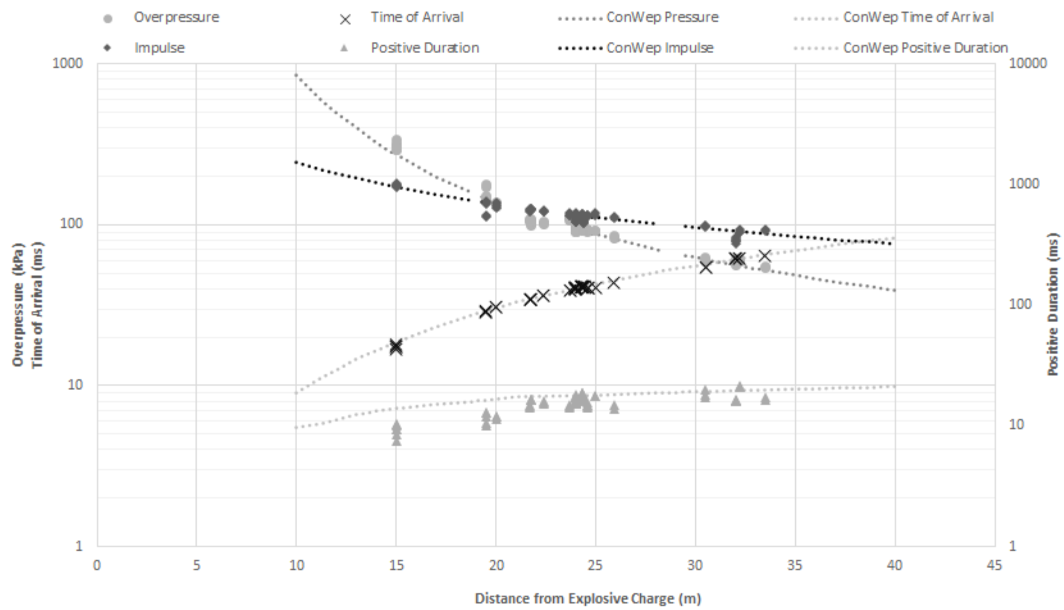

Figure 5.9: Comparison of 2019 - 2021 reflected data with ConWep

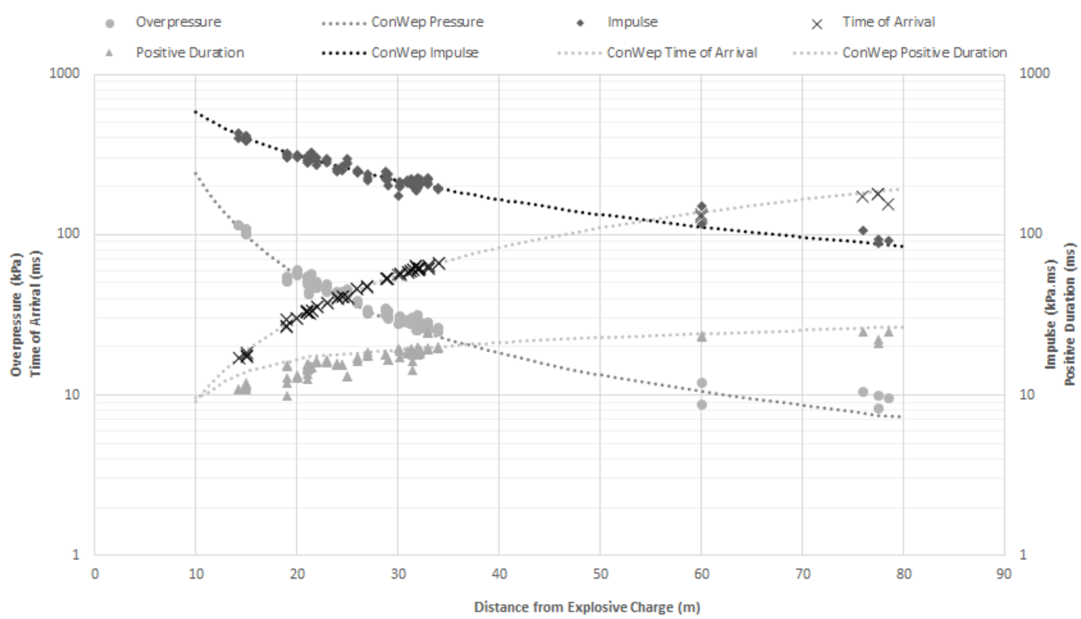

Figure 5.10: Comparison of 2019 - 2021 incident data with ConWep

From these graphs it can be seen that the majority of data is a good fit with the ConWep data. The exception here is the positive duration which, for both reflected and incident data is consistently low at all distances. The impulse is slightly lower closer to the explosive charge. Johnson and Claber [88] state in their paper that for close-in explosions on targets, ConWep produces non-conservative predictions for free air as well as for near air blasts. It is likely that for the positive duration and the impulse that this is again due to the explosive type. If the positive duration and the impulse are the main target factors, the author would recommend to increase the charge size in order to closely match this explosive type to TNT, although this would of course cause higher pressures and earlier times of arrival. This reaffirms the issue mentioned in Section 2.4 where a single value of TNT equivalence may not be suitable for producing equivalent pressures and impulses. The incident measurements in the far far-field (60 metres or a scaled distance of 12 $mkg^{-\frac{1}{3}}$), have a wider variation than closer in. The author suspects this maybe due to experimental setup where the accuracy of measurements is harder to control the larger the distances being measured. If the incident gauges are not at the exact measurement position or are misaligned by more than a degree, this would impact the pressure, impulse, time of arrival and positive duration measured. This is further confirmed in a study by Rigby et al. [124].

5.5 Calculating Uncertainty Factors

In 2014, Bogosian et al. [21] published a paper analysing statistical variation of air blast parameters in a series of experimental trials conducted in the USA. Bogosian developed a methodology for calculating an uncertainty factor based on the assumption of a normal distribution of the data in logarithmic space. Bogosian developed the following steps for calculating an uncertainty factor:

1. Calculate the natural logarithm of each data point
2. Calculate the mean m and the standard deviation σ of the logarithm data set
3. Calculate the mean as the exponential of the average value
4. Calculate the upper and lower bounds on the data as the exponential of $(m \pm 2\sigma)$
5. Calculate the uncertainty factor as a ratio of the upper bound to the average

This methodology was used and applied to the data set in this chapter for incident and reflected pressure, impulse, time of arrival and positive duration. Where there were only one or two measurements at a specific stand-off, these values have not been included in this uncertainty factor calculation.

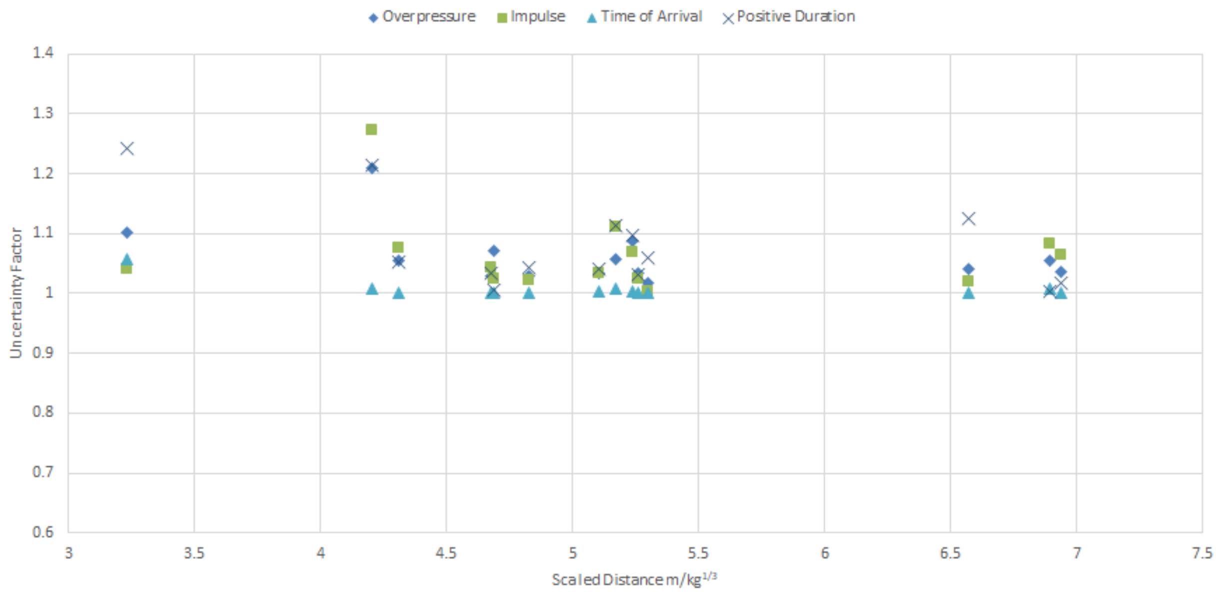

Figure 5.11: Uncertainty factors of reflected data

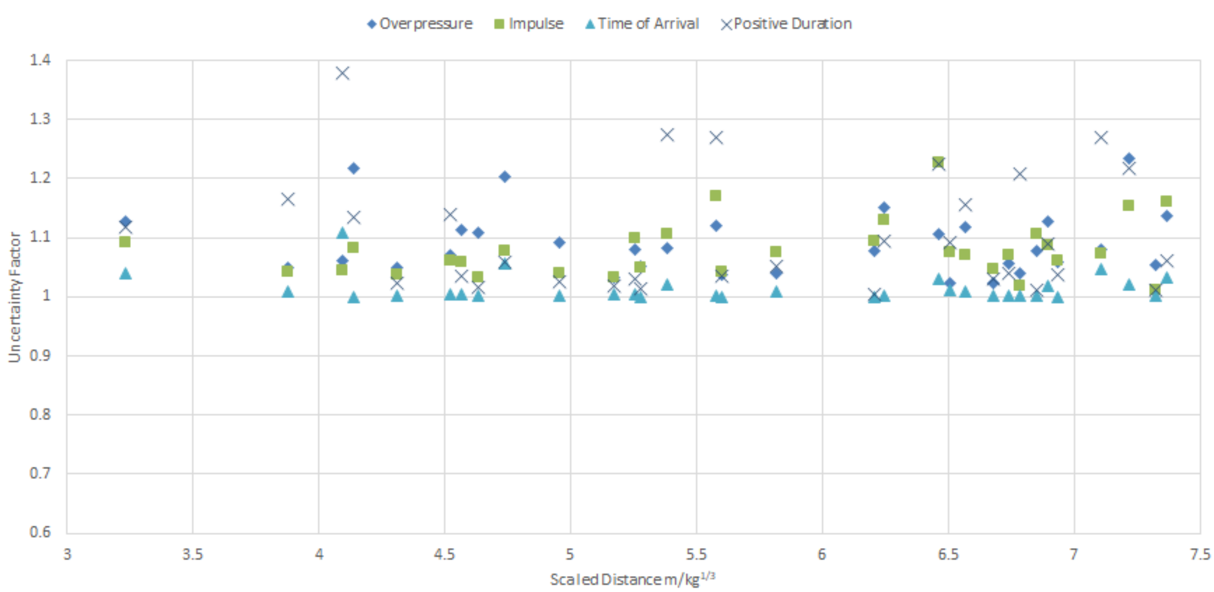

Figure 5.12: uncertainty factors of incident data

Much like the Coefficient of Variation values and the standard deviation, it can be seen that the time of arrival shows very low uncertainty (1.01 for incident measurements and 1.007 for reflected measurements), particularly when compared to other parameters, especially the positive duration (1.1 for incident and 1.07 for reflected). For both incident and reflected data, there is slight evidence that the uncertainty increases in all parameters closer to the explosive charge, but more data would be required at the smaller scaled distances to be able to confirm this further. Bogosian stated from their historical data [21] that they had significantly higher uncertainty factors for peak overpressure versus impulse data, but this is not evident in this current data set, although it does agree that even closely spaced gauges do not produce truly repeat measurements.

5.6 Comparison with Historical Spadeadam Data

Conclusions from Section 4 were taken, particularly with regards to the gauge type for incident measurements and the increased reflected surface size for the reflected measurements.

The same methodology used in Section 5.5 has been applied to the historical data to produce uncertainty factors allowing direct comparison between data sets. Due to improved modelling that allowed for more accurately planned distances for specific overpressures or impulses in the recent data set, there are a much larger number of stand-off distances and therefore only values with corresponding stand-offs from the historical data have been compared. Table 5.5 and Table 5.6 show the comparison in uncertainty factors for pressure and impulse for reflected and incident data respectively. The number of data points for each stand-off has also been included. Graphs showing the calculated historical and recent uncertainty factors have also been plotted in figure 5.13 and figure 5.14 on the same scale to show the improvement of uncertainty.

Scaled Distance	Pressure		Impulse		No. of Data Points	
from Charge ($m/kg^{\frac{1}{3}}$)	Pre 2019	Post 2019	Pre 2019	Post 2019	Pre 2019	Post 2019
3.23	1.17	1.10	1.17	1.04	54	7
4.31	1.02	1.05	1.09	1.08	3	3
4.74	1.04	1.03	1.17	1.02	9	3
5.39	1.26	1.02	1.30	1.00	59	5
6.46	1.24	1.04	2.27	1.02	13	3
6.89	1.31	1.06	1.26	1.08	6	6
Average	1.17	1.05	1.38	1.04	-	-

Table 5.5: Uncertainty factors for reflected data

Scaled Distance from Charge ($m/kg^{\frac{1}{3}}$)	Pressure		Impulse		No. of Data Points	
	Pre 2019	Post 2019	Pre 2019	Post 2019	Pre 2019	Post 2019
3.23	3.93	1.13	1.54	1.09	16	12
4.31	3.01	1.05	1.42	1.04	24	3
4.52	1.51	1.07	1.03	1.06	3	9
4.74	2.04	1.20	1.03	1.08	3	5
4.96	1.21	1.09	1.02	1.04	3	3
5.39	2.51	1.08	1.38	1.11	76	5
5.82	1.23	1.04	1.25	1.08	3	3
6.46	1.95	1.11	1.74	1.23	41	3
7.11	1.86	1.08	1.36	1.07	27	6
Average	2.14	1.09	1.31	1.09	-	-

Table 5.6: Uncertainty factors for incident data

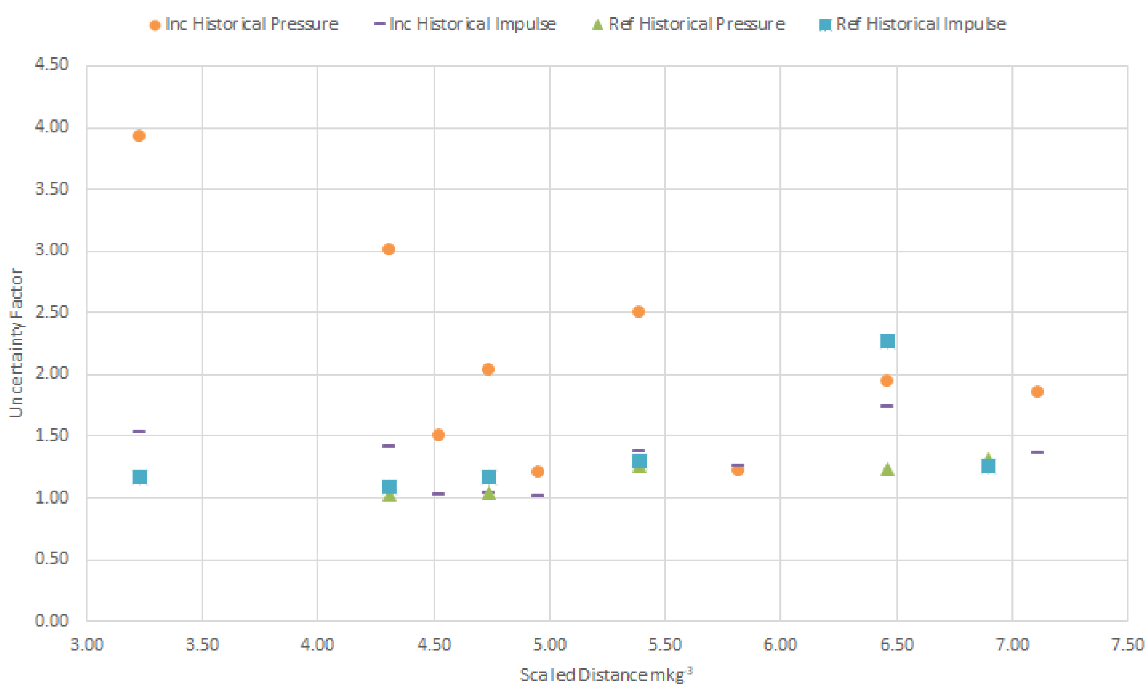

Figure 5.13: Historical Uncertainty Factors

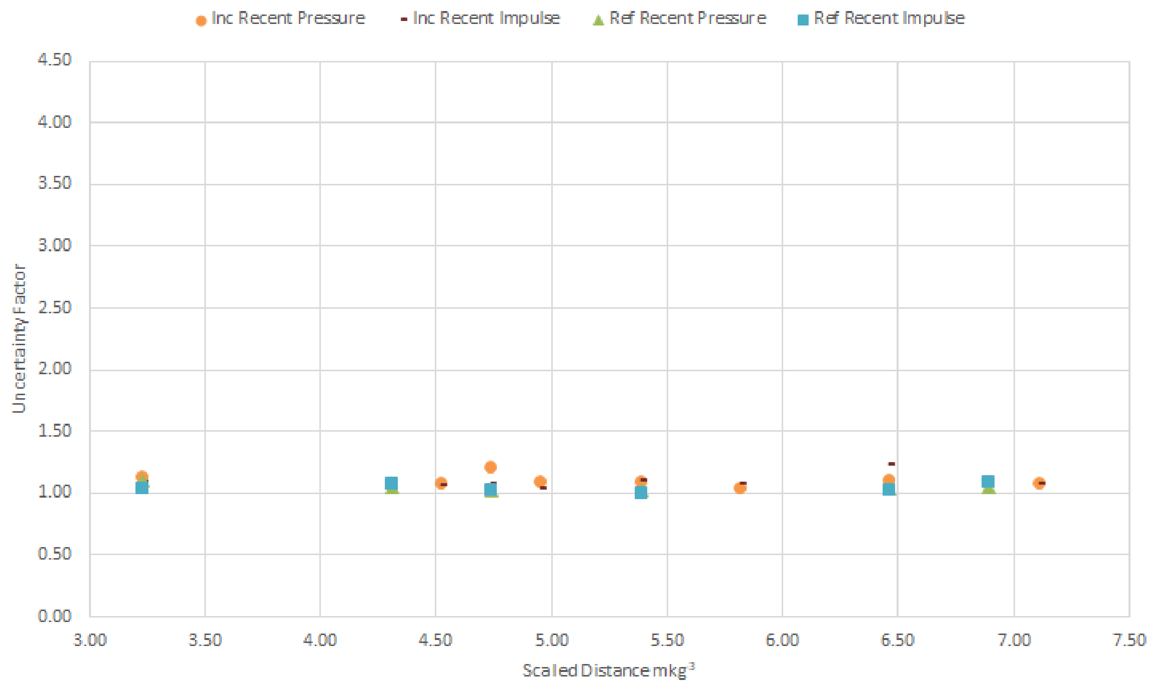

Figure 5.14: Recent Uncertainty Factors

Table 5.5 shows that for both reflected pressure and impulse, there is clear improvement on the uncertainty factors between the two data sets, especially at the further distances. This is also the case for the incident data (Table 5.6) where the uncertainty factors are greatly reduced. However, it should be noted that within the historical data set there are significantly more data points which would naturally be expected to produce a greater variability and greater uncertainty. This can be seen for the incident data (Table 5.6) where there are only a small number of data points at some of the scaled distances for pre-2019 data. When compared with post 2019 data, the analysis shows an increased uncertainty factor for the impulse measurements in the post 2019. The improvement is likely to be due to the increased gauge block size to mitigate the clearing effect but also suggests that variation in gauge block size becomes less important once the gauge block is sufficiently large to mitigate the clearing effect. There is also an improvement in the variation of incident data for both pressure and impulse. This is likely due to the use of pencil gauges, instead of the pancake and bullnose gauges, as they produce pressure-time curves which more closely match the actual curve. When compared to the Bogosian conclusions [21], the average uncertainty for the recent data is significantly lower than those calculated from the Bogosian data sets. The data set presented in this thesis also does not show the same uncertainty difference between the peak pressure and the impulse presented in the Bogosian paper; Bogosian found the peak pressure uncertainties were significantly higher than those for impulse, while in the author's data both factors are very similar.

5.7 Conclusion of Data Review

The data comparison in Section 5.6 demonstrates that it is possible through the techniques discussed to significantly improve the reliability and accuracy of the produced data through adjusted setups and measurements, providing greater repeatability between trials regardless of stand-off. If a blast test can produce high quality and repeatable data that takes into account the blast parameter sensitivities, it has the potential to be used for different applications beyond validating the response of a target to an explosive charge. The following chapters use experimental data that has been collected using the best practices mentioned in Section 4 for further assessment of blast parameters. The improved accuracy of the data produced in the recent trials allows for its further use in numerical and investigative studies as the data sets are more reliable, leading to more credible studies. This analysis utilised 100 kg TNT equivalent charges only with identical charge geometries which allows only limited conclusions to be drawn as the influence of the change in geometries can further affect the sensitivities. The following chapter utilises the methodologies and practices reviewed to investigate the change in charge size and whether the sensitivities are affected further.

6 Do Sensitivities Change with Scale?

The previous sections dealt with 100 kg TNT equivalent explosive charges as the author had the largest quantity of identical test set-ups with the same charge size and only varying the stand-off distances. As discussed in Section 2.4.4, it is a common requirement to perform a scaled down version of a blast test, often due to cost and feasibility. The Hopkinson-Cranz scaling law has long been used to calculate scaled up or down explosives and distances. This section investigates if the most common and usable targeted blast parameter sensitivities change with scale. This investigation of sensitivities changing with scale considers scaled distances of 2.43 to 12.93 $mkg^{-\frac{1}{3}}$ and investigates the changes in pressure, impulse, time of arrival and positive duration over these scaled distances.

6.1 Experimental Study

Using data from trials carried out on the smaller scale by Blastech by the University of Sheffield and at the larger scale by the author at DNV Spadeadam (utilising the good practice techniques referred to in Section 5) to consider and validate the Hopkinson-Cranz scaling law. These trials covered a range of charge sizes from 0.22 kg up to 500 kg of PE4. A consistent explosive type was used to remove any inconsistencies that may exist from comparing between Nitromethane, ANFO and PE4. Measurements were taken for reflected and incident pressures at set distances. These measurements were then converted to their scaled equivalents using the Hopkinson-Cranz scaling law and compared in order to validate the scaling law.

Table 6.1 gives the charge sizes and scaled distances that were recorded in the trials. The data for explosive charges less than 1 kg was collected by Sheffield and only reflected measurements were taken. These were hemispherical explosive charges located on a flat plate on the ground (Figure 6.1). Trials for explosive charges greater than 1 kg were conducted at Spadeadam using spherical charges placed at 1.2 metres above ground, except for the 640 kg charge which was placed 2 metres above ground. Explosive charges between 2.5 kg and 15 kg were shaped in black plastic bags with electrical tape used to secure their shape (Figure 6.2). For explosive charges larger than 15 kg, ABS plastic spheres were vacuum moulded to the correct size for holding the appropriate amount of explosive; PE4 was then packed by hand into the lower hemisphere of the plastic sphere before the top half was then attached and the rest packed in with the aid of a wooden baton (Figure 6.3). Reflected and incident gauges were positioned at set distances from the centre of the explosive charge. Due to their size and short distance from the ground, the shock wave can be considered hemispherical and so directly comparable with the hemispherical explosive results from Blastech.

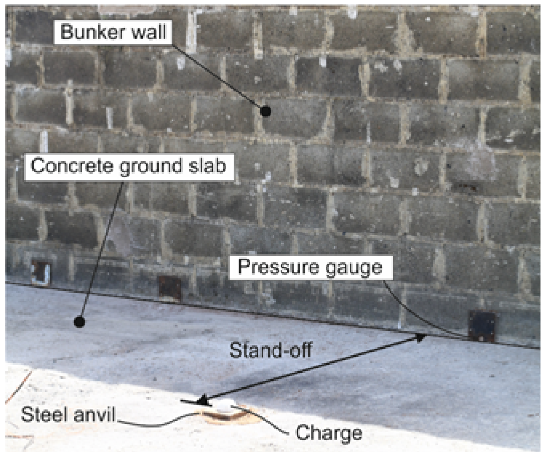

Figure 6.1: Experimental setup at Blastech by the University of Sheffield [128]

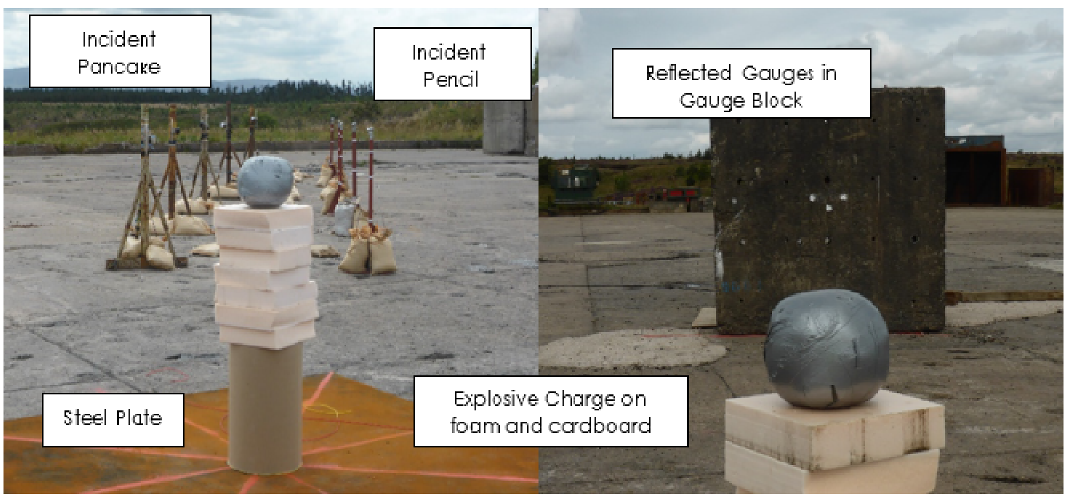

Figure 6.2: Experimental setup at Spadeadam by the author and DNV

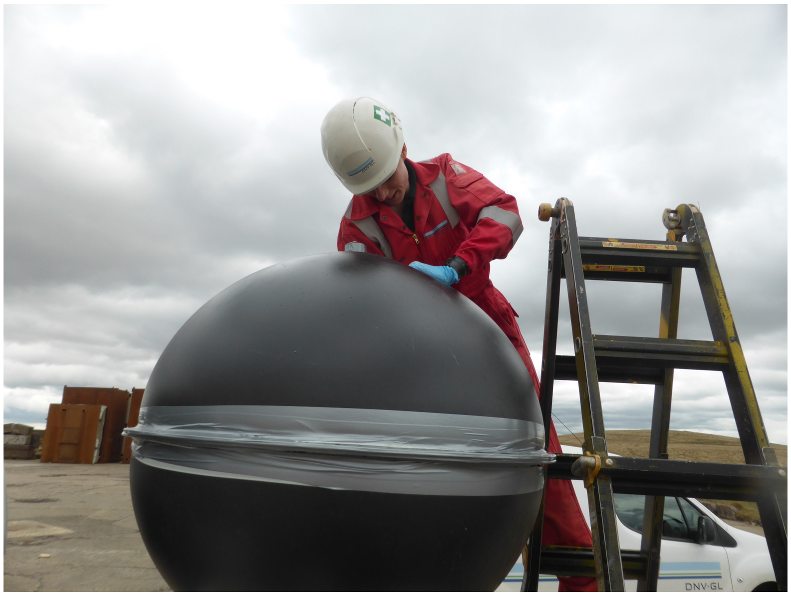

Figure 6.3: The author packing the 640 kg PE4 explosive charge into a plastic sphere

Table 6.1 displays the charge sizes, stand-off distances (in metres and as the scaled distance based on the Hopkinson-Cranz scaling law) and type of measurement (incident or reflected) used in this scaling analysis.

TNT Equivalent Charge Size (kg)	**Distance from Charge (m)**	**Measurement Type**	**Scaled Distance**
0.22	4	Reflected	6.63
0.3	4	Reflected	5.98
	6	Reflected	8.96
0.35	6	Reflected	8.51
0.42	4	Reflected	5.34
	6	Reflected	8.01
2.5	6	Incident	4.42
	9	Incident	6.63
	9	Reflected	6.63
	12	Incident	8.84
	15	Reflected	11.05
	15	Incident	11.05
	18	Incident	13.26
10	6	Incident	2.78
	9	Incident	4.18
	9	Reflected	4.18
	12	Incident	5.57
	15	Incident	6.96
	15	Reflected	6.96
15	17.5	Incident	7.10
	6	Incident	2.43
	10	Incident	4.05
	15	Incident	6.08
100	15	Incident	3.23
	15	Reflected	3.23
	21	Incident	4.52
	24	Incident	5.17
	25.9	Reflected	5.58
	30	Incident	6.46
	30.5	Reflected	6.57
	33	Incident	7.11
	33.5	Reflected	7.22
	60	Incident	12.93
640	22	Incident	2.55
	30	Incident	3.48
	30	Reflected	3.48
	40	Incident	4.64

Table 6.1: Hopkinson-Cranz validation data measurements

The figures below show the results of the trials, plotting scaled distance against the incident and reflected pressure using the Hopkinson-Cranz scaling law.

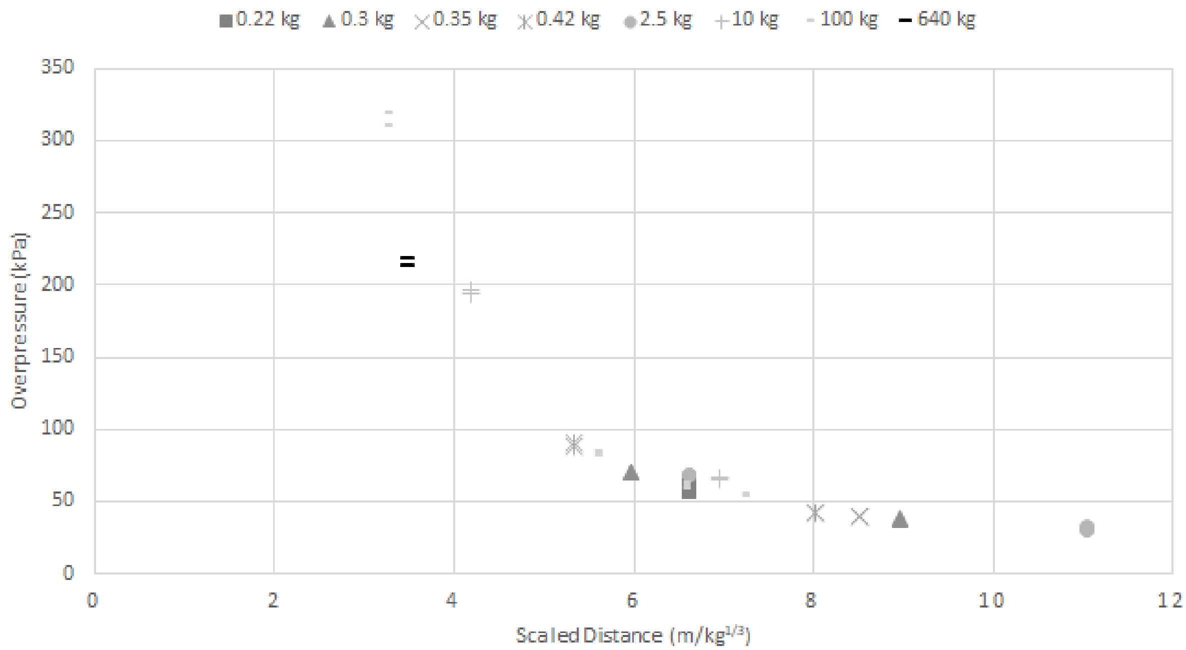

Figure 6.4: Reflected pressure vs scaled distance

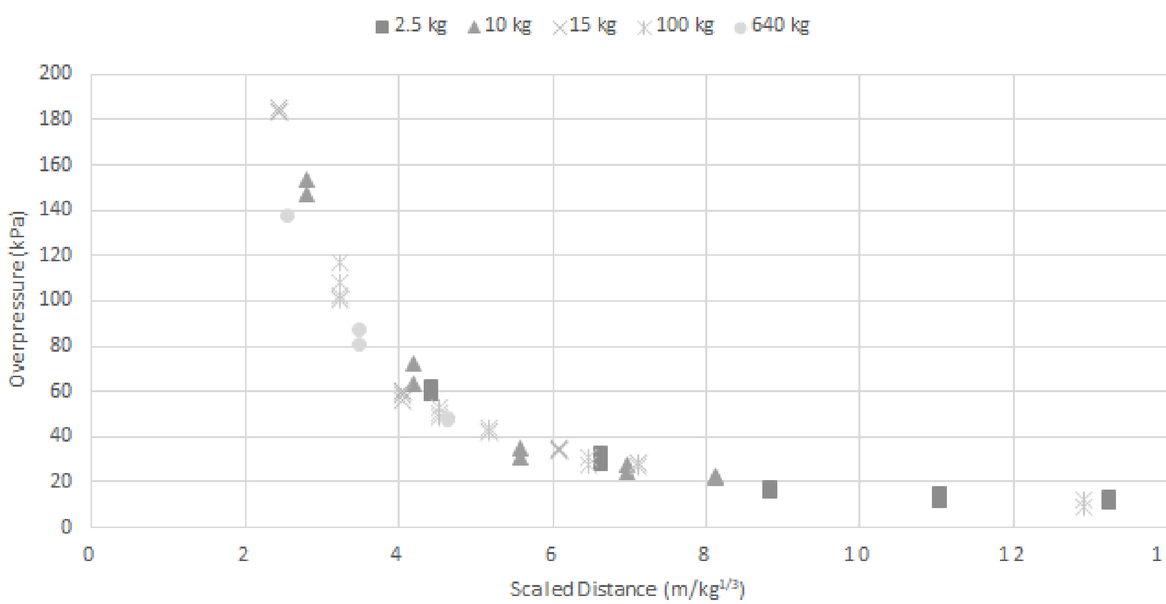

Figure 6.5: Incident pressure vs scaled distance

From this set of trials, the data demonstrates a clear relationship between the scaled distance and the overpressure, regardless of charge size. There is good correlation between the smaller charge; less than a kilogram and the larger charge sizes, with no obvious outliers. This suggests that the Hopkinson-Cranz scaling law is valid at least for these charge sizes and scaled distances.

When considering the impulse (i) and time of arrival (t), unlike the scaled pressure vs actual pressure, the length factor k ($W^{\frac{1}{3}}$) needs to be included [12] where:

$$P_{actual} = P_{scaled} \tag{6.1}$$

$$t_{actual} = t_{scaled} W^{\frac{1}{3}} \tag{6.2}$$

$$i_{actual} = i_{scaled} W^{\frac{1}{3}} \tag{6.3}$$

Using these equations, Figure 6.6 to Figure 6.9 plot scaled impulse and scaled time of arrival against scaled distance.

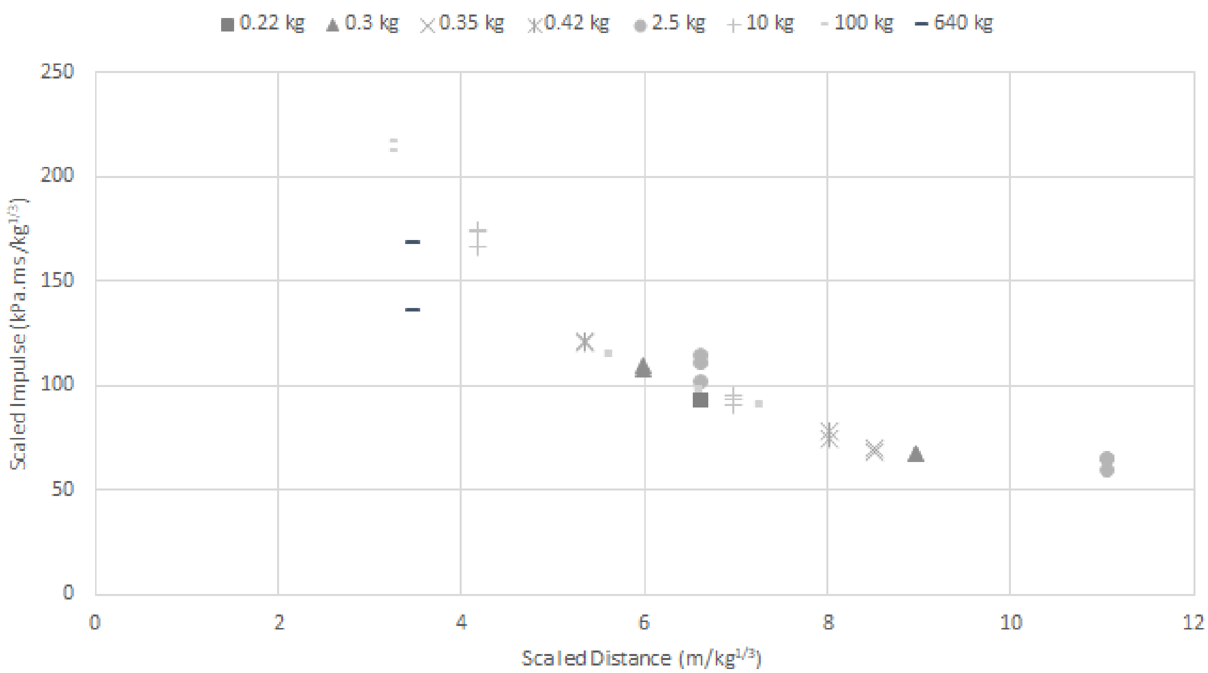

Figure 6.6: Scaled reflected impulse vs scaled distance

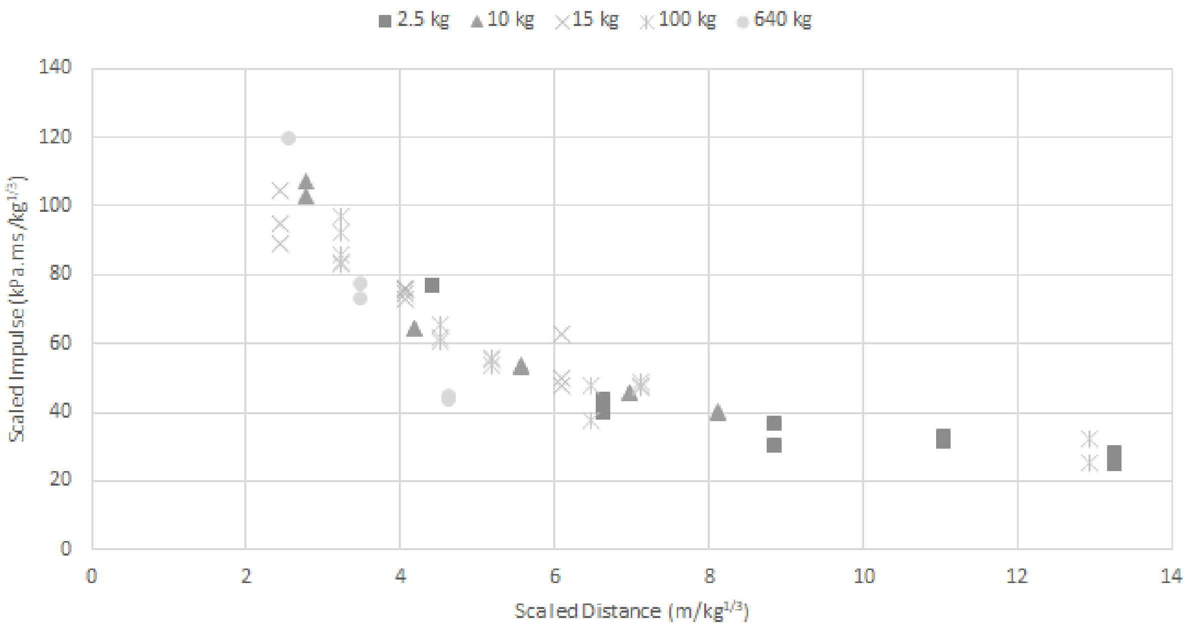

Figure 6.7: Scaled incident impulse vs scaled distance

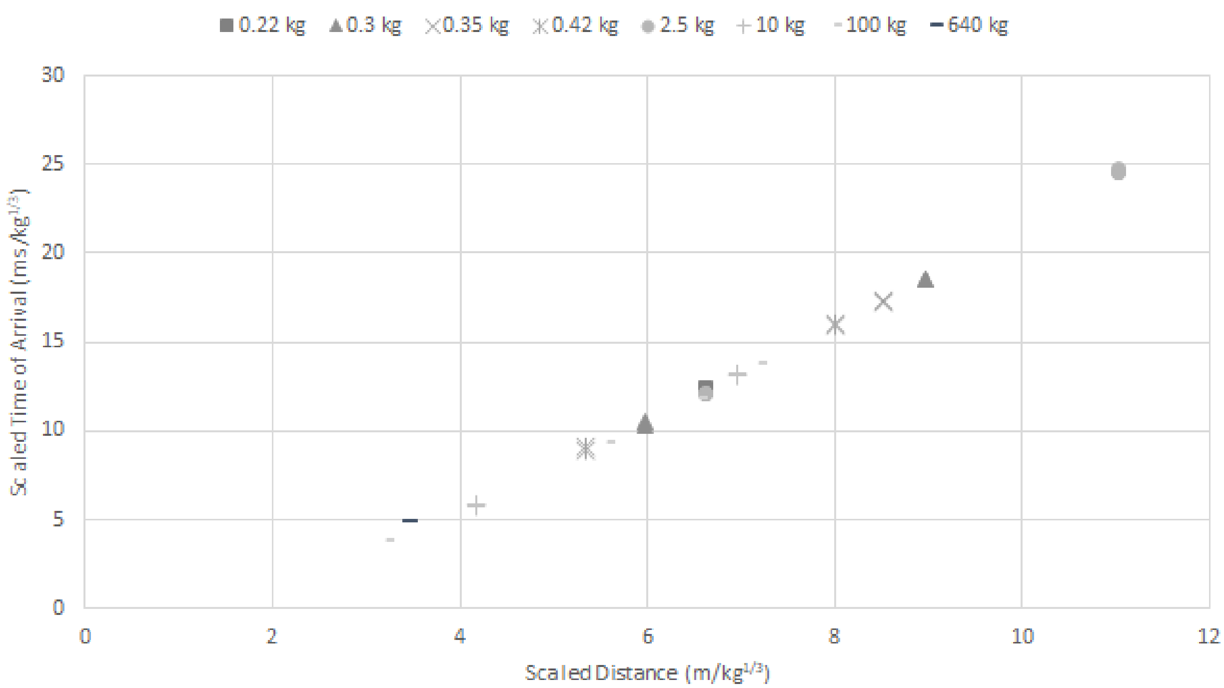

Figure 6.8: Scaled reflected time of arrival vs scaled distance

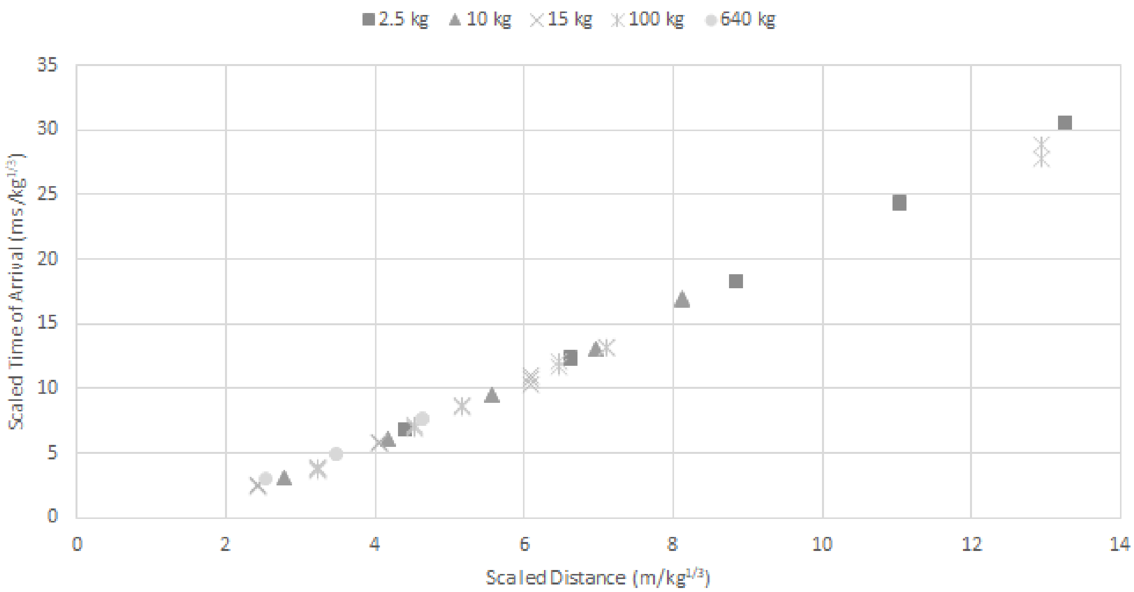

Figure 6.9: Scaled incident time of arrival vs scaled distance

As with the overpressure results, the above figures demonstrate a clear relationship between the scaled distance, the scaled impulse and the scaled time of arrival, regardless of charge size. There is particularly good correlation for the time of arrival versus scaled distance, with a slightly wider spread of impulse. This wider spread is expected based on the standard deviation results shown in Section 5. These results again suggest that the Hopkinson-Cranz scaling law is valid at least for these charge sizes and scaled distances. There is a lack of reflected data at the smaller scaled distances for larger charge sizes which makes it difficult to definitively conclude that the scaling law is valid for reflected pressure, impulse and time of arrival. Likewise, with the absence of incident data for smaller charge sizes, conclusions cannot be drawn to include these values.

6.2 Comparison with ConWep

Since Section 5.4 suggested that ConWep is a suitable tool for the validation of experimental data, it is informative to investigate the validity of ConWep for pressure and impulse and the repeatability of the experimental data, regardless of charge size and stand-off. In order to perform this investigation, the data collected for this analysis were divided by the respective ConWep values and plotted against the scaled distance. For the ConWep values, the charge size and stand-off were modelled for each set of trials using the TNT equivalent values. Figure 6.10 to Figure 6.13 display the results of this analysis for reflected and incident data respectively. A solid line at 1 has been plotted to show the variation around the ConWep values.

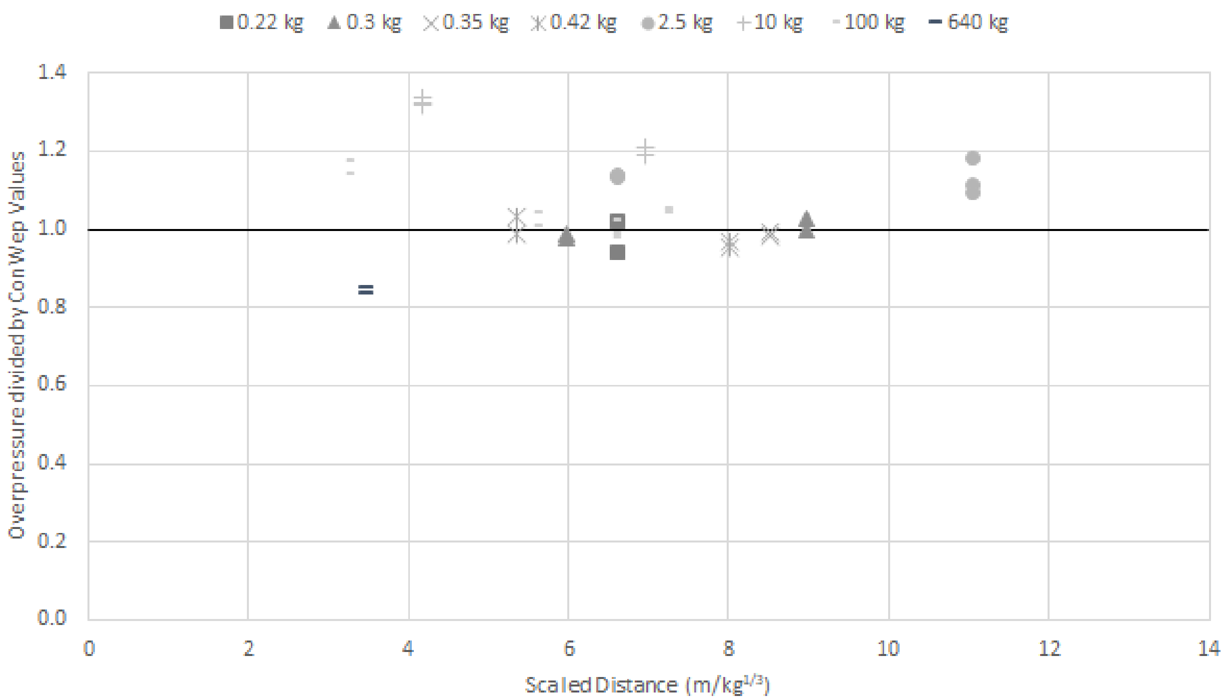

Figure 6.10: Reflected pressure divided by ConWep values

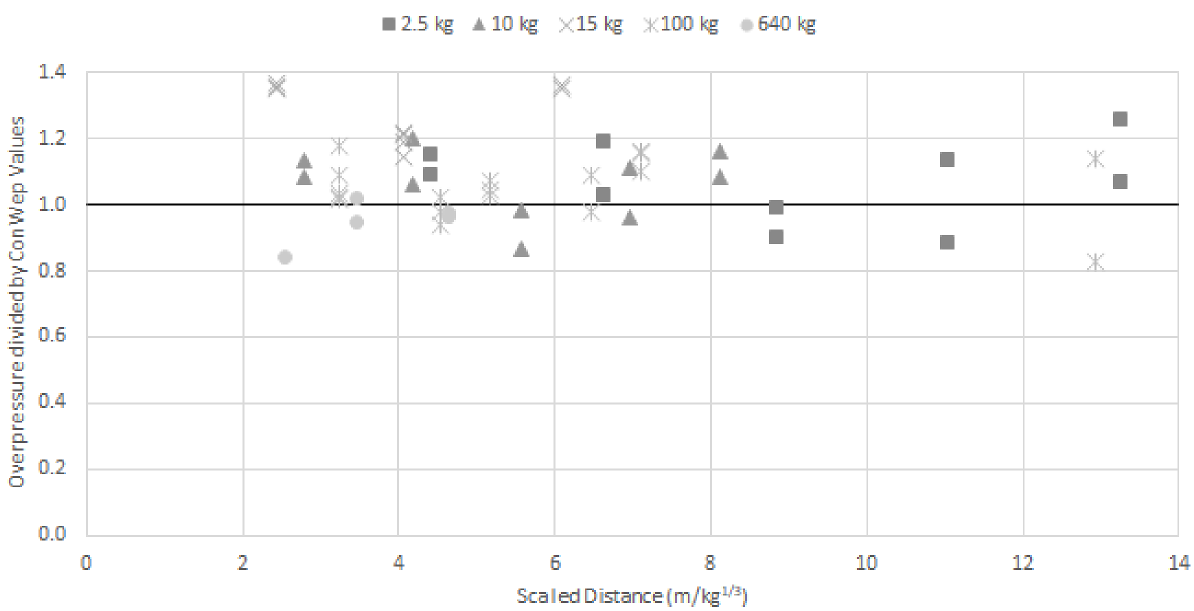

Figure 6.11: Incident pressure divided by ConWep values

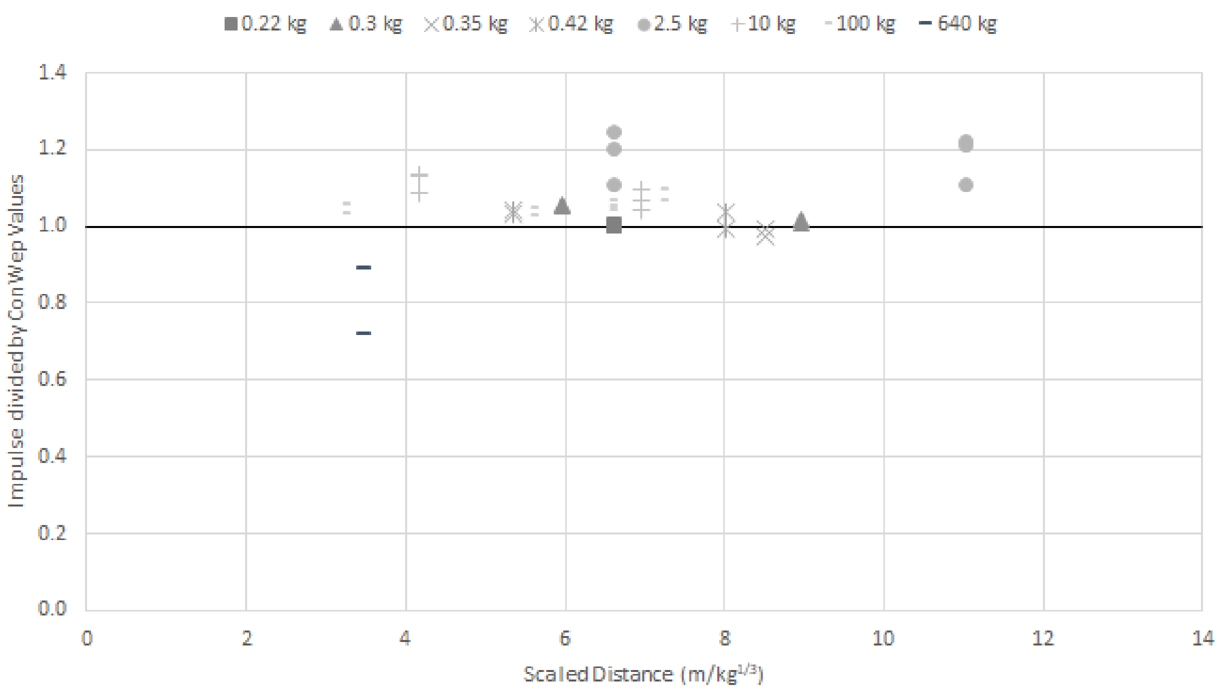

Figure 6.12: Reflected impulse divided by ConWep values

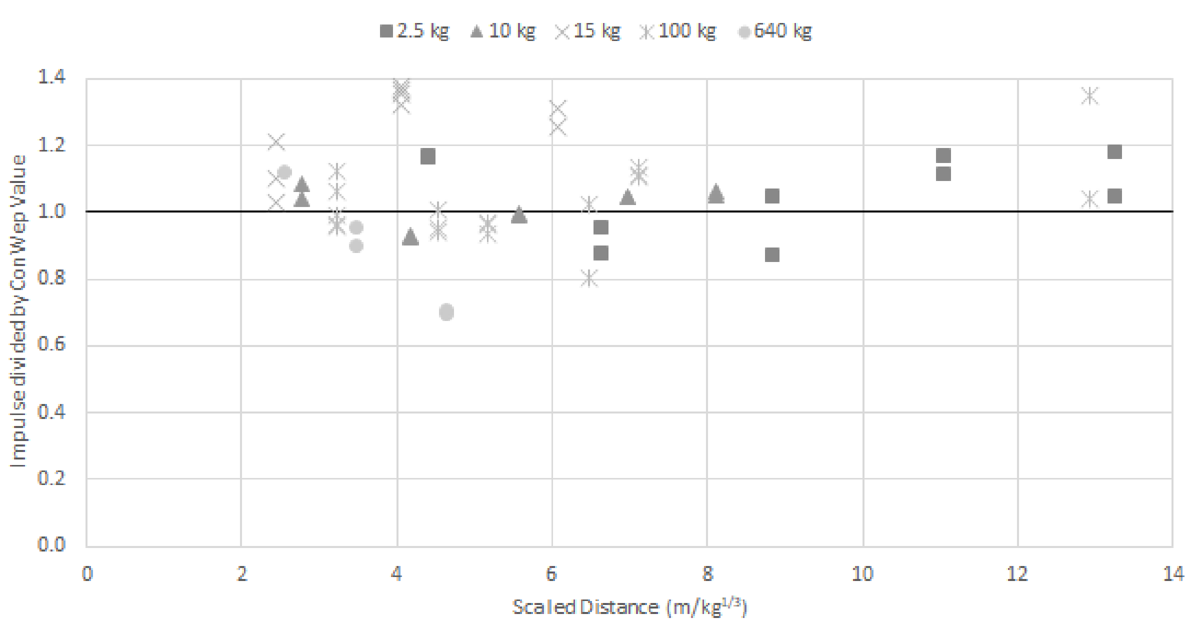

Figure 6.13: Incident impulse divided by ConWep values

Analysis of these graphs along with those produced in the next section with Air3D will be discussed in Section 6.4.

6.3 Comparison with Air3D

Analogous with ConWep in the previous section, Air3D was used to model each individual test set up, matching the charge size and stand-off to those in the experimental trials. The overpressure and impulse were recorded and the experimental values divided by the predicted values and then plotted in Figure 6.14 to Figure 6.17 to show the accuracy of the Air3D in predicting the parameters.

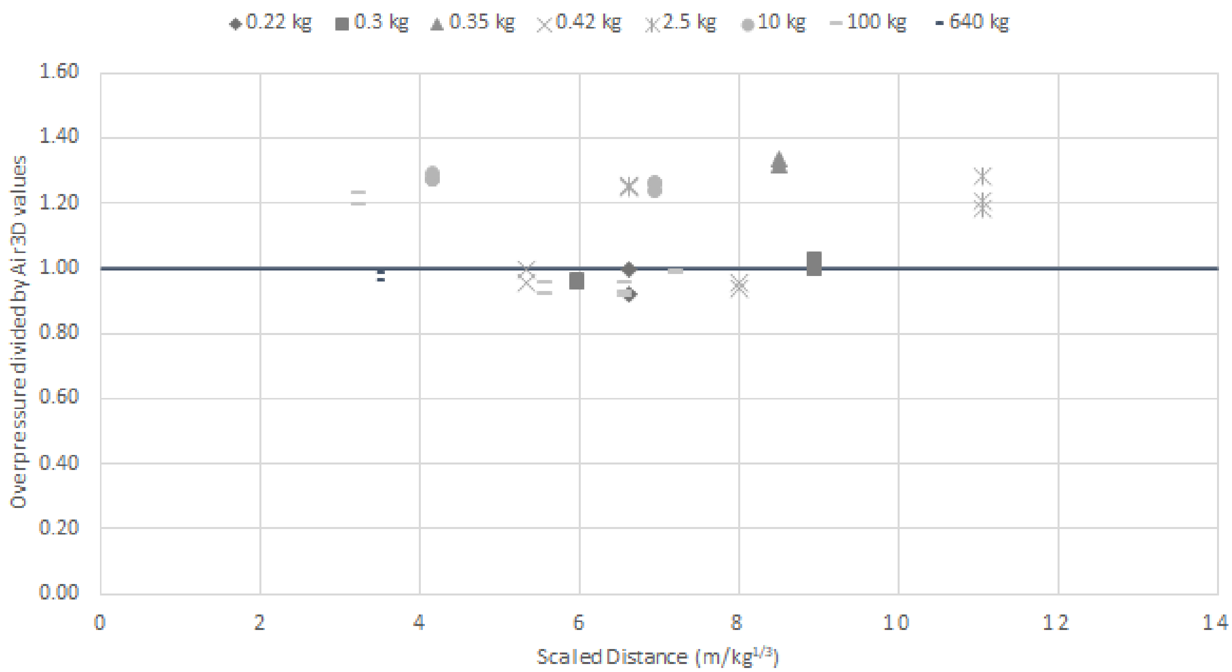

Figure 6.14: Reflected pressure divided by Air3D values

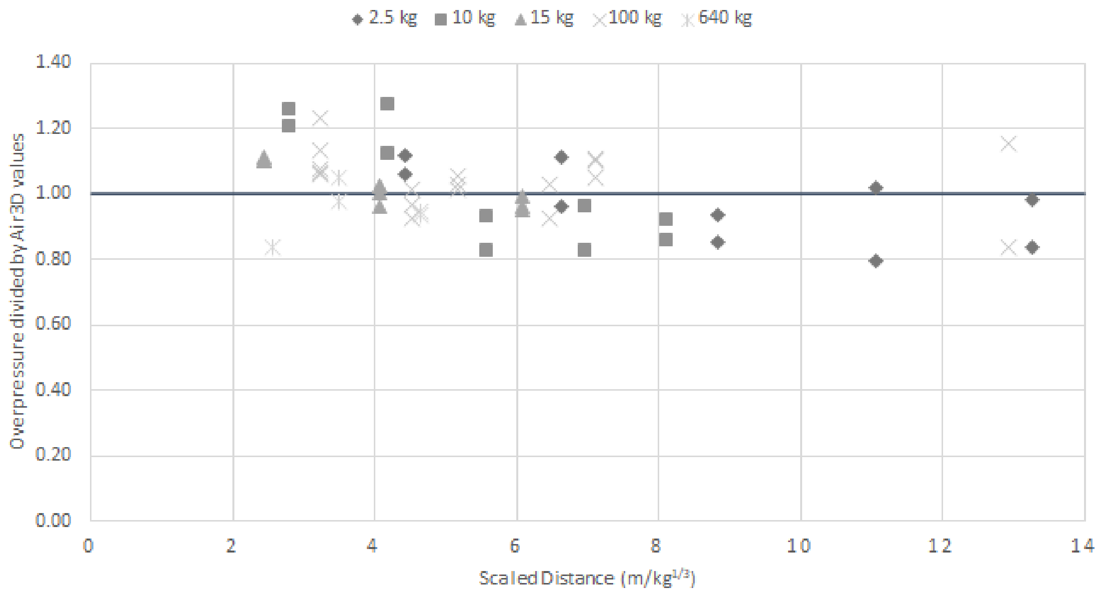

Figure 6.15: Incident pressure divided by Air3D values

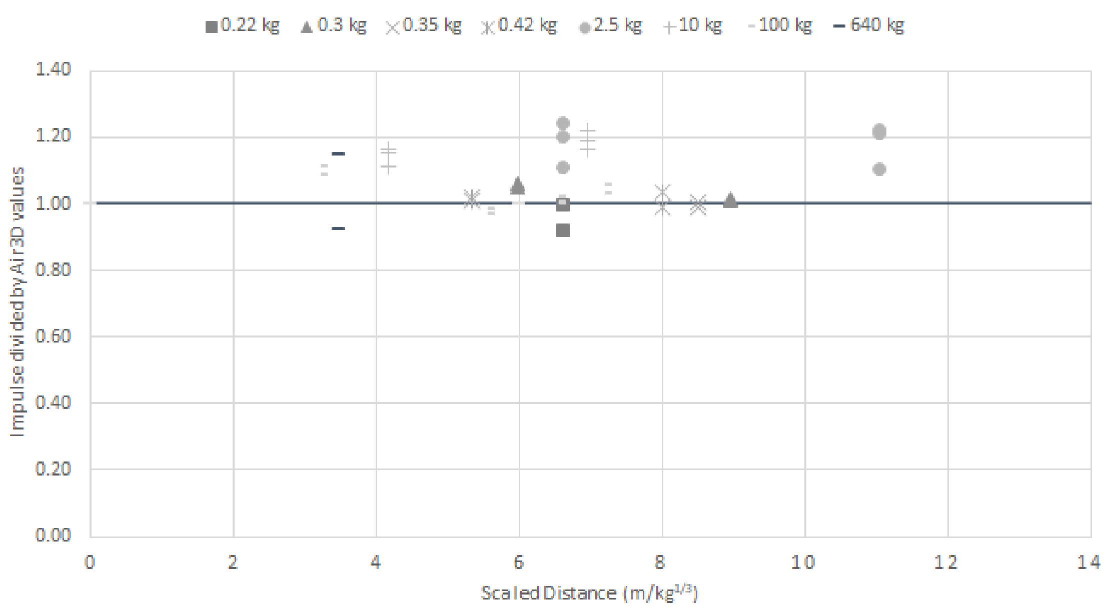

Figure 6.16: Reflected impulse divided by Air3D values

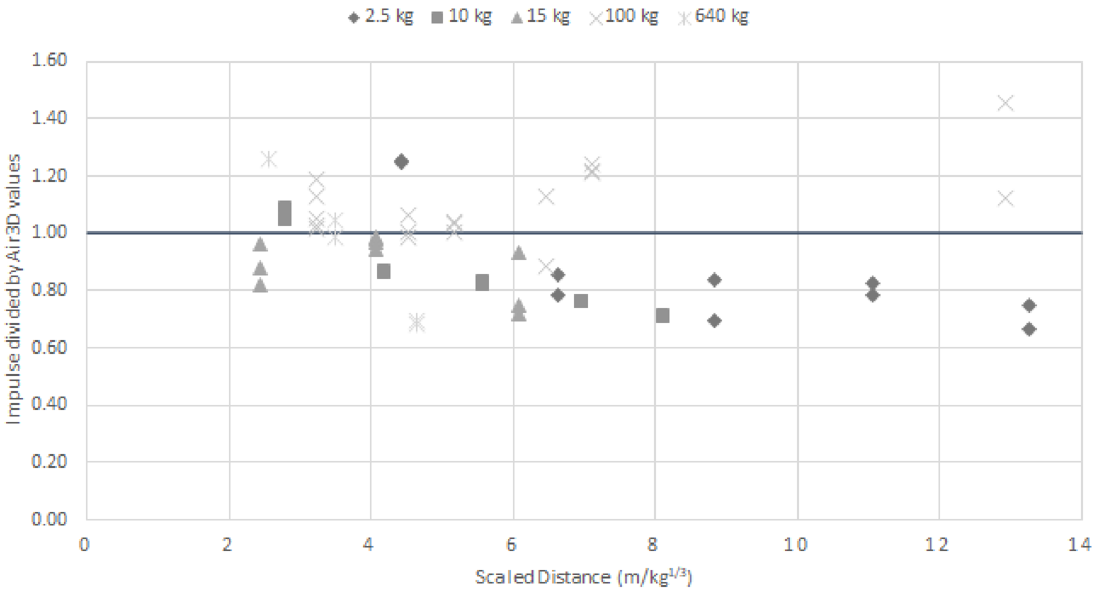

Figure 6.17: Incident impulse divided by Air3D values

Analysis of these graphs along with the graphs produced with ConWep data is discussed in section 6.4.

6.4 Model Comparisons

From the data in Sections 6.2 and 6.3, the mean, standard deviation and coefficient of variation for both the reflected and incident pressure and impulse data divided by their equivalent ConWep and Air3D predictions have been calculated. To allow an assessment of small scale setups versus larger scale setups to be compared, which gives the ability to compare the data that was collected at Spadeadam with the data collected at Blastech, Sheffield, the values below have also been calculated for smaller than 1 kg and larger than 1 kg. The split between mid-field scaled distances of less than 4.5 $mkg^{-\frac{1}{3}}$ and the far-field scaled distance of 4.5 $mkg^{-\frac{1}{3}}$ have also been calculated to allow comparisons between the smaller and larger scaled distances to determine if this has an impact upon the data sensitivities. The following three graphs display the mean (Figure 6.18), standard deviation (Figure 6.19) and the coefficient of variation (Figure 6.20). Analysis has been drawn for each graph.

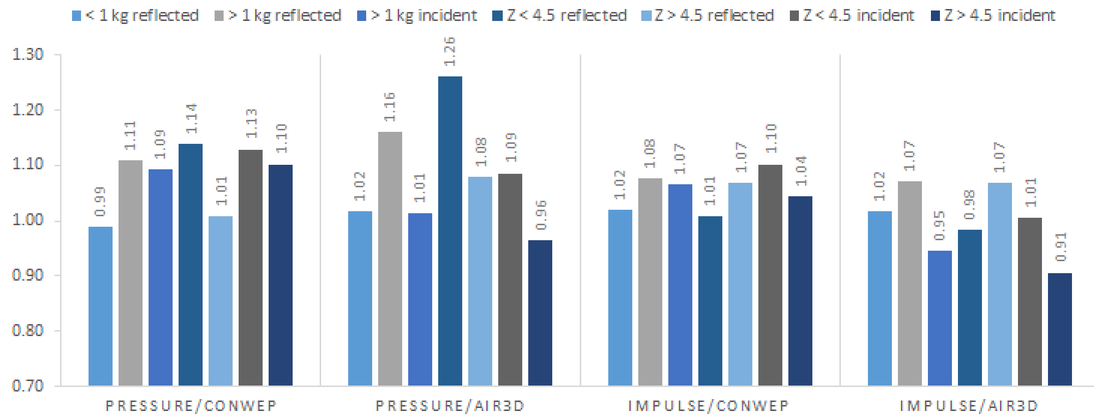

Figure 6.18: Mean of normalised data when compared to ConWep and Air3D

This graphs shows generally good agreement between Air3D and ConWep when the normalised mean experimental values are compared to the predicted values. It can be seen that the smaller charge sizes of less than one kilogram are more closely matched to the ConWep predictions for reflected data. There was no incident data for the small charge sizes, so conclusions on this cannot be drawn. When considering scaled distance, Air3D appears to overpredict both the incident impulse and overpressure when compared to ConWep in the far field, however this is not the case for reflected data or closer to the explosive charge. There is no evidence of any better or worse agreement for ConWep and Air3D between reflected or incident data.

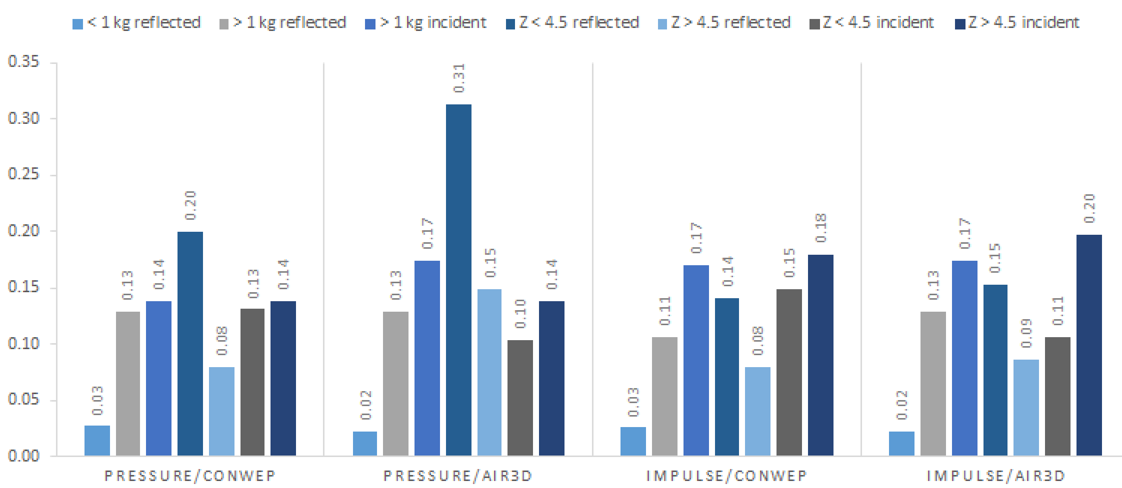

Figure 6.19: Standard deviation of data when compared with ConWep and Air3D

Immediately evident from this graph is the small standard deviation seen in the data for less than 1 kg collected from Blastech. This suggests a small spread of data, regardless of comparisons between pressure and impulse and between ConWep and Air3D. This is most likely due to the level of control that is possible for smaller scaled tests, allowing for a setup that more effectively matches the idealised geometric assumptions, such as hemispherical charge shape and surface denotations to an extent which is not possible in large-scale arena trials. This low standard deviation seen in the Blastech results compared with other experimental measurements may also be due to differences in setup between different test houses, stemming from the lack of standard or best practice method for trial and instrument setup.

Figure 6.19 shows that observations of a wider spread of incident data than in the reflected data. This could be primarily due to the difficulty in recording pressure data which was covered in Section 4.1, particularly when considering the increased difficulty with accuracy in instrument placement for the far field. Many of the issues found with the recording of the incident pressure data are not found in the recording of reflected pressure data, which can explain the improved repeatability of the reflected data versus the incident data, as shown by the increased standard deviation at larger scale.

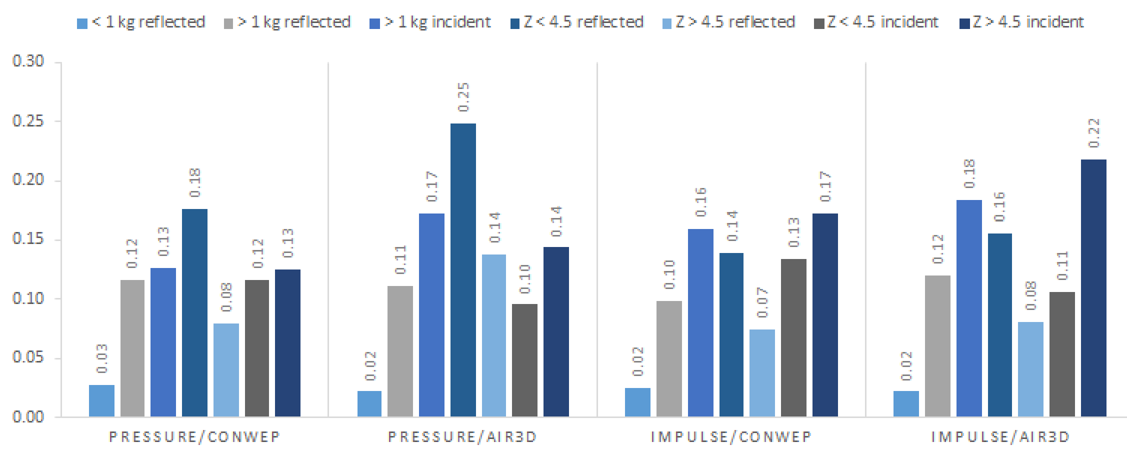

Figure 6.20: Coefficient of variation of data when compared with ConWep and Air3D

The coefficient of variability has been calculated for the data and shows very similar conclusions to the Figure 6.19. This is explained as the mean values show good correlation with the data, and therefore the values of the coefficient of variation would not be expected to vary considerably from the standard deviation.

The reviews in this section show that, in principle, smaller scale tests can give more consistent and repeatable results than the larger scale tests, particularly if only considering reflected pressure. As discussed, there are inherent difficulties in measuring incident data, which become increasingly difficult as the scaled distance increases. Further investigation in this area would require additional trials measuring incident pressure on smaller charge sizes to determine if the same sensitivities are seen as equivalent scaled distances to those observed with the larger charge sizes.

6.5 Literature Comparison

UFC-3-340-02 has comprehensive plots of overpressure, impulse and time of arrival for both reflected and incident data for hemispherical charges [158] over a very wide range of scaled distances. This data has been compiled through both experimental trials and computer models. In Section 6.1, the data from the trials has been plotted in the same units and scale as the data produced in UFC-3-340-02 and a line of best fit plotted for direct comparison. In Figure 6.22, the experimental data points are overlaid on the data from the literature. It can be seen from this overlay that the experimental data matches exceptionally well for pressure, but the experimental data provides slightly higher values than the literature data for impulse and time of arrival, although still with the same trends. This is true regardless of whether considering the reflected or incident measurements and also regardless of scale.

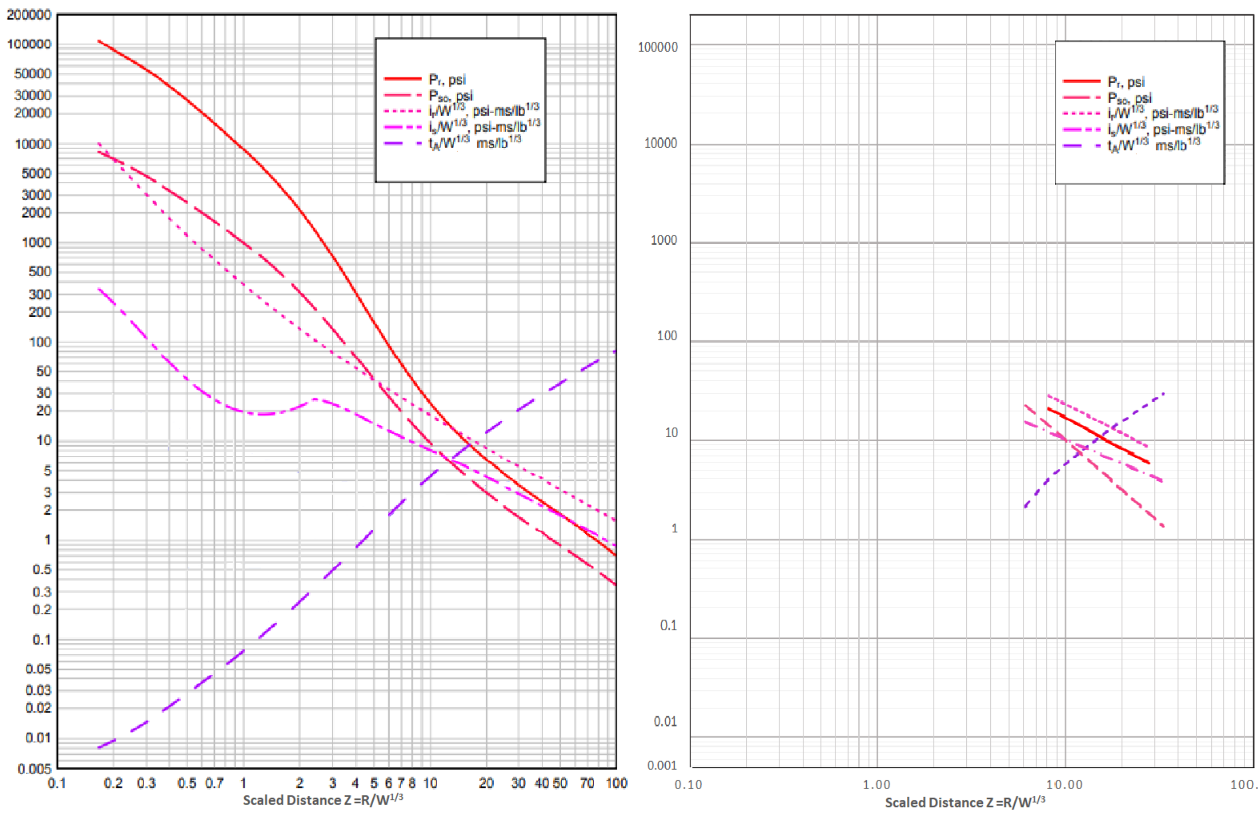

Figure 6.21: Comparison of blast parameters with scaled distance with literature [158]

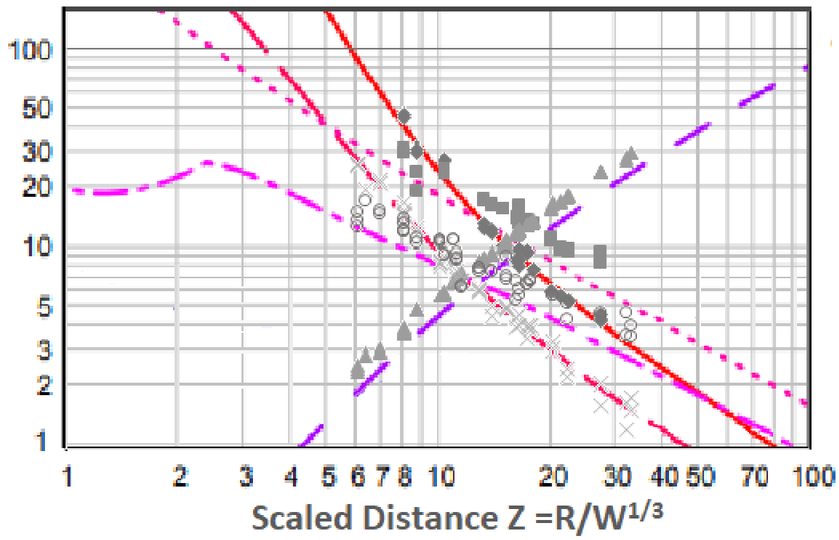

Figure 6.22: Direct overlay of experimental data points over UFC data

6.6 Conclusions

From the data collected in Section 6.1 and the analysis that followed, it can be concluded that for the scales considered in this set of trials, the Hopkinson-Cranz Scaling Law can be considered valid. The experimental data showed good fit with ConWep, Air3D and also the data provided in UFC-3-340-02. This allows for scaled down trials to replicate larger trials where possible. However, care should be taken when assessing targets, particularly large targets or complex arrangements, such as multiple targets or varied shapes, as this study considered only incident pressures and reflections over a large flat reflected surface; omitting investigation of complex shapes, complex charge sizes, arena set-up or interactions between charges and/or targets. It should also be noted, and is evident from Figure 6.21, that the experimental data considered in this study covers only a very small area of scaled distances especially when compared to the full scales of the UFC graphs. To further confirm that the full curves in UFC-3-340-02 are valid, further investigations are needed to cover the near field and far far-field, and also with a more varied charge size than in the restricted data set investigated in this chapter.

7 Energy Flux

7.1 Calculating Energy Flux

As previously mentioned in Section 2.7.1, the energy flux in air can be calculated in different ways such as those shown in both Swisdak [137] and Grisaro [70]. Swisdak calculated it using the characteristic impedance and a pressure-time curve as defined below and in Section 2.7.1 using the following equation:

$$E_f = \int_{t_a}^{t_a+t_{d+}} (\frac{1}{\rho_{so} u_{so}}) \, [p(t) - p_0]^2 \, dt \tag{7.1}$$

Grisaro used a similar methodology but based on the particle velocity instead of the characteristic impedance using equation:

$$E_f = \int_{t_a}^{t_a+t_{d+}} [p(t) \cdot u_p(t)] \, dt \tag{7.2}$$

For this energy flux study, both methodologies will be considered.

7.2 Total Available Energy and Relative Energy

If the explosive charge is spherical or hemispherical (depending on the set-up) it can be assumed to produce a spherical or hemispherical shock wave. The total energy output of the shock wave can be calculated by multiplying the measured energy flux at a known distance by the surface area of the shock wave at that distance. This gives a total value of energy emitted in the shock wave of the explosive. If this value is then divided by the mass of explosive used, it will give a value for energy per kilogram. This allows a comparison to be made as to whether the charge size has an impact on the energy available - i.e. does a larger charge size convert a greater or lesser proportion of energy to the shock wave than a smaller charge size?

As well as using the shock wave energy to analyse the variance of efficiency from differing charge sizes, the value for energy per kilogram can also be divided by the calorific value for one kilogram of the explosive. This will give a value for relative energy for a particular explosive - the amount of energy in that explosive which is converted to the pressure wave.

7.3 Energy Flux Calculations for TNT Based on the Swisdak Method

Initially, the energy flux methodology proposed by Sadwin and Swisdak [137] will be used to calculate the energy flux, total available energy, energy per kilogram of explosive and relative energy for TNT. Using the quick-to-run computer programme ConWep (2.8), full pressure-time curves from TNT blasts can be produced which can be used to calculate the energy flux of TNT at a set distance. The method calculates the characteristic impedance based on the equations given in Section 2.2. The below set of graphs show the steps (1 to 8) used to calculate the energy flux and, from there, the total shock energy, energy per kg and the relative energy.

This example uses a pressure-time curve for a 100 kg TNT charge at a stand-off of 40 metres. The calorific value for TNT is 4560 kilojoules per kilogram [129].

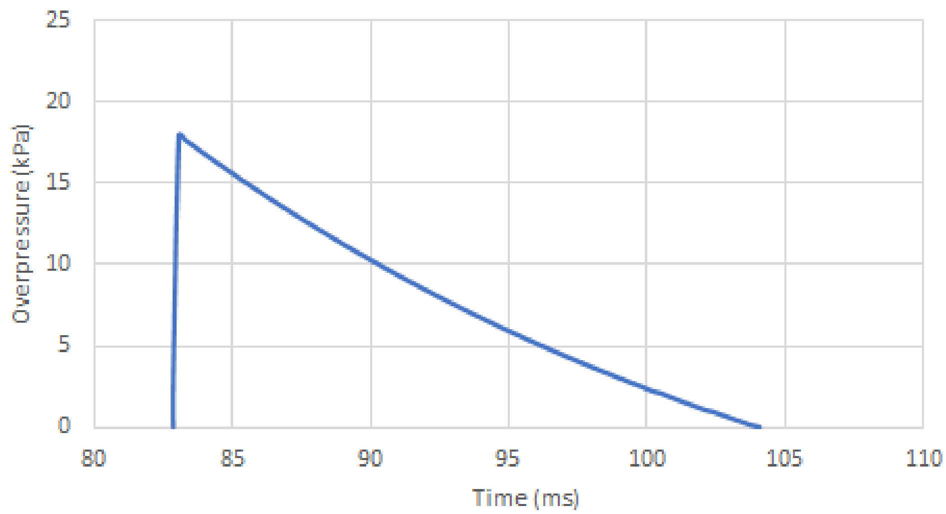

Figure 7.1: ConWep incident pressure-time curve for 100 kg at 40m

1. Using the equations in Section 2.2, the characteristic impedance ($\rho\mu$) at each time step is calculated:

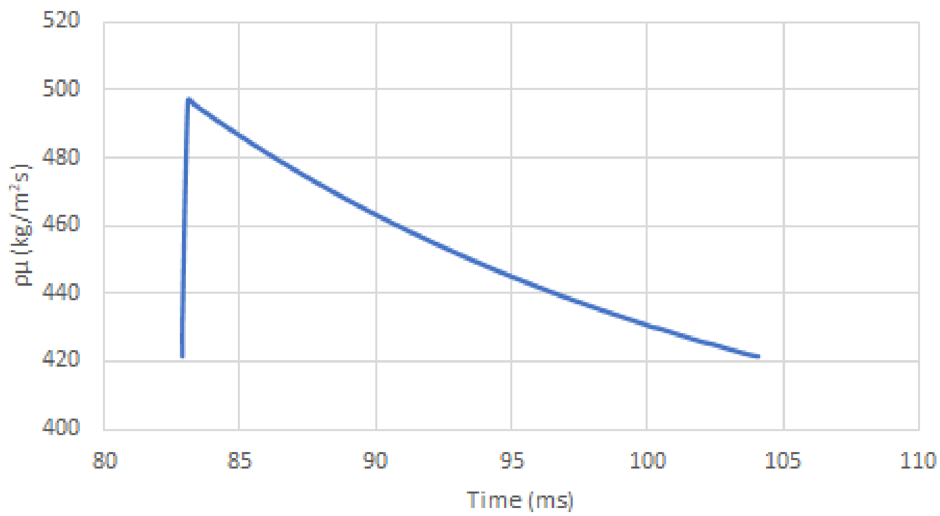

Figure 7.2: Characteristic impedance for incident pressure-time curve for 100 kg at 40m

2. Next the squares of the pressure values are multiplied by the characteristic impedance at each time step:

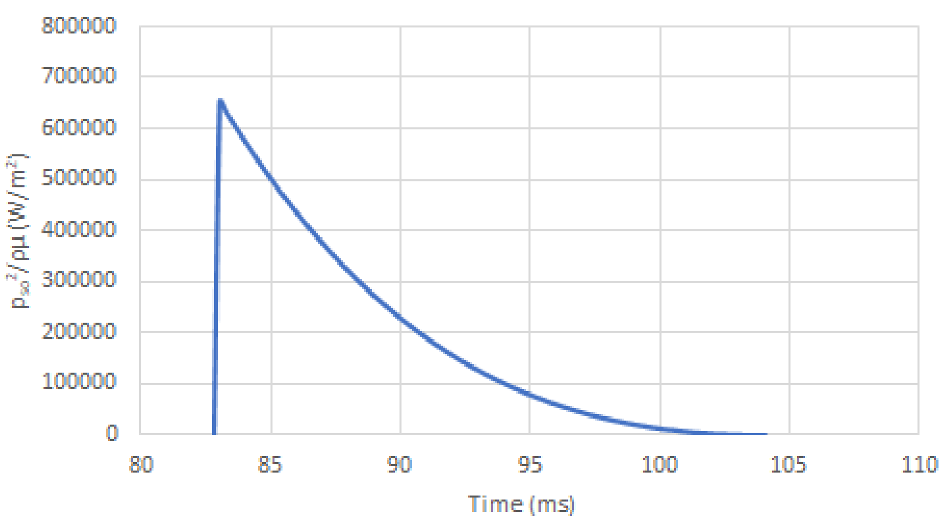

Figure 7.3: p_{so}^2 multiplied by $\rho\mu$ for 100 kg at 40m

3. Next the integral of the above curve is produced. This was calculated using the trapezoidal method.

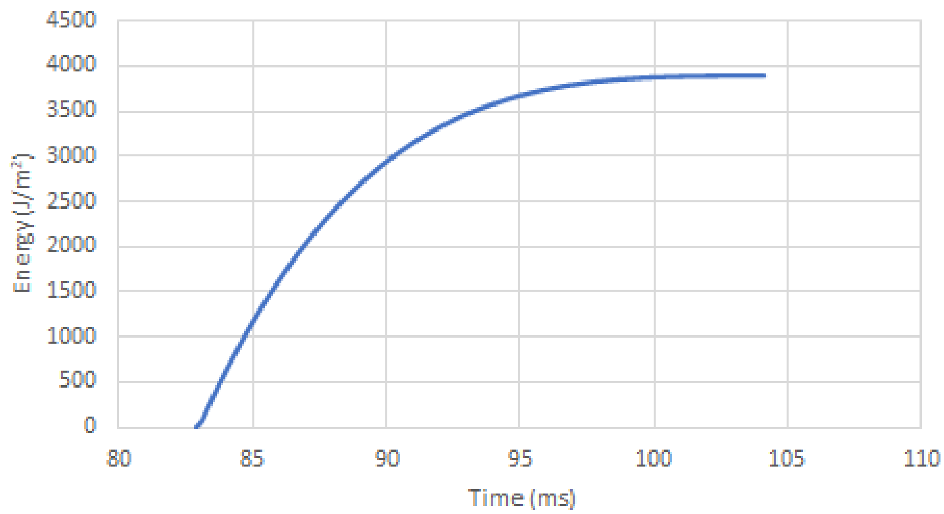

Figure 7.4: Integral of p_{so}^2 multiplied by $\rho\mu$ for 100 kg at 40m

4. The peak of this integral gives the value for energy flux as $3900.11 J/m^2$.

5. The surface area for a 40 metre radius hemisphere is given by $= 2\pi r^2 = 2 \cdot \pi \cdot 40^2 = 10,053.1 m^2$

6. The total shock energy is the energy flux multiplied by the surface area.$= 3900.11 \cdot 10053.1 = 39208.18 kJ$

7. The energy per kilogram of TNT is given by the total shock energy divided by the mass of explosives $= 39208.18/100 = 392.08 kJ/kg$

8. The relative energy is calculated by dividing the energy per kilogram measured from the energy flux in the blast, divided by the amount of available energy in one kilogram of TNT $= 392.08/4560 = 8.59\%$

The above steps to calculate total shock energy, energy per kilogram and relative energy were conducted on 42 different pressure-time curves with varying charge size of 25 kg to 200 kg and scaled distances between 2 and 18 $mkg^{-\frac{1}{3}}$. The output was used to produce graphs showing how the energy per kilogram and relative energy of TNT vary with scaled distance.

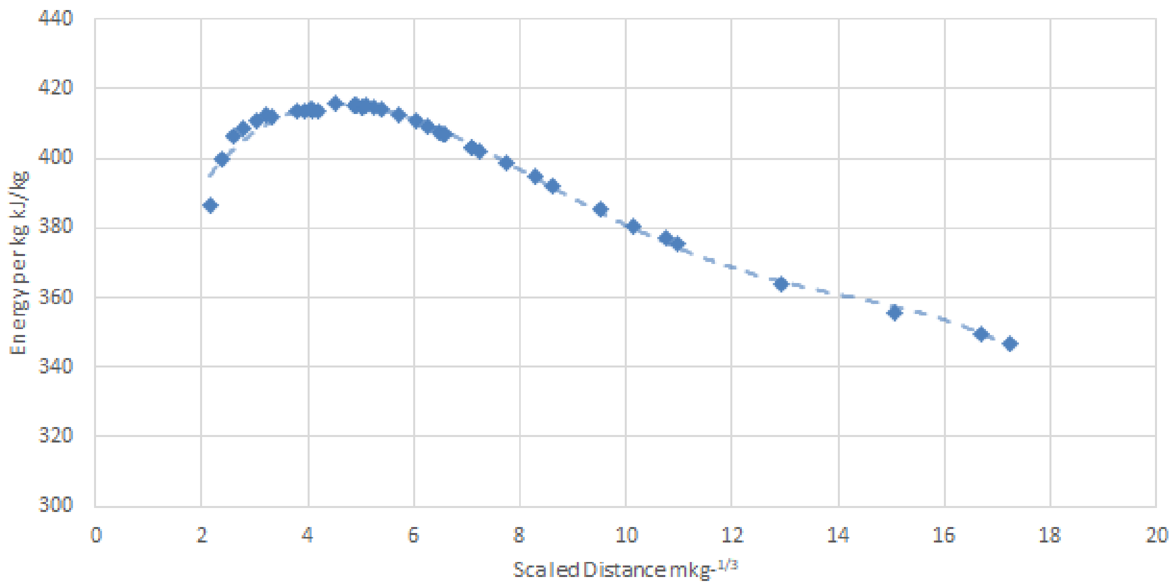

Figure 7.5: Total shock energy calculated at each distance divided by the mass of explosives to give energy per kilogram of TNT with scaled distance from Swisdak Method

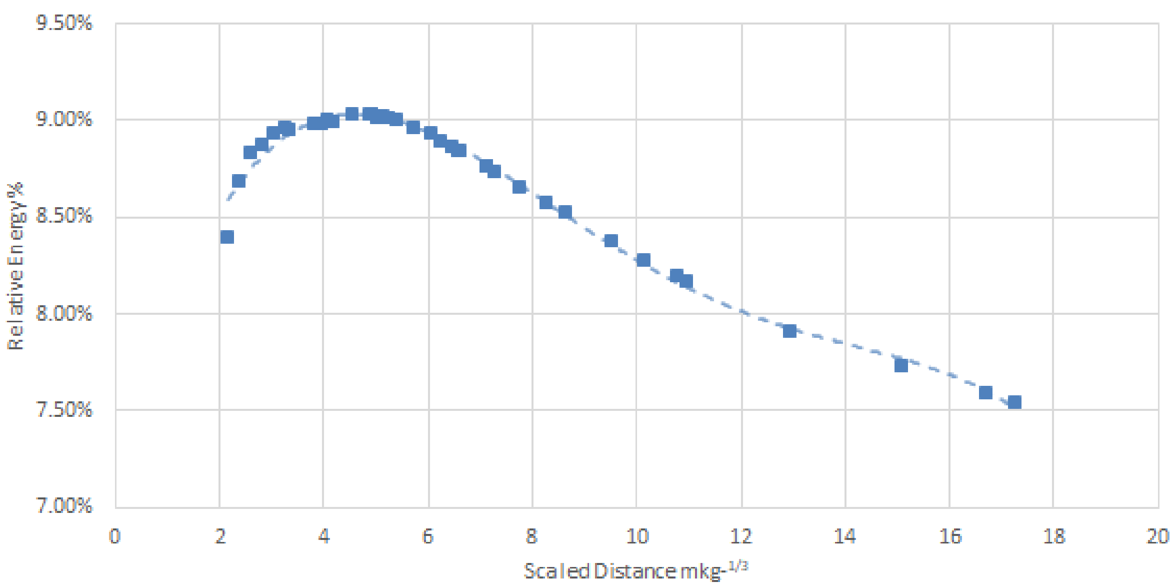

Figure 7.6: Relative energy of TNT at each scaled distance calculated from the energy per kilogram of TNT from the measured pressure data divided by the total energy available in TNT from Swisdak Method

Figure 7.5 and Figure 7.6 suggest that between a scaled distance of 2 and 4 $mkg^{-\frac{1}{3}}$, the energy transmitted within the shock wave (and therefore relative energy) increases, before then decreasing again almost linearly with scaled distance. A scaled distance of 2 $mkg^{-\frac{1}{3}}$ is outside of the fireball zone where the shock wave has separated from the fireball and so the shock wave would generally be assumed to be constant at this point, rather than being expected to shown an increase and then decrease of energy over a short scaled distance. It should also be noted that there are some discrepancies between the papers produced by Sadwin and Swisdak in the energy flux equation with the characteristic impedance being excluded outside of the integral in some cases ([136] and [147] but inside the integral in others [137]). The author trialled the characteristic impedance outside of the integral but this gave unrealistic results that did not take into account how the characteristic impedance would change with overpressure, and therefore considers including it inside the integral to be correct.

7.4 Energy Flux Calculations for TNT Based on Grisaro Method

Grisaro used a different methodology for calculating the energy flux. Using the same pressure-time curves used in Section 7.3, the method will be applied and values calculated.

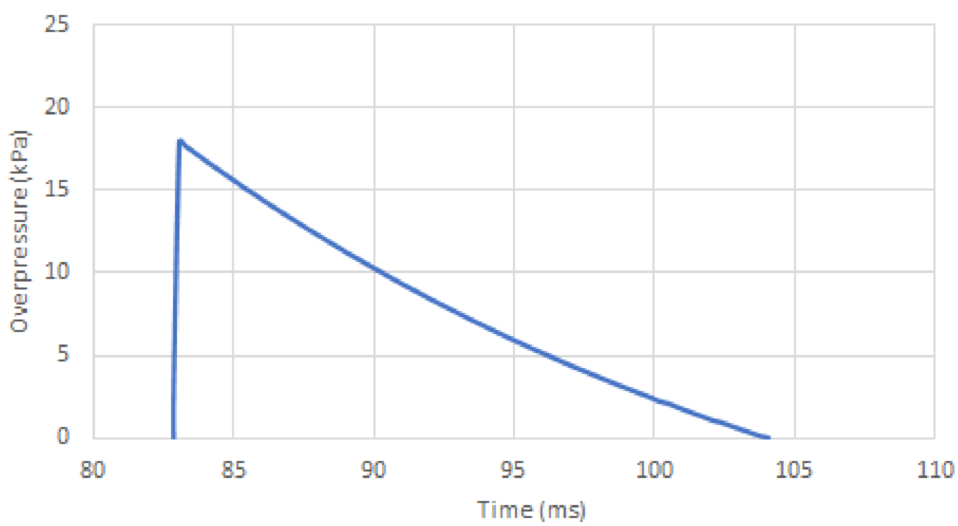

Figure 7.7: ConWep incident pressure-time curve for 100 kg at 40m

1. Using the equations in Section 2.2, the particle velocity at each time step is calculated:

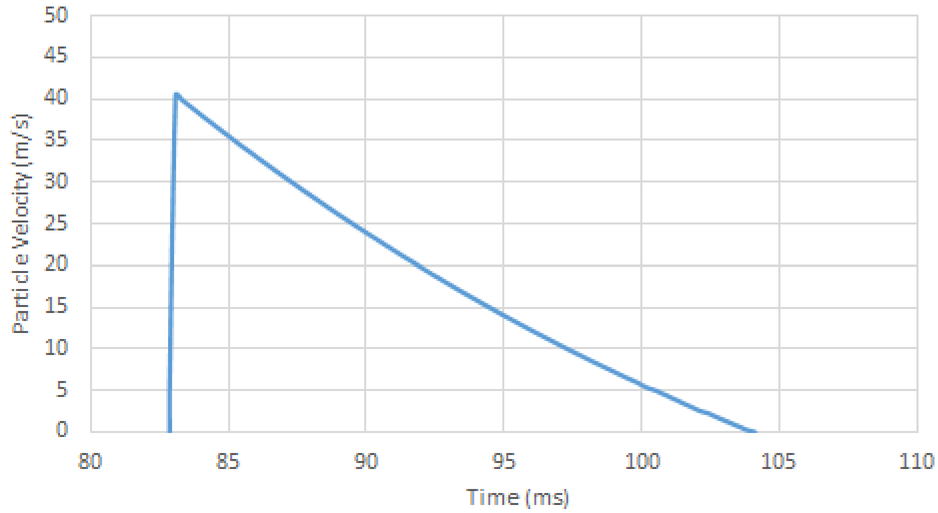

Figure 7.8: Characteristic impedance for incident pressure-time curve for 100 kg at 40m

2. Next the square of the pressure values are multiplied by the particle velocities at each time step:

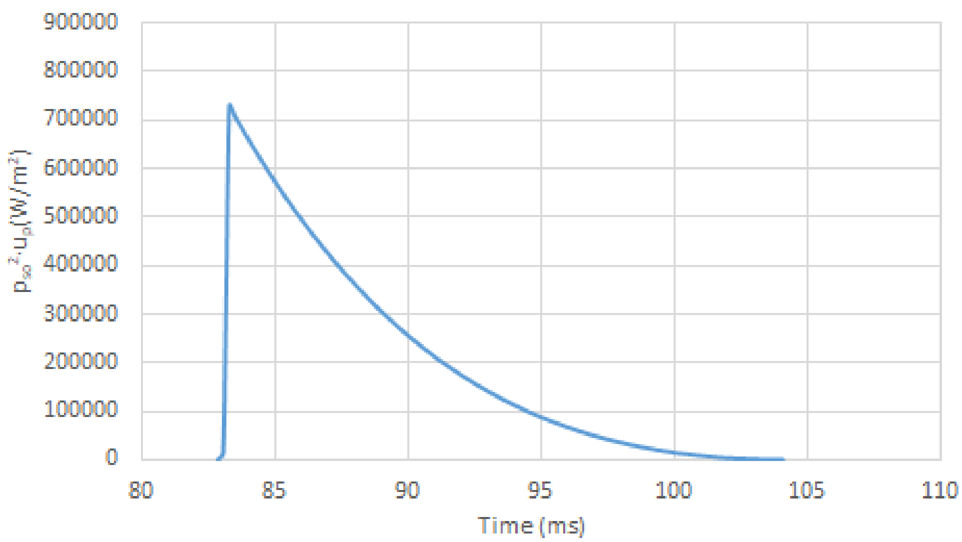

Figure 7.9: p_{so}^2 multiplied by $\rho\mu$ for 100 kg at 40m

3. Next the integral of the above curve is produced. This was calculated using the trapezoidal method.

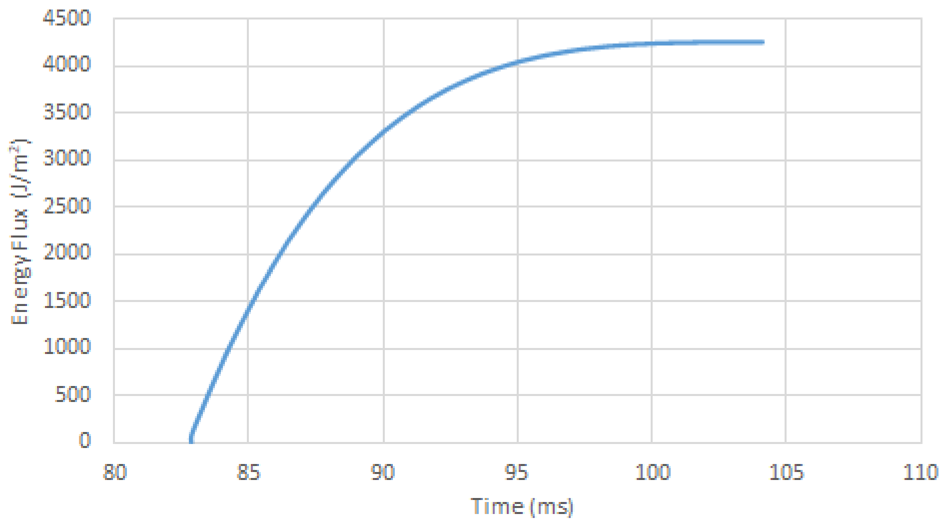

Figure 7.10: Integral of p_{so}^2 multiplied by $\rho\mu$ for 100 kg at 40m

4. The peak of this integral gives the value for energy flux as $4251.14J/m^2$.

5. The surface area for a 40 metre radius hemisphere is given by $= 2\pi r^2 = 2 \cdot \pi \cdot 40^2 = 10,053.1m^2$

6. The total shock energy is the energy flux multiplied by the surface area.$= 4251.14 \cdot 10053.1 = 42,737.16kJ$

7. The energy per kilogram of TNT is given by the total shock energy divided by the mass of explosives $= 42,737.16/100 = 427.37kJ/kg$

8. The relative energy is calculated by dividing the energy per kilogram measured in the blast from the energy flux, divided by the amount of available energy in one kilogram of TNT $= 427.37/4560 = 9.37\%$

The above steps to calculate total shock energy, energy per kilogram and relative energy were conducted on 42 pressure-time curves from varying charge sizes of 25 kg to 200 kg and scaled distances between 2 and 18 $mkg^{-\frac{1}{3}}$. The output was used to produce graphs of how the energy per kg of TNT and relative energy vary with scaled distance.

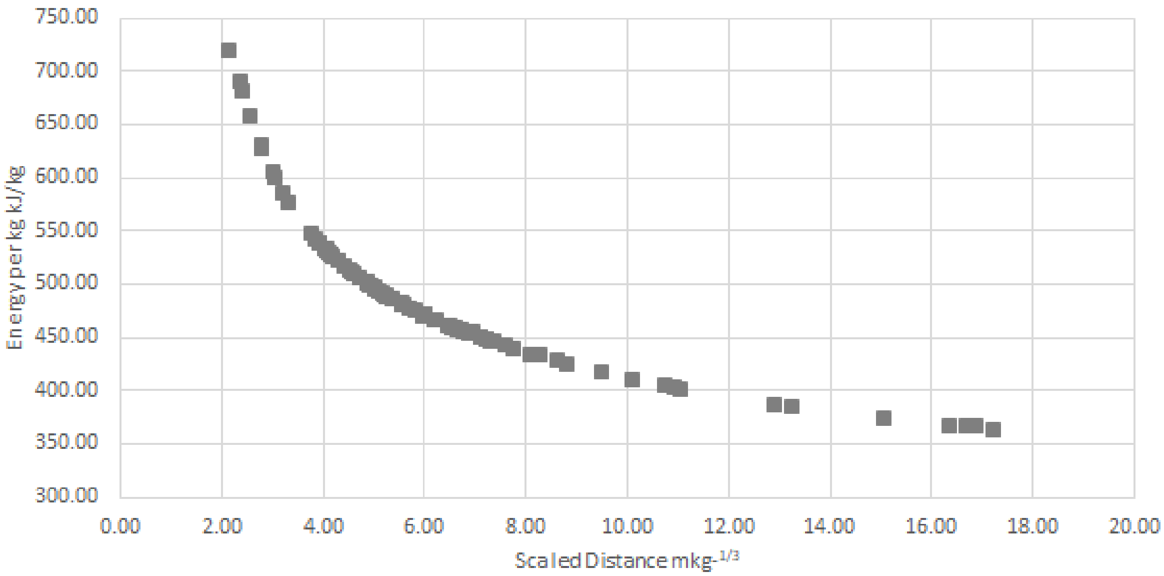

Figure 7.11: Total shock energy calculated at each distance divided by the mass of explosives to give energy per kilogram of TNT with scaled distance from Grisaro Method

This graph suggests very clearly that the energy carried in the shock wave that is measured at a set stand-off varies considerably with scaled distance regardless of charge size; larger values of total energy flux are measured at smaller scaled distances. As the distance from the charge increases, the energy per kilogram calculated decreases as the energy is dissipated over a wider area. No measurements have been taken at the smaller scaled distances due to the difficulties in producing usable pressure-time curves, but if it were possible to do so, it would be expected that the total energy flux at a very small distance would approach the total energy released in the detonation.

By comparing the amount of energy per kg with the amount of energy available in a single kilogram of TNT, the relative energy can be calculated and assessed as to how it varies over scaled distance.

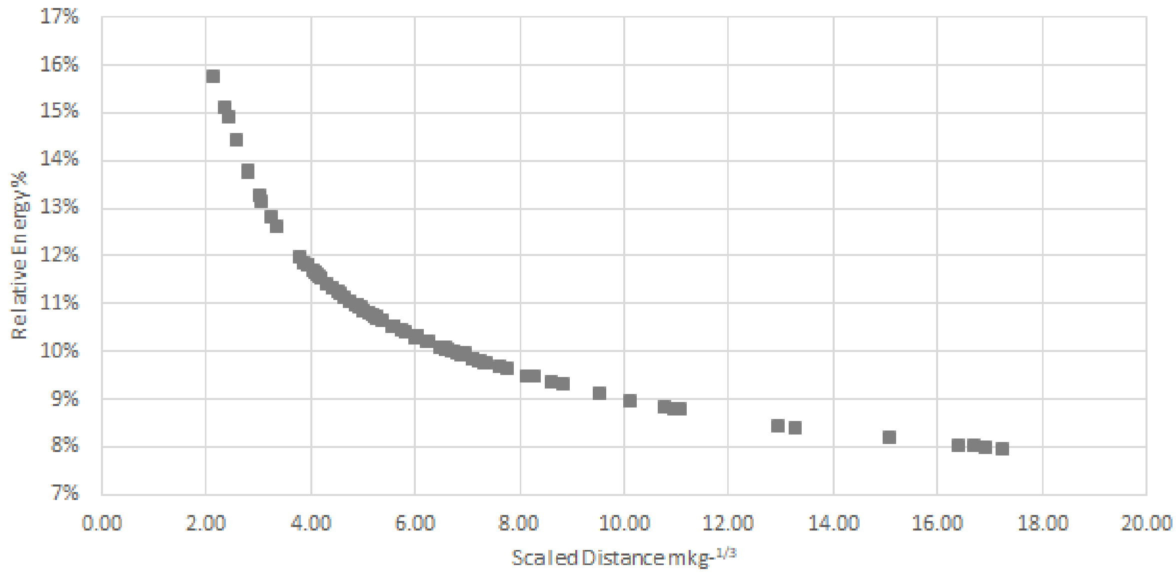

Figure 7.12: Relative energy of TNT at each scaled distance calculated from the energy per kilogram of TNT from the measured pressure data divided by the total energy available in TNT from Grisaro Method

This graph, and the previous one, show that, despite the same amount of energy being available in the explosive, the further away the target, the lower the amount of energy that is converted to blast pressure. This is as expected as the shock wave loses velocity and therefore energy as it travels over distance, potentially due to the heating up of a greater volume of air. This method produces a more reliable and scientifically sound result compared to the Swisdak method and will therefore be used for calculations of energy flux in the remainder of this chapter.

7.5 Sensitivities of Energy Flux Calculations

Calculating the energy flux relies on the full pressure-time curve of each measurement. If the pressure-time curve is not complete due to instrument damage or faults, or is a particularly noisy curve due to external impacts (as discussed in Section 4.1) then, when it is squared and multiplied by the particle velocity, this noise is amplified significantly producing an unreliable, potentially artificially high or low value for the energy flux. For these studies, pressure-time curves for each pressure measurement were loaded in to the graphing programme DPlot and a Modified Friedlander Curve fitted, based on the time of arrival as shown in Figure 2.13. This takes into account every data point but fits a smooth curve to noisy pressure-time data that can be used for the energy flux calculations. Where there was an incomplete pressure-time curve, although it may have been acceptable for determining a time of arrival and peak pressure, since the trace was incomplete these have been omitted from the data set.

All data collected in the trials assessed in this thesis have involved spherical charges placed a small distance above a large flat concrete pad and so the shock wave can be considered a uniform hemispherical shape. If a charge is shaped, the energy flux can still be calculated at any given distance from the charge, but the shape of the shock wave from the charge will not be uniform across the hemisphere or sphere. This means that it would not be possible to calculate a total energy flux or energy per kg based on pressure curves from a set distance.

If a charge is cased in any way, for example in metal casings, energy is lost in the detonation process through the break up of the casing and the fragmentation throw. The energy flux would still be able to be calculated and the total energy released calculated. However the relative energy would be expected to be significantly lower than that of a bare charge, depending on wall thickness of the casing.

As would be expected, the energy flux is dependent upon the charge size and the stand-off, showing a positive correlation with charge size, and an inverse correlation to the stand-off distance. To test if the Hopkinson-Cranz scaling law (Figure 2.9) is valid for energy flux as well as pressure, impulse and time of arrival, the measured energy flux for TNT at various stand-off distances and charge sizes has been compared with the scaled energy flux calculated according to the Hopkinson-Cranz law as the energy flux divided by the charge size to the power of -1/3. This has been plotted in Figure 7.13 which clearly shows that, once the scaling law has been applied, there is a clear relationship between the energy flux and distance.

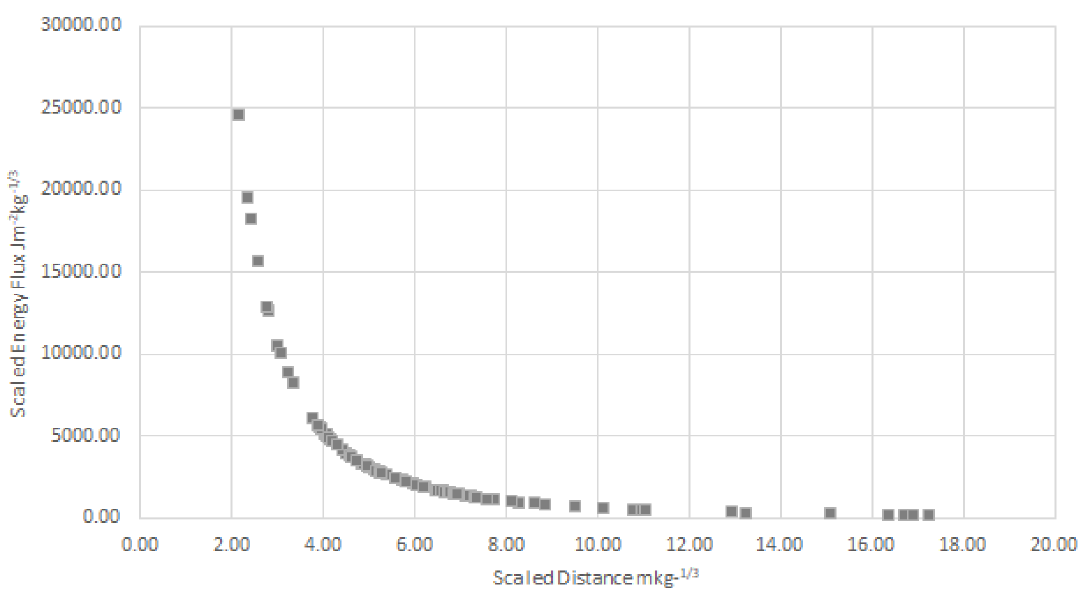

Figure 7.13: Scaled energy flux vs scaled distance for TNT

To investigate the validity of this method of calculating TNT equivalence using energy flux, this method will be applied to Nitromethane, PE4 and ANFO in the next sections.

7.6 TNT Equivalence of Nitromethane using the Energy Flux Method

Using the process described in Section 7.4 it is possible to calculate a TNT equivalence based upon energy flux by comparing the energy per kg of another explosive with that of TNT. The energy flux, total available energy, energy per kilogram and relative energy were calculated for Nitromethane using 147 pressure-time curves from the data from Section 5. Each pressure-time curve was smoothed with a smoothing window of 20 points and had an exponential curve fitted as described in Figure 2.13. It was this exponential curve that was used to calculate the energy flux. Where there were repeats of distance from charge, the average of the calculated values were taken. The same charge size was used in every measurement. Figure 7.14 shows the energy flux against scaled distance. Figure 7.15 shows the energy per kilogram of Nitromethane, calculated from the total available energy divided by the charge mass. The values on the y-axis have all been redacted.

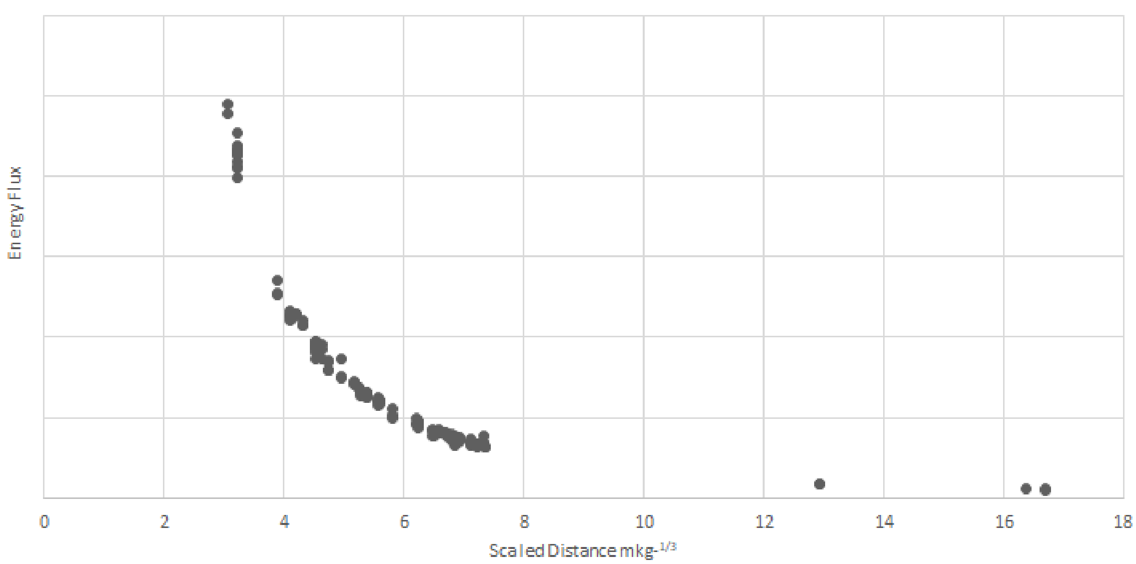

Figure 7.14: Energy flux vs scaled distance for Nitromethane (values redacted)

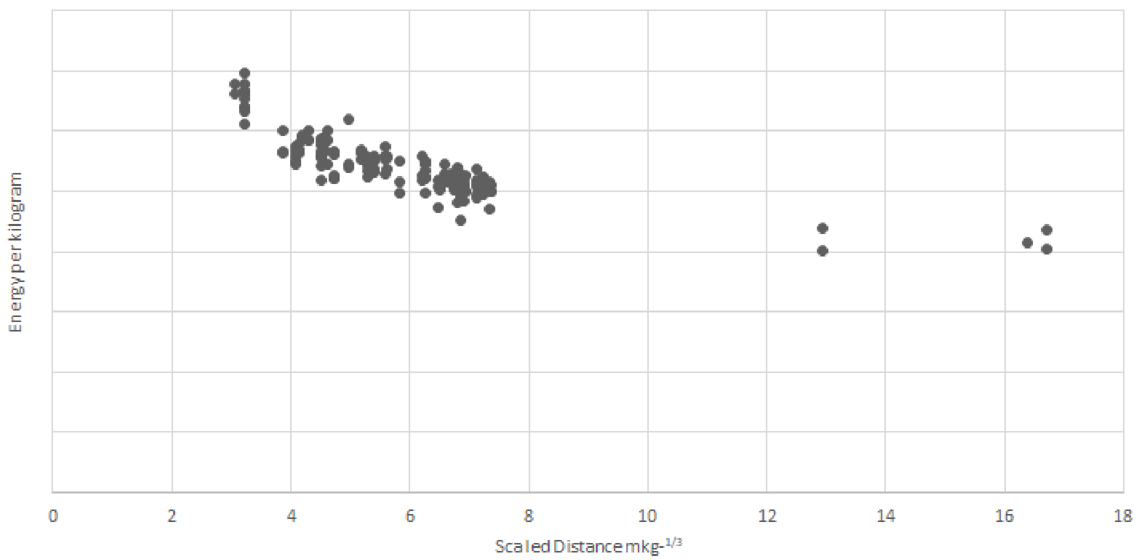

Figure 7.15: Energy per kg vs scaled distance for Nitromethane (values redacted)

By dividing the energy per kg of Nitromethane, by that of TNT calculated in Section 7.3, it is possible to determine a TNT equivalence based on energy flux, taking into account how this may change over scaled distance. Where there was more than one value per scaled distance, the average value was taken and used to calculate the equivalence factor. As previous, the y-axis has been redacted.

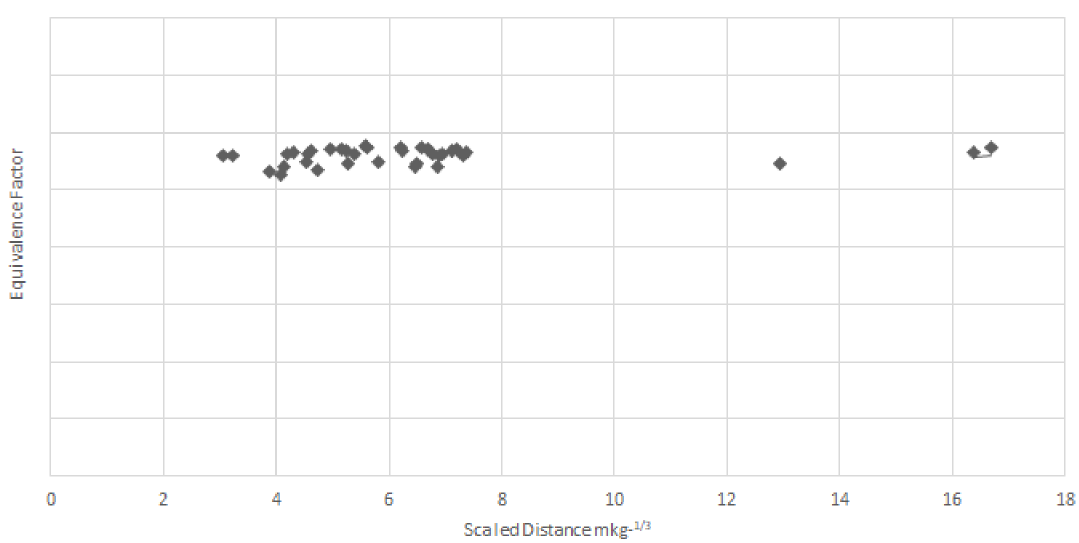

Figure 7.16: TNT equivalence vs scaled distance for Nitromethane (values redacted)

Despite the difficulties in displaying this data redacted, it can be seen that, although there is no definitive single value for TNT equivalence with variation even at very similar scaled distances, the spread is quite minimal. To assist in understanding the variation, the standard deviation has been calculated as 0.042 equivalence factor variation. This is actually surprisingly small, and therefore suggests that taking an average value across all the scaled distances shown in this data set for the TNT equivalence would give a valid and constant equivalence factor regardless of stand-off. To investigate this method further, other explosive types with known and publishable TNT equivalence factors will be compared.

7.7 TNT Equivalence of ANFO using the Energy Flux Method

The process displayed in Section 7.6 has been repeated for ANFO (Ammonium Nitrate Fuel Oil) using 37 pressure-time curves collected over five tests. The explosive set up for this was very similar to that of the Nitromethane tests, with a spherical charge located 1.2 metres above a steel plate located on a flat 100 m x 100 m concrete pad. The ANFO was commercial grade and initiated using a 450 gram Pentolite ANFO booster. This 450 g booster has been included in the overall explosive weight for each test. The tests were conducted using charge sizes of between 31.25 kg and 250 kg of ANFO with scaled distances between 3.3 and 10.9 $mkg^{-\frac{1}{3}}$. The considerations from Section 4 were also taken into account for these tests. The individual pressure-time curves were smoothed with a smoothing window of 20 points and then a exponential curve fitted, which was then used for the calculation of the energy flux. Whereas the previous Nitromethane tests considered only one charge size, to enable investigation as to whether the charge size has an effect upon the energy flux and the TNT equivalence, each charge size has been plotted separately on the graphs, allowing identification of any differences that may occur between the different charge sizes. Since Figure 7.13 concluded that the Hopkinson-Cranz Scaling Law was reliable for energy flux, the law has been applied to this data. Figure 7.17 shows scaled energy flux versus scaled distance for the five different charge sizes.

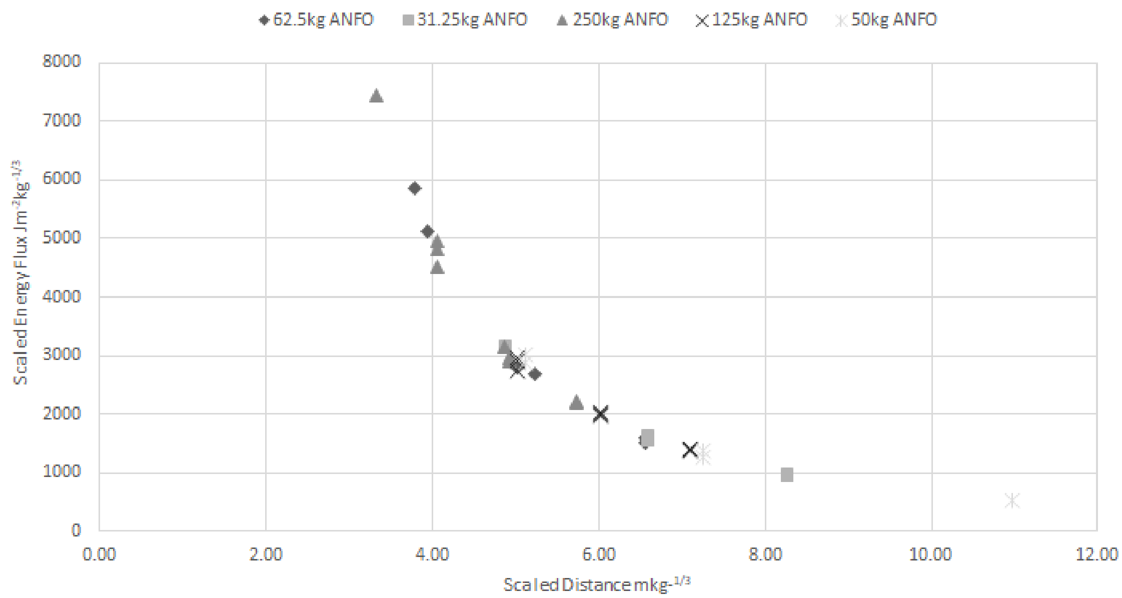

Figure 7.17: Scaled energy flux vs scaled distance for ANFO

The energy per kilogram was next calculated by dividing the energy flux values by the mass of explosive used.

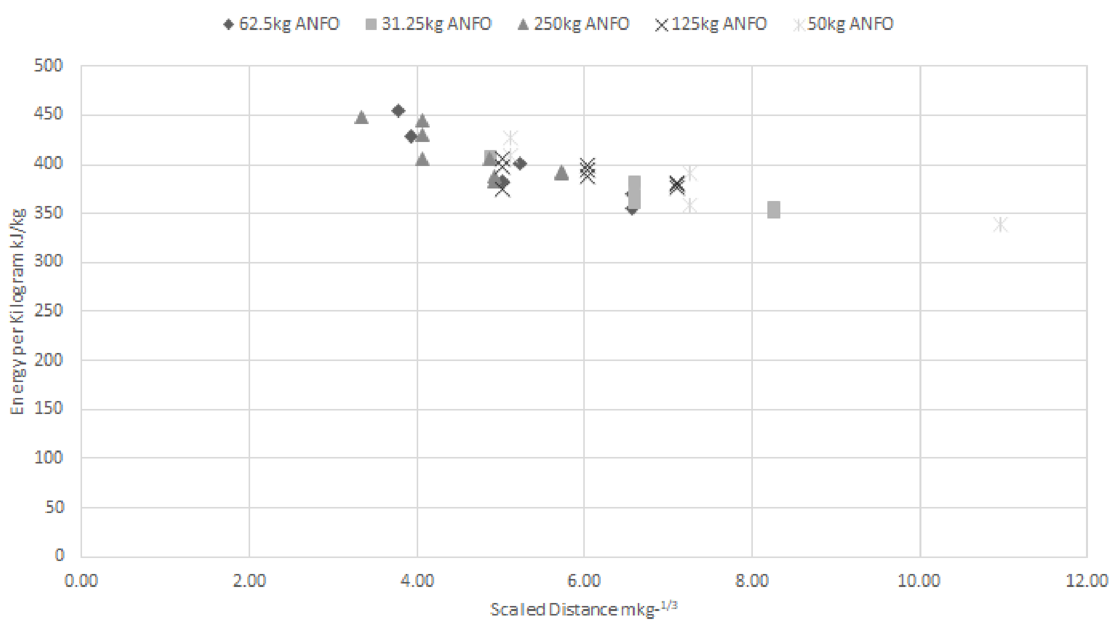

Figure 7.18: Energy per kg vs scaled distance for ANFO

By dividing the energy per kg of ANFO by that of TNT as calculated in Section 7.3, the TNT equivalence of ANFO can be calculated based upon the energy flux, taking into account the possibility of this changing over scaled distances. Where there were multiple values for a single scaled distance, an average for energy per kilogram was calculated.

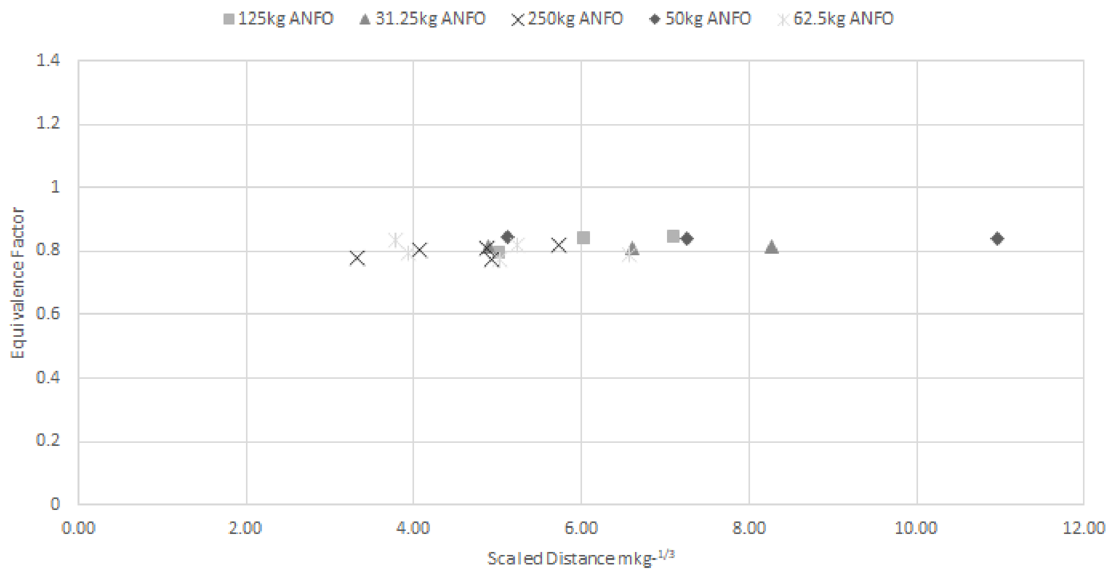

Figure 7.19: TNT equivalence vs scaled distance for ANFO

Figure 7.19 suggests an average TNT equivalence factor of 0.81, meaning that 1.23 kilograms of ANFO would be required to produce the same energy flux as 1 kilogram of TNT. This aligns closely with the TNT equivalence factor 0.82 given in Figure 2.8 [1]. The standard deviation over the 37 measurements is 0.028. This is not a statistically significant variation and does not appear to change over scaled distance, implying that a single value of TNT equivalence for ANFO is valid between the scaled distances of 3.3 and 10.9 $mkg^{-\frac{1}{3}}$ for charge sizes in the range of 31.25 kg to 250 kg.

7.8 TNT Equivalence of PE4 using the Energy Flux Method

The process displayed in Section 7.6 has again been repeated for PE4 using 46 pressure-time curves collected over six tests. The blast pressures were measured using charge sizes of between 2.5 kg and 128 kg of PE4 with scaled distances between 2.43 and 13.26 $mkg^{-\frac{1}{3}}$. The setup for the PE4 explosive charges was similar to that of the Nitromethane and ANFO trials, comprising a spherical charge positioned 1.2 metres above a steel plate located on a flat 100 m × 100 m concrete pad. The shock wave has been assumed to be hemispherical. To investigate if the charge size has an effect upon the energy flux and the TNT equivalence, each charge size has been plotted separately on a graph to identify any differences that may occur. Figure 7.20 shows scaled energy flux versus scaled distance for the five different charge sizes.

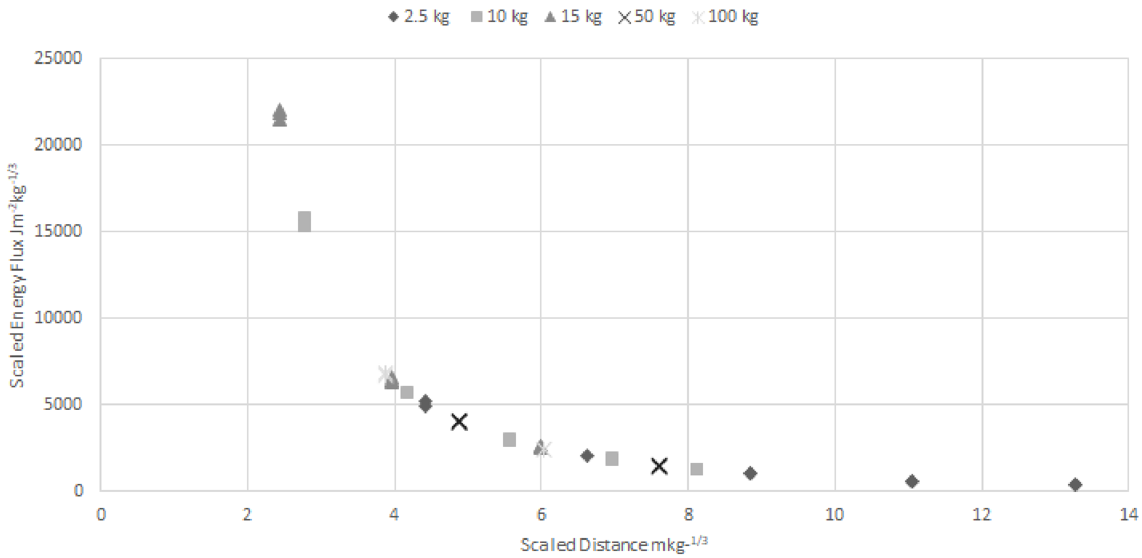

Figure 7.20: Scaled energy flux vs scaled distance for PE4

The values of energy flux were divided by the mass of the explosive in order to calculate the energy per kilogram of PE4. This has been plotted in Figure 7.21.

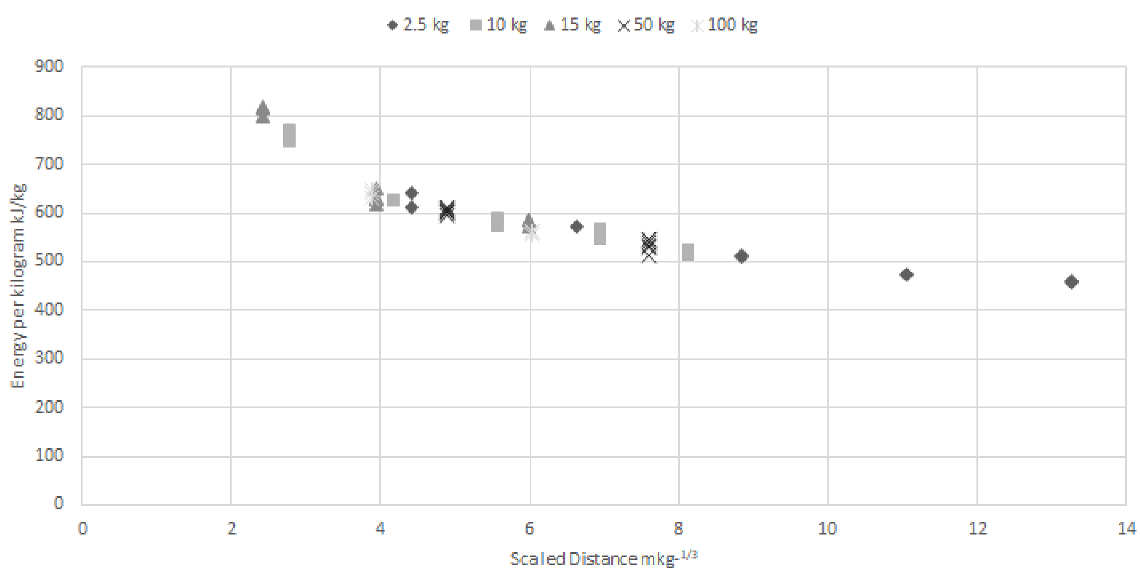

Figure 7.21: Energy per kg vs scaled distance for PE4

By dividing the energy per kg of PE4 by that of TNT as calculated in Section 7.3, a TNT equivalence for PE4 has been calculated based on energy flux, taking in to account the scaled distances. Where there were multiple values for a single scaled distance, an average for energy per kilogram was taken.

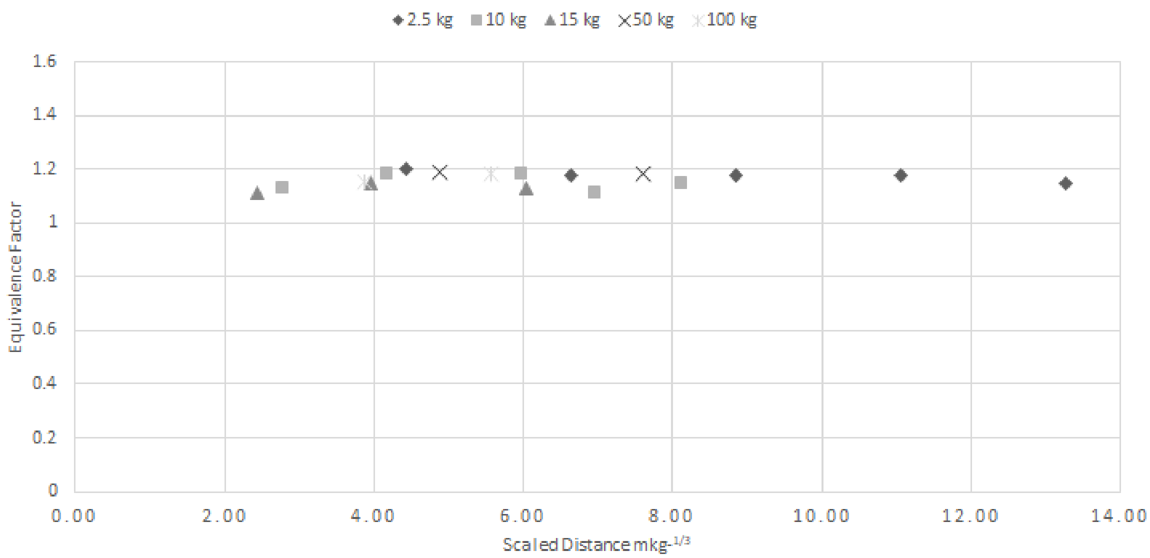

Figure 7.22: TNT equivalence vs scaled distance for PE4

When all the values of TNT equivalence for each measurement are considered, Figure 7.22 provides an average TNT equivalence Factor of 1.2 with an upper value of 1.25 and a lower value of 1.14, implying that 0.83 kilograms of PE4 would be required to produce the same energy flux as 1 kilogram of TNT. Figure 2.8 [1] provides TNT equivalence factors for pressure of 1.2 and for impulse of 1.08. The value calculated here aligns with the higher of these suggesting that the TNT equivalence factor calculated from energy flux more closely aligns with that of the equivalence factor based upon pressure. This also matches the results from Rigby and Sielicki, in which they calculated a TNT equivalence of 1.2 for positive phase parameters [128]. The standard deviation over the 46 measurements in the above data set is 0.024. This is minimal variation and does not appear to change over scaled distance, implying a single value of TNT equivalence for PE4 is valid over scaled distances of 2.43 to 13.26 $mkg^{-\frac{1}{3}}$ for charge sizes between 2.5 kg and 100 kg. There is a suggestion from the data that for scaled distances below 4 the equivalence factor reduces to 1.18 - this is based upon 12 measurements from 3 charge sizes at 4 different scaled distances. It would be recommended that more measurements are undertaken to confirm it.

7.9 Energy Flux for Calculating TNT Equivalence in Vapour Cloud Explosions

Although this thesis concentrates on the effects and parameters produced from high explosives, vapour cloud explosions as a result of gas releases of hydrocarbons or hydrogen can produce comparable devastating effects, particularly if the detonation of the vapour cloud produces significant overpressures, and more often longer durations and therefore high loading [17]. This has been seen on multiple scales, ranging from domestic gas explosions up to large detonations such as those seen at Buncefield [27] and Jaipur [85]. As part of a commitment to decarbonisation within the global energy transition, there is a large push to introduce hydrogen both domestically and commercially as a commonplace fuel to replace natural gas. When considering this transition, it is vital to consider the effects on public safety which could be considerable due to properties of hydrogen including wide flammability limits, very low minimum ignition and very high burning velocities.

7.9.1 Hydrogen Detonation Setup

Consistent with the arena trial setup for high explosive charges, the setup for the hydrogen cube involved locating pencil pressure gauges at set distances from the hydrogen detonation. To produce the detonation, a polythene sheet cube with dimensions 2.5 × 2.5 × 2.5 m, producing a volume of $15.6m^3$ was clamped to a concrete pad. A feed of air and hydrogen was supplied to the side of the cube, initially at 7 bar, but controlled through a rotameter to enable the target concentration to be met. As the fuel-air mixture enters the polythene cube it inflates as seen in Figure 7.23. Two oxygen sensors were located inside the polythene cube: one at the inlet point; the other centrally at the base adjacent to the initiation point allowing accurate measurement of the concentration of hydrogen in the cube. In order to initiate a detonation of the hydrogen-air mixture, a 30 gram Semtex booster charge was moulded around a non-el detonator and initiated using shocktube. The booster and detonator were located centrally at the base of the cube. The concentration at the time of ignition was 33.2 % gas in air, equating to 0.434 kg of Hydrogen which, when combined with the 30 grams of high explosive gives a the total mass of 0.464 kg. Dewey in his 2014 paper [47] discussed the difficulties in identifying parameters in experimental trials of vapour cloud explosions; despite the difficulties he agreed that over the scaled distances considered in this study the Friedlander curve was a good fit for detonation waves from a vapour cloud explosion.

Figure 7.23: Setup of Hydrogen cube with fuel-air feed input bottom left

7.9.2 Results

Figure 7.24 shows four stills from a video of the detonation of the hydrogen-air mixture from a 3000 f.p.s high speed Photron Fastcam [115]. The pressure-time curves from one of these trials can be seen in Figure 7.25.

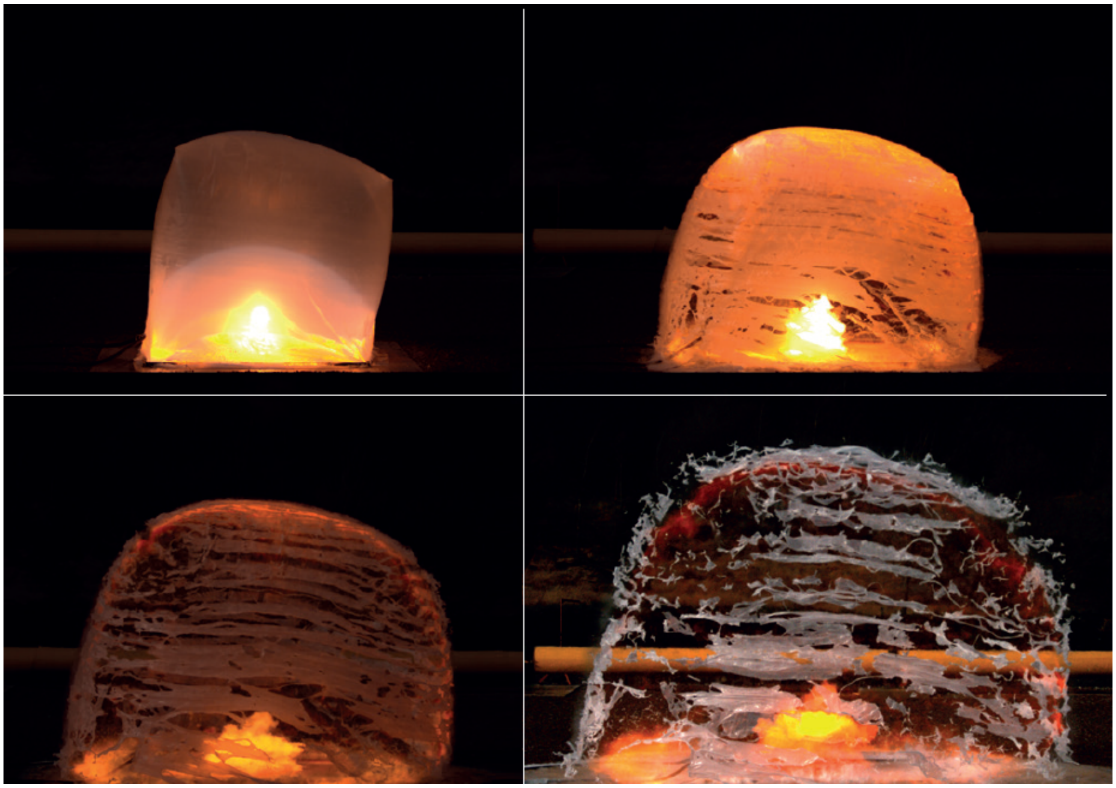

Figure 7.24: High speed video frames of detonation of the Hydrogen cube

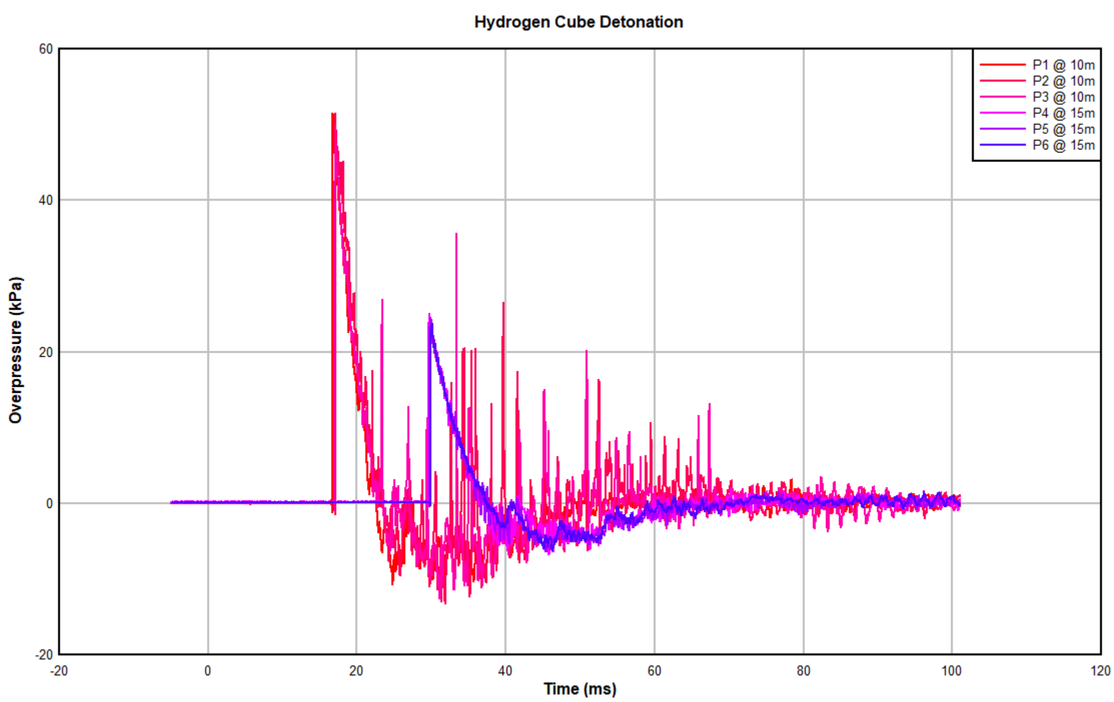

Figure 7.25: Pressure-time curves from Test 1

7.9.3 Energy Flux and TNT Equivalence Calculations

Using the same methodology as for high explosives earlier in the chapter, the curves were smoothed and a modified Friedlander Curve fitted. This curve was then used to calculate the energy flux using the Grisaro method. Once the energy flux was calculated, the total air blast energy and energy per kilogram of Hydrogen (plus booster) was calculated. The energy per kilogram of Hydrogen was then compared to that of TNT to produce a TNT equivalence with scaled distance. These steps can be seen in Figure 7.26 to Figure 7.30.

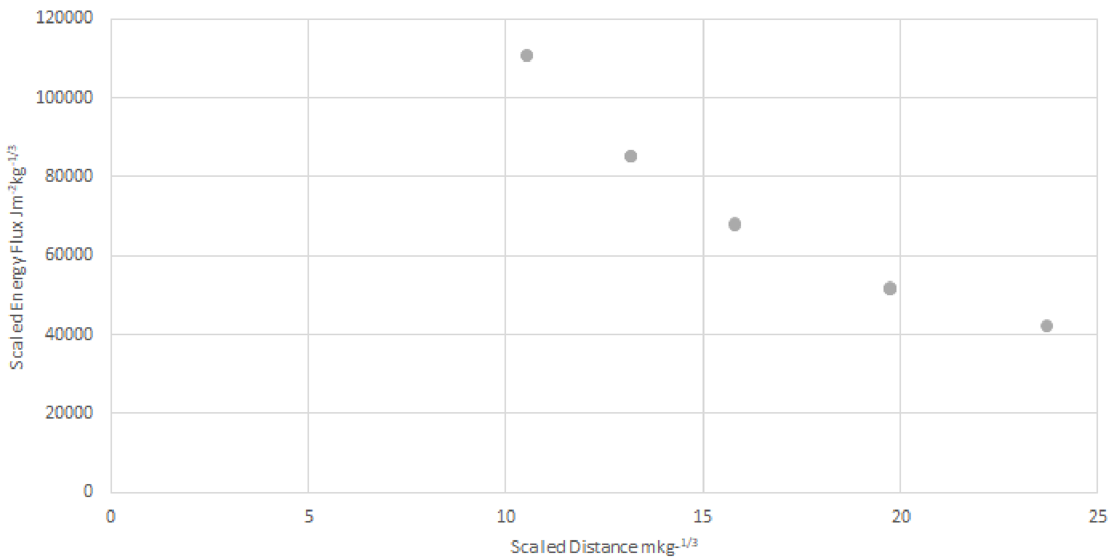

Figure 7.26: Scaled energy flux vs scaled distance

The energy flux at each distance was multiplied by the surface area of the shock wave hemisphere to provide a total air blast energy at each distance.

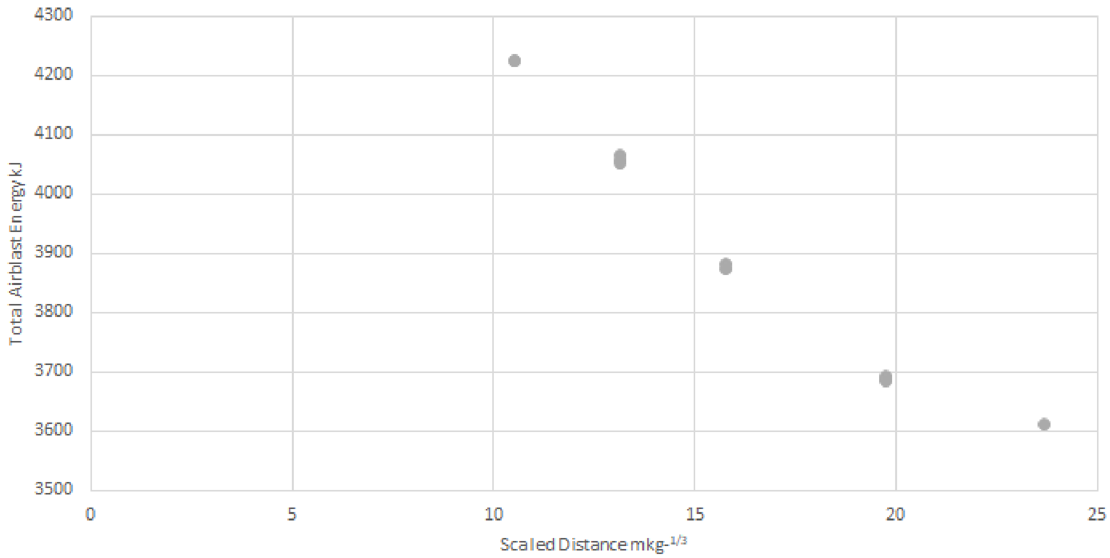

Figure 7.27: Total air blast energy vs scaled distance

The total air blast energy at each distance was then divided by the total mass of Hydrogen (plus booster) to provide an energy per kilogram value.

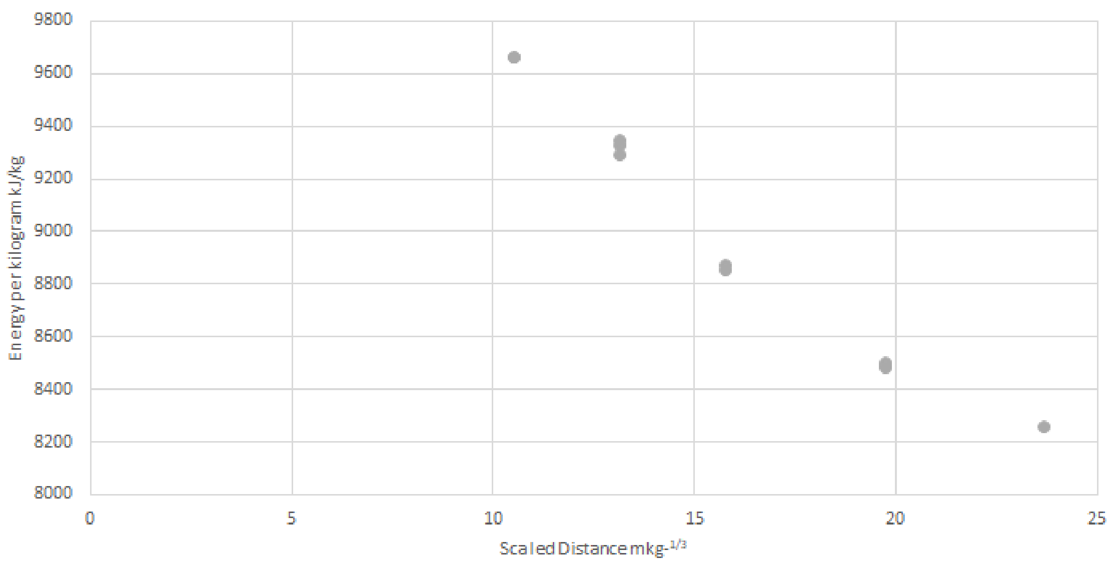

Figure 7.28: Energy per kilogram of Hydrogen vs scaled distance

Based upon the calorific value of Hydrogen of 141,900kJ [30], the relative efficiency of the blast can be calculated based upon the amount of energy measured at the set distance divided by the total energy available.

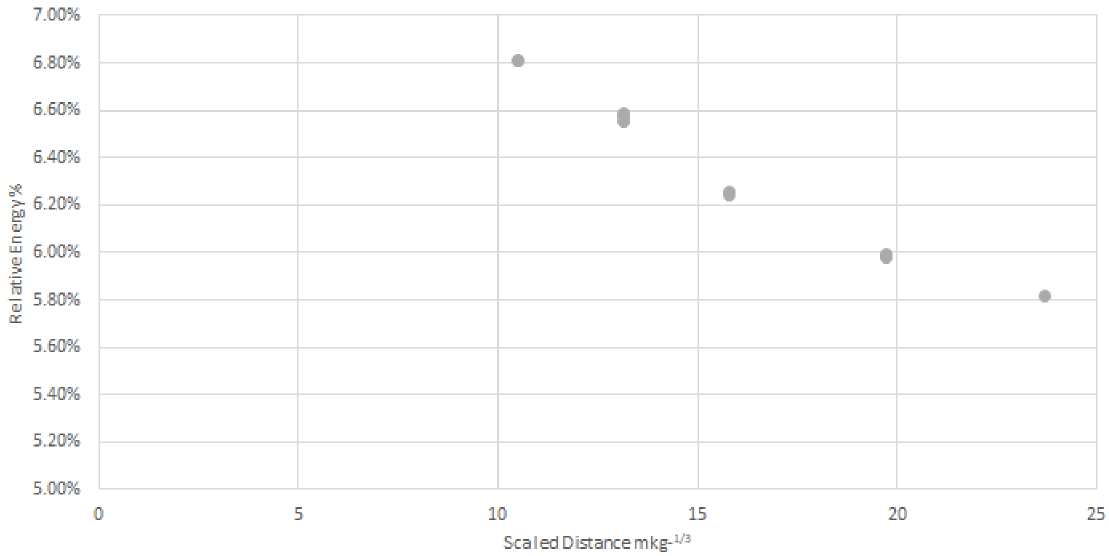

Figure 7.29: Relative energy of Hydrogen vs scaled distance

The energy per kilogram value of Hydrogen at each distance was compared directly to the equivalent energy per kilogram of TNT of the same mass at the same distance to provide a TNT equivalence for Hydrogen.

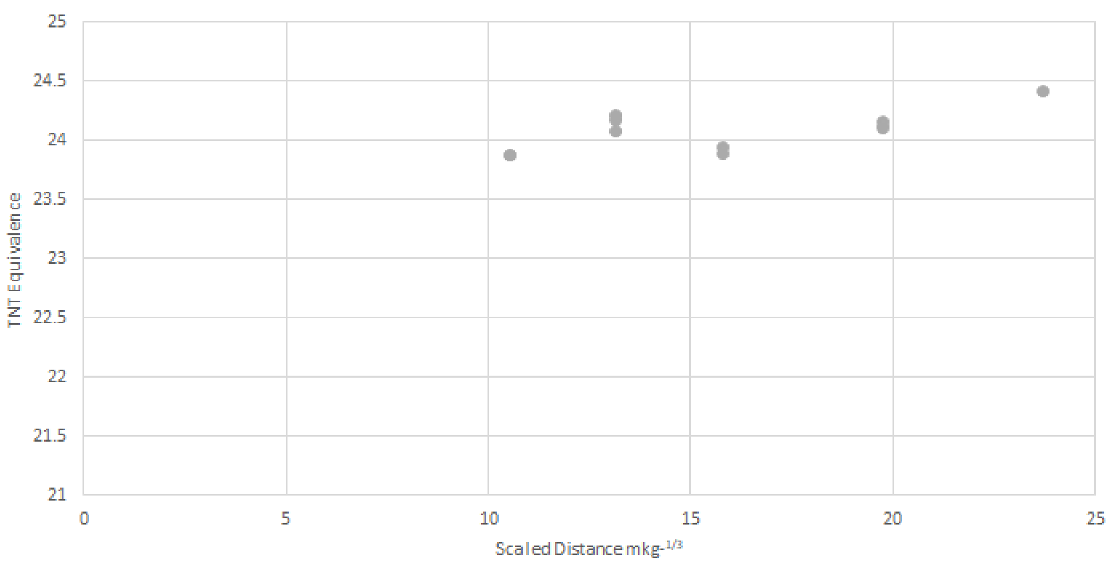

Figure 7.30: TNT equivalence of Hydrogen vs scaled distance

The method given in CCPS Guidelines for Vapour Cloud Explosions, Pressure Vessel Burst, BLEVE and Flash Fire Hazards [30] provides a methodology for calculating the TNT equivalence of a vapour cloud explosion utilising the below equation:

$$W_{TNT} = \alpha_e \frac{W_f H_f}{H_{TNT}} = \alpha_m W_f \tag{7.3}$$

where W_f =mass of fuel involved, W_{TNT} =equivalent mass of TNT, H_f =heat of combustion of the fuel, H_{TNT} =TNT heat of combustion, α_e =TNT equivalency based on energy and α_m =TNT equivalency based on mass. A theoretical maximum efficiency coefficient of 40 % is generally used for calculated the equivalency for vapour cloud detonations under atmospheric conditions with a value of 20% used for vapour cloud deflagrations [74]. However, most real-life incidents do not involve the full amount of available fuel, so the practical values for the TNT equivalence may be much lower than the theoretical upper limit. Gugan [72] and Pritchard [118] state that for historical incidents, this is typically between 1 and 10 %, based on the heat of combustion of the full quantity of fuel released. This is evident in figure 7.29 which suggests that between 5 % and 7 % of the available energy in the Hydrogen is converted to air blast energy.

Using Equation 7.3, a mass of fuel of 0.437 kg of Hydrogen, a heat of combustion of Hydrogen of $141.9 MJ/kg$, a heat of combustion for TNT of $4.6 MJ/kg$ and a maximum theoretical efficiency of 40%, a TNT equivalence charge size of 5.5 kg is calculated, and therefore a general TNT equivalence factor of 12.5. Using the average of the values calculated in figure 7.30, this gives a TNT equivalence of 24.06, and an equivalent explosive charge size of 10.5 kg, significantly higher than that calculated using the method in the CCPS guidelines.

However, both these methods are potentially flawed for calculating TNT equivalence in a detonating volume of gas. Once a detonation wave has been triggered in a vapour cloud, as long as the fuel-air mixture is within the detonation limits (generally considered to be very close to the flammability limits of a fuel - for hydrogen in air the exceedingly wide range of between approximately 8 and 85 %), then the detonation wave will propagate, producing the same burning velocities and overpressure regardless of the mass of fuel within the cloud [30]. Therefore, in an incident, if the extents of the vapour cloud size is known, and it is known that the vapour cloud detonated, the actual value for mass and therefore concentration of fuel in the vapour cloud could vary significantly whilst still producing the same overpressures and impulses. The author theorises that, through assessment of damage in an incident to produce estimations on overpressure and impulse, a TNT equivalence can be produced for the vapour cloud based upon the upper and lower masses of fuel in the detonating cloud. Based on the detonation limits, a 15.6 m^3 fuel-air cloud as used in the setup described in Section 7.9.1 could contain between 0.104 kg (8 % fuel in air) and 1.11 kg (85 % fuel in air) of Hydrogen to produce the same overpressure and impulse loadings.

7.10 Energy Flux Conclusions

Both the Grisaro and Swisdak methods of calculating energy flux were used to produce energy flux values from the pressure-time curves calculated using ConWep. These are smooth and reliable curves and the most appropriate for testing two separate methods. The results showed the Grisaro method to be more reliable and in keeping with expected behaviour of a shock wave, particularly as the Swisdak method showed the energy flux increasing in the early scaled distances before then decreasing. If this increase was seen at scaled distances where measurements would have been taken inside the fireball region, it might be expected that the energy flux measured may increase due to other influences. However, as this is not the case in these calculations one would not expect the energy flux to be impacted and therefore the rise shown by the Swisdak method does not have an explanation as to why this may occur. Outside of the fireball region, the energy flux per kilogram is expected to decrease with the square of the scaled distance as the energy in the shock wave is spread over the increasing hemispherical shell as the wave progresses away from the charge location. Since the Grisaro method aligned more closely with expected principles, this method was used to calculate the energy flux and the energy per kilogram of TNT from ConWep curves.

The Grisaro method for calculating energy flux was then utilised for Nitromethane, ANFO and PE4 to calculate energy flux, energy per kilogram and then a TNT equivalence. The values for Nitromethane were redacted but showed good consistency between scaled distances. For ANFO and PE4, the TNT equivalence factors were calculated and shown to align closely with values from literature such as that produced in ISO16933 [1]. The Grisaro method was then applied to a detonation of a cloud of Hydrogen to investigate the effectiveness of using the energy flux in determining the TNT equivalence of a vapour cloud detonation. The method was successfully applied producing a consistent value for the TNT equivalence of a $15.6m^3$, 33.2% fuel in air vapour cloud. However, it was discussed that due to the nature of detonations of vapour clouds, that once a detonation wave has been initiated, the burning velocity and therefore overpressure is a function of the extents of the vapour cloud, and not of the fuel concentration. Therefore, the method of using energy flux to produce a TNT equivalence can be used but it would be more appropriate to use it to produce upper and lower masses of fuel to produce a detonable vapour cloud. The values for TNT equivalence calculated using this method can be seen in Table 7.1.

Explosive/Fuel	Energy Flux Method
Nitromethane	redacted
ANFO	0.81
PE4	1.2
Hydrogen (detonation with explosive initiation)	25

Table 7.1: TNT equivalences calculated from the energy flux method

It should be noted that when using either method of calculating the energy flux, the eventual values are very sensitive to the quality of pressure-time curves. A variation in time of arrival could be the difference of a centimetre stand-off, will produce two different values of energy flux. This highlights the sensitivities of the blast parameters to setup and analysis of the experimental data when it comes to further calculations. It was for this reason that only data gathered with the revised methodologies were used, and when used, an exponential curve fit used to smooth the data. Despite this, there was still a wide variation of values at the same scaled distances. Regardless of the sensitivities, this method of producing energy flux has shown using this data to produce a single value of TNT equivalence for each explosive type, regardless of stand-off and charge size. It also takes in to account the atmospheric conditions at the time of firing, allowing for predictions of blast parameters based upon weather conditions for planning of trials.

8 Conclusions and Further Work

This chapter summarises and discusses the research presented in this thesis and makes recommendations for future work.

8.1 Summary

The TNT equivalence of an explosive is a standard way of expressing the energy released by an explosive in relation to that of TNT. There are many methods available to predict this value. However, no single definitive method exists, with methodologies usually chosen depending on the scenario in which the explosive is to be used. This thesis considered the way in which TNT equivalence can be calculated using experimental data, and contrasts the relative equivalence factors they produce, aiding an appropriate choice of methodology for future trials. Outside of controlled experimental trials, if an incident happens, whether a terrorist attack or accidental explosion, it is possible to use known parameters such as blast damage or time of arrival from CCTV and camera footage to calculate estimates for explosive charge size and/or equivalent TNT charge size using proven methodologies of calculating TNT equivalence. This thesis reviewed different methodologies of predicting explosive size for the Beirut Ammonium Nitrate incident in 2020.

This thesis has also shown the importance of fully understanding and considering the sensitivities of blast parameters when conducting experimental small and large scale trials for the production of reliable and accurate experimental data that can be used for further studies. When a trial is conducted and the blast pressure measured by gauges, this produces a curve that can be best described by the modified Friedlander pressure-time curve. This curve can be used to identify blast parameters such as the peak overpressure, time of arrival, impulse loading and positive phase duration. These parameters are sensitive to many factors that include explosive charge size, charge geometry, gauge type and interactions with structures. If the setup is fully and accurately known, it is possible to predict blast parameters using computer models such as ConWep and Air3d. This thesis has shown the output of these programmes to fit well with experimental data for predicting blast parameters, particularly time of arrival.

Using data collected at Spadeadam Research and Development over the past few years, analysis has been conducted on blast parameters for assessing the reliability and accuracy of the trials in one of the largest experimental comparisons seen in literature. This has involved comparing the data with prediction models, as well as assessing validity of the Hopkinson-Cranz Scaling Law. This law was shown to be valid for Nitromethane, PE4 and ANFO of charge sizes from 150 grams up to 640 kilograms with scaled distances between 2 and 14 $kgm^{-\frac{1}{3}}$. Understanding the validity of this scaling law allows conclusions to be drawn across variable charge sizes and distances.

Energy flux is a relatively new idea investigated by both Grisaro [70] and Swisdak [147]. Two methodologies were considered for the calculation of energy flux, with the Grisaro method deemed to be more appropriate. Energy flux was then calculated for variable charge sizes and charge stand-offs for Nitromethane, PE4 and ANFO. The energy flux was shown to scale according to the Hopkinson-Cranz scaling law. The values of energy flux from these explosives were compared to those calculated for TNT based on pressure-time curves produced by ConWep. Not previously investigated, the author compared the energy flux of TNT with that of other explosives, a TNT equivalence value was produced. For Nitromethane, PE4 and ANFO, this produced a TNT equivalence factor was shown to be constant regardless of charge size and stand-off for the ranges considered in this study, a key and new takeaway from this thesis. The values also provided a good fit with those produced in the literature. The same method was used to calculate the energy flux from a Hydrogen detonation, showing the same methodology can be applied to vapour cloud explosions.There are few and far between methodologies for calculating TNT equivalences for hydrogen and so this thesis provides a new methodology that could be further used for gases and high explosives alike.

Findings from this thesis have highlighted the importance of reliable measurements in experimental trials especially when the data is further used for model validation, incident investigation and methodology analysis. This thesis has considered only limited charge size, type and stand-offs, but shown that at least for the parameters considered, a good understanding of blast sensitivities can contribute to reliable and accurate data sets that can be used for further studies.

8.2 Conclusions

Conclusions of this thesis have been summarised below. They are listed in the order in which they appear in the thesis:

- Blast parameters measured in a blast test can be sensitive to the setup, explosive type and way in which they are measured. Confidence in the way blast parameters are produced allows for further use in the assessment of real-life incidents, model validation and further study.

- If the parameters are not understood, data can be produced that are not wholly reliable or suitable for further use. Although not a direct conclusion from this work, it is clear that if poor quality data is cited and used in studies to validate models or create predictions, there is a risk that inaccurate outputs could have serious ramifications if used to predict injury or blast protection.

- Improving the way measurements are taken and then analysed can produce a more accurate and reliable data set that can be used for further analysis studies. Small improvements in the way blast arenas are set out and measurements are taken have the ability to greatly improve the quality of the recorded data.

- Air3D and ConWep predictions for peak pressure, impulse, time of arrival and positive duration have excellent agreement with the data produced in experimental trials for Nitromethane and PE4 when the blast parameter sensitivities have been considered in the largest comparison of experimental data with these computer models seen in literature.

- Using the Coefficient of Variation is a good tool for analysis of variation of experimental data as it allows comparison across different parameters and scales. Calculating the Uncertainty Factor of data also allows for further comparison across experimental trials.

- Hopkinson-Cranz scaling law is valid for PE4, ANFO and Nitromethane charge sizes from 150 grams to 640 kilograms with scaled distances between 2 and 14 $kgm^{-\frac{1}{3}}$. The law was shown to be valid for overpressure, impulse, time of arrival, positive duration and even energy flux which had previously not been investigated prior to this thesis.

- The energy flux was calculated for TNT using values produced from ConWep. The energy flux was shown to decay over distance with the relative energy decreasing from 16% at smaller scaled distances to 8% at larger scaled distances. Energy flux has not been considered for TNT previously - this thesis provides a data set for TNT alongside other explosives for energy flux. The method was shown to be sensitive to the quality of pressure-time curves.

- Energy flux was calculated for PE4, Nitromethane and ANFO, and compared to that of TNT to producing a new way of calculating providing a TNT equivalence factor of 1.2 for PE4 and 0.81 for ANFO. It was shown that the value of TNT equivalence remained constant in the far-field. A preliminary study of the energy flux measured from a hydrogen vapour cloud detonation at 33.2% gas in air was conducted, producing a TNT equivalence factor of 25, showing that the energy flux method is also suitable for vapour cloud detonations. By proving this method for hydrogen as well as high explosives, it shows that this energy flux method could be used to study relative rates of energy release for non-ideal explosives, and can be linked directly to its TNT equivalence. This new methodology could be further used to determine TNT equivalence for cased charges and non-spherical explosive charges.

- This thesis has considered mostly hemispherical bare explosive charges with measurements taken in the far field in one of the largest experimental data sets from one author of its kind. There are many complex considerations that should be further investigated to enable the findings to be extended to real-world scenarios including cased charges and the effects of interactions of structures on the shock wave.

8.3 Future Work

This work has investigated parameters and TNT equivalence based upon specific geometries and test setups, often relating directly to test standards. These are standard and very repeatable, producing data sets that can be meaningfully directly compared. This final section discusses some of the complex scenarios that would be of interest for the conduct of further research into the impact of the blast parameters.

The effect of explosive casing has not been investigated in depth within this thesis. Multiple mechanisms can affect the detonation of a cased charge; for example the energy required to break up the case will be in turn mitigated by the additional energy build-up caused by the case. This would directly impact the energy flux measured at a set stand-off, causing a different relative energy and also TNT equivalence compared to a bare charge. The influence of case thickness and material will have a direct effect upon this and would be of interest to investigate further.

As discussed in the literature review, data is often produced from trials that may not be of the highest quality. Flaws in these trials can include poorly packed explosive charges, perhaps with non-uniform density or variable charge size. A study to investigate the effect of charge size versus density and the energy output would allow conclusions to be drawn as to whether it is is the mass or the diameter of the explosive that is the leading effect of the energy measured. Likewise, if the charge is not spherical or hemispherical, and therefore does not produce a spherical or hemispherical shock wave, can the measured energy flux be used to estimate a total available energy in the explosive charge by considering the different shapes and surface areas of the shock wave produced?

Predominantly at Spadeadam, charge sizes are rarely below 5 kg. By including some PE4 data produced by the University of Sheffield at Blastech in this thesis, this has extended the range of charge sizes investigated to 150 grams, but this was restricted only to the single explosive type. With this smaller charge size, smaller stand-off distances were also possible to measure. It would be beneficial to extend the studies conducted in this thesis to include a greater range of scaled distances for more explosive types, including Nitromethane and ANFO, particularly at the smaller scaled distances. Figure 6.22 showed the very small spread of data that had been considered in the PE4 study compared to that of literature, demonstrating the need to cover a wider range of scaled distances in order to investigate the validity further. It would be of interest to use the results of trials over a wide range of charge sizes to investigate whether the efficiency of an explosive varies with charge size.

Consideration has been made during this thesis to vapour cloud explosions. Historically, incidents involving vapour cloud detonations have been devastating, including Flixborough, Buncefield and Jaipur. With the ongoing energy transition, moving from a natural gas distribution system to one based on hydrogen, incidents may become more frequent. Hydrogen has a high burning velocity with a severe risk of transition to detonation if ignited. Further studies for understanding the energy produced from an ignited hydrogen vapour cloud are key for industry as hydrogen moves to a domestic fuel. The effect of confinement and congestion, while understood with natural gas, may have significant impact upon Hydrogen.

The conclusions from this thesis can be used as a basis for further investigations for future research studies, building upon the work already conducted.

References

[1] ISO 16933: 2007 Glass in Building - Explosion Resistant Security Glazing - Test and Classification for Arena Air-Blast Loading.

[2] K. Ackland, H. Bornstein, and D. Lamos. An Analysis of TNT Equivalencies Using AUTODYN. In *Australasian Structural Engineering Conference 2012: The past, present and future of Structural Engineering, Perth Australia*, 2012.

[3] J. Akhaven. *The Chemistry of Explosives.* Royal Society of Chemistry, Cambridge, UK, 2nd edition, 2004.

[4] D. Allason and D. M. Johnson. Appendix H: Detonation Characteristics of Large Flammable Vapour Clouds (Large Scale Tests). In *Dispersion and Explosion Characteristics of Large Vapour Clouds Volume 2: Appendices.* Steel Construction Institute, UK, 2014.

[5] C. Anderson, W. Baker, D. Wauters, and B. Morris. Quasistatic Pressure, Duration, and Impulse for Explosions in Structures. *International Journal of Mechanical Sciences*, 25(6):455–464, 1982.

[6] ANSYS. ANSYS AUTODYN Product Specification. Website, accessed August 2022, 2022.

[7] Ansys Inc. Ansys Autodyn - Short Duration, Severe Loading Simulations. Website, accessed August 2022, 2022.

[8] C. Aouad, W. Chemissany, P. Mazzali, Y. Temsah, and A. Jahami. Beirut explosion - TNT Equivalence from the Fireball Evolution in the First 170 Milliseconds. *Shockwaves*, 31:813–827, 2021.

[9] Z. Bajic, J. Bogdanov, R. Dimitrijevi, and R. Jeremic. Investigation of Scaled Distance Influence on Shockwave Overpressure for Plastic Explosive PPE-01. In *19th International Seminar on New Trends in Research of Energetic Materials, Pardubice*, number April, 2016.

[10] Z. Bajic, J. Bogdanov, and R. Jeremic. Blast Effects Evaluation Using TNT Equivalence. *Scientific Technical Review*, 59(3-4):50–53, 2009.

[11] Q. Baker. Vapour Cloud Explosion Analysis. *Process Safety Progress*, 15(2):106–109, 1996.

[12] Wilfred E. Baker. *Explosions in Air.* University of Texas Press, Austin and London, 1973.

[13] G. Ballantyne, A. Whittaker, G. Dargush, and A. Aref. Air-Blast Effects on Structural Shapes of Finite Width. *Journal of Structural Engineering*, 136(2):152–159, 2009.

[14] J. Baum, E. Mestreau, H. Luo, and J. Gran. Modeling of Near-field Blast Wave Evolution. In *The 44th AIAA Aerospace Sciences Meeting and Exhibit, Nevada*, 2006.

[15] A. Benselama, M. William-Louis, and F. Monnoyer. Prediction of Blast Wave Effects on a Developed Site. *International Journal of Impact Engineering*, 37(4):385–396, 2010.

[16] M. Berthelot. *Explosives and Their Power.* John Murray, London, 1892.

[17] F. B. A. Beshara. Modelling of Blast Loading on Aboveground Structures - I. General Phenomenology and External Blast. *Journal of Computers and Structures*, 51(5):585–596, 1994.

[18] blastFoam. ERDC Small-Scale High-Explosive Airblast Experiments. website available at https://www.blastfoam.org/examples/erdc-internal-blast-test, 2019.

[19] blastFoam. Simulation of the RECONASS 400kg TNT NEQ Explosive Test. Website available at https://www.blastfoam.org/examples/reconass-explosive-test.md, 2019.

[20] D. Bogosian, M. Yokota, and S. E. Rigby. TNT Equivalence of C4 and PE4: A Review of Traditional Sources and Recent Data. In *The 24th International Symposium on the Military Aspects of Blast and Shock, Halifax NS, Canada*, 2016.

[21] D. Bogosian, A. Yu, T. Dailey, and A. Ohrt. Statistical Variation in Reflected Airblast Parameters from Bare Charges. In *The 23rd International Symposium on the Military Aspects of Blast and Shock, Oxford UK*, 2014.

[22] E. Borenstein. *Loading and Structural Response Models for Transverse Deflection of Circular Plates Subjected to Near Field Explosions.* PhD thesis, 2010.

[23] J. B. W. Borgers and J. Vantomme. Towards a Parametric Model of a Planar Blast Wave Created with Detonating Cord. *The 19th International Symposium on the Military Aspects of Blast and Shock, Calgary Canada*, 2006.

[24] I. Bowen, E. Fletcher, and D. Richmond. Estimate of Man's Tolerance to the Direct Effects of Air Blast. Technical report, Defence Atomic Support Agency, 1968.

[25] T. Bowles, D. Stevens, and M. Stanley. Assessment of Blast Load Prediction in an Urban Environment. In *The 22nd International Symposium on the Military Aspects of Blast and Shock, Bourges, France*, 2012.

[26] P. S. Bulson. *Explosive Loading of Engineering Structures.* Taylor & Francis, New York, 1997.

[27] Buncefield Major Incident Investigation Board. *The Buncefield Incident - 11 December 2005: The Final Report of the Major Incident Investigation Board.* HSE, UK, 2008.

[28] B. A. Burgan. Dispersion and Explosion Characteristics of Large Vapour Clouds. Technical report, Joint Industry Project with the Steel Construction Institute, 2014.

[29] C. Catlin, M. Ivings, S. Myatt, D. Ingram, D. Causon, and L. Quian. Explosion Hazard Assessment: A Study of the Feasibility and Benefits of Extending Current HSE Methodology to take Account of Blast Sheltering. Technical report, Health and Safety Laboratory, UK, 2001.

[30] Centre for Chemical Process Safety. *Guidelines for Vapor Cloud Explosion, Pressure Vessel Burst, BLEVE, and Flash Fire Hazards.* John Wiley and Sons Inc, 2nd Edition edition, 2010.

[31] David B Chang and Carl S. Young. Probabilistic Estimates of Vulnerability to Explosive Overpressures and Impulses. *Journal of Physical Security*, 4(2):10–29, 2010.

[32] R. Cheesman. Definition and Use of TNT Equivalencies in Assessing Loading in Confined Structures. In *ICPS Conference, Manchester UK*, 2010.

[33] A. Chester. A Comparison of Far Field Explosive Loads from a Selection of Current and Emerging Blast Software. In *The 2022 DNV PhD Symposium, Cumbria UK*, 2022.

[34] K. Cheval, O. Loiseau, and V. Vala. Laboratory Scale Tests for the Assessment of Solid Explosive Blast Effects. Part I: Free-field test campaign. *Journal of Loss Prevention in the Process Industries*, 23(5):613–621, 2010.

[35] K. Cheval, O. Loiseau, and V. Vala. Laboratory Scale Tests for the Assessment of Solid Explosive Blast Effects. Part II: Reflected Blast Series of Tests. *Journal of Loss Prevention in the Process Industries*, 25(3):436–442, 2012.

[36] S. Christenensen. The Use of Numberical Calculations in Forensiv Investigation of the 22nd July Bombing in Oslo. In *The 10th International Seminar on Fire and Explosion Hazards*, 2022.

[37] B. Clark. Some Basic Principles of Scaling Explosion Produced Damage to Deep nline Openings in Rock. Technical report, Research and Development Command, US Army, 1965.

[38] T. Cloete and G. Nurick. Blast Characterisation using a Ballistic Pendulum with a Centrally Mounted Hopkinson Bar. *International Journal of Protective Structures*, 7(3):367–388, 2016.

[39] P. Cooper. Comments on TNT equivalence. *The 20th International Pyrotechnics Seminar, Colorado USA*, 1994.

[40] P. Cooper. *Explosives Engineering.* Wiley VCH, London, 1996.

[41] Cranfield University. Prosair computational blast loading tool, 2022.

[42] I. Cullis. Blast Waves and How They Interact With Structures. *Journal of the Royal Army Medical Corps*, 147(1):16–26, 2001.

[43] W. E. Deal. Shock Hugoniot of Air. *Journal of Applied Physics*, 28(7):782–784, 1957.

[44] Department of Defense USA. *TM 5 - 855-1 Design and Analysis of Hardened Structures to Conventional Weapon Effects.* Department of Defense USA, 2002.

[45] J. M. Dewey. 53 Years of Blast Wave Research - A Personal History. In *The 21st International Symposium on the Military Aspects of Blast and Shock, Jerusalem, Israel*, 2010.

[46] J. M. Dewey. The TNT and ANFO Equivalences of the Beirut Explosion. *Shockwaves*, 31(1):95–99, 2021.

[47] M. C. Dewey and J. M. Dewey. The Physical Properties of the Blast Wave produced by a Stoichiometric Propane/Oxygen Explosion. *Shock Waves*, 24(6):593–601, 2014.

[48] M. V. Dharaneepathy, M. N. Keshava-Rao, and A. R. Santhakumar. Critical Distance for Blast-Resistant Design. *Computers and Structures*, 54(4):587–595, 1995.

[49] V. DharmaRao, K. Srinivas Adapaka, K. Venkateswara Rao, and V. S. R. Krishna Prasad. Theoretical and Experimental Studies on Blast Wave Propagation in Air. *Propellants, Explosives, Pyrotechnics*, 40(1):138–143, 2015.

[50] J. S. Díaz. Explosion Analysis from Images: Trinity and Beirut. *European Journal of Physics*, 42(3), 2021.

[51] (DoA) Department of the Army. *Design and Analysis of Hardened Structures for Conventional Weapon Effects (TM 5-855-1).* Washington DC, USA, 1986.

[52] H. Draganic, D. Varevac, and S. Lukic. An Overview and of Methods and for Blast and Load Testing and Devices for Pressure and Measurement. In *Hindawi Advances in Civil Engineering*, volume 2018, pages 1–20, 2018.

[53] J. E. Drotleff, C. T. Vincent, S. A. Mullin, J. D. Walker, and B. L. Morris. Research in Close-In Blast Loading From High Explosives. Technical report, Army Research Laboratory, 1996.

[54] D. Dusenberry, editor. *Handbook for Blast Resistant Design of Buildings.* John WIley and Sons, Inc., 2010.

[55] I. Edri, V. R. Feldgun, Y. S. Karinski, and D. Z. Yankelevsky. Afterburning Aspects in an Intenal TNT Explosion. *International Journal of Protective Structures*, 4(1), 2013.

[56] D. H. Edwards, G. O. Thomas, A. Milne, G. Hooper, and D. Tasker. Blast Wave Measurements Close to Explosive Charges. *Shock Waves*, 2(4):237–243, 1992.

[57] D. E. Esparza. Blast Measurements and Equivalency for Spherical Charges at Small Scaled Distances. *International Journal of Impact Engineering*, 4(1):23–40, 1986.

[58] European Commission. Coefficient of Variation. *European Commission Website - Data Calls and Uploading*, 2022.

[59] M. G. Evinrude. Minor Scale Event Test Execution Report. Technical report, Defence Nuclear Agency, 1986.

[60] G. E. Fairlie, N. F. Johnson, and K. C. Moran. Validated Numerical Simulations of Blast Loads on Structures. In *The 16th International Symposium on the Military Aspects of Blast and Shock, Oxford, UK*, 2000.

[61] D. G. Farrimond, S. E. Rigby, S. D. Clarke, and A. Tyas. Time of Arrival as a Diagnostic for Far-Field High Explosive Blast Waves. *International Journal of Protective Structures*, 13(2):379–402, apr 2022.

[62] J. R. Florek and H. Benaroya. Pulse-Pressure Loading Effects on Aviation and General Egineering Structures - A Review. *Journal of Sound and Vibration*, 284(1-2):421–453, 2005.

[63] S. A. Formby and R. K. Wharton. Blast Characteristics and TNT Equivalence Values for Some Commercial Explosives Detonated at Ground Level. *Journal of Hazardous Materials*, 50(2-3):183–198, 1996.

[64] F. G. Friedlander. The Diffraction of Sound Pulses I. Diffraction by a Semi-Infinite Plane. *Proceedings of the Royal Society of London Part A*, (186):322–344, 1946.

[65] B. Fuchs, J. Covino, and E. Baker. A Critical Review of TNT Equivalency. In *International Explosives Safety Symposium and Exposition, San Diago, USA*, 2018.

[66] J. Ge, G. W. Li, and S. W. Chen. Theoretical and Experimental Investigation on Fragment Behavior of Architectural Glass Panel Under Blast Loading. *Engineering Failure Analysis*, 26:293–303, 2012.

[67] F. R. Gilmore. Equilibrium Composition and Thermodynamic Properties of Air to 24,000K. *U.S. Air Force Project Rand Research Memorandum*, 1955.

[68] M. D. Goel, V. A. Matsagar, A. K. Gupta, and S. Marburg. An Abridged Review of Blast Wave Parameters. *Defence Science Journal*, 62(5):300–306, 2012.

[69] S. A. Granström. Loading Characteristics of Air Blasts from Detonating Charges. *Transactions of the Royal Institute of Technology, Stockholm, Sweden*, 1956.

[70] Hezi Grisaro and Idan Edri. Numerical Investigation of Explosive Bare Charge Equivalent Weight. In *International Journal of Protective Structures*, volume 8, 2017.

[71] E. Gruss. A Correction for Primary Blast Injury Criteria. *The Journal of Trauma*, 60(6):1284–9, 2006.

[72] K. Gugan. *Unconfined Vapour Cloud Explosions*. IChemE, London, 1978.

[73] J. Hallquist. *LS-DYNA® Theory Manual*. March 2006.

[74] R. J. Harris and M. J. Wickens. Understanding Vapour Cloud Explosions: An Experimental Study. Technical report, Institution of Gas Engineers, London, 1989.

[75] M. Held. Blast Load Diagnostics. *Propellants, Explosives, Pyrotechnics*, 34(3):194–209, 2009.

[76] B. Hopkinson. A Method of Measuring the Pressure Produced in the Detonation of High Explosives or by the Impact of Bullets. volume 213, pages 497–508, 1913.

[77] Y. Huang, M. R. Willford, and L. E. Schwer. Validation of LS-DYNA ® MMALE with Blast Experiments. *The 12th international LS-Dyna User Conference, Detroit USA*, (3):1–12, 2012.

[78] C. Hudson. Blast Loading End Effects I. *Armed Forces Special Weapons Project 461*, 1954.

[79] C. C. Hudson. Sound Pulse Approximations to Blast Loading (With Comments on Transient Drag). 1955.

[80] C. Huescar Medina. High Frequency Transducer Functionality Trials. Technical report, DNV, Cumbria UK, 2020.

[81] D. Hyde. DPlot User Manual. Vicksburg, Mississippi, May 2018.

[82] IEP. Global Terroism Index 2022. Technical report, Institute for Econoics and Peace, UK, 2022.

[83] C. M. Jenkins, Y. Horie, and C. Wu. Particle Velocity and Structures in Blast Waves Imaged Using Particle Image Velocimetry. *International Journal of Multiphase Flow*, 36(1):88–91, 2010.

[84] R. Jeremić and Z. Bajić. An Approach to Determining the TNT Equivalence of High Explosives. *Scientific Technical Review*, 3(1):58–62, 2006.

[85] D. M. Johnson. Vapour Cloud Explosion at the IOC Terminal in Jaipur. *Loss Prevention Bulletin*, 229:11–18, 2013.

[86] M. Johnson and D. Allason. Explosion Characteristics of Large Shallow Vapour Clouds: Full Scale Experiments. Technical report, DNV, 2022.

[87] M. Johnson and P. Cronin. Beirut Disaster: Analysis of Video Recordings. Technical report, FABIG Newsletter Issue 078, 2020.

[88] N. Johnson and K. Claber. Blast Measurements - Trends and Anomalies. In *The 16th International Symposium on the Military Aspects of Blast and Shock, Oxford, UK*, 2000.

[89] N. F. Johnson. Discussion: Clearing of Blast Waves from Building Facades. *Proceedings of the Institution of Civil Engineers - Structures and Buildings*, 140(4), 2000.

[90] D. Kakogiannis, D. Van Hemelrijck, J. Wastiels, S. Palanivelu, W. Van Paepegem, J. Vantomme, A. Kotzakolios, and V. Kostopoulos. Assessment of Pressure Waves Generated by Explosive Loading. *CMES - Computer Modeling in Engineering and Sciences*, 65(1):75–93, 2010.

[91] V. Karlos, G. Solomos, and M. Larcher. Analysis of the Blast Wave Decay Coefficient using the Kingery–Bulmash Data. *International Journal of Protective Structures*, 7(3):409–429, jul 2016.

[92] W. D. Kennedy. Explosions and Explosives in Air. *Effects of Impact and Explosion*, 1, 1946.

[93] M. P. Kerry, P. E. Riddle, and B. J. Bibby. Blast Propagation Modification Caused by Regualr and Irregular Multiple Object Arrays. In *The 16th International Symposium on the Military Aspects of Blast and Shock, Oxford, UK*, 2000.

[94] C. N. Kingery and G. A. Coulter. Reflected Overpressure Impulse on a Finite Structure. Technical report, Ballistic Research Laboratory Aberdeen, UK, 1983.

[95] H. Kleine, E. Timofeev, and K. Takayama. Laboratory-scale blast wave phenomena - Optical diagnostics and applications. *Shock Waves*, 14(5-6):343–357, 2005.

[96] C. Knock, N. Davies, and T. Reeves. Predicting Blast Waves from the Axial Direction of a Cylindrical Charge. *Propellants, Explosives, Pyrotechnics*, 40(2):169–179, 2015.

[97] G. S. Langdon, S. Chung Kim Yuen, and G. N. Nurick. Experimental and Numerical Studies on the Response of Quadrangular Stiffened Plates. Part II: Localised Blast Loading. *International Journal of Impact Engineering*, 31(1):85–111, 2005.

[98] C. Langran-Wheeler, S. E. Rigby, S. D. Clarke, A. Tyas, C. Stephens, and R. Walker. Near-field Spatial and Temporal Blast Pressure Distributions from Non-spherical Charges: Horizontally-Aligned Cylinders. *International Journal of Protective Structures*, 12(4):492–516, may 2021.

[99] G. LeBlanc, M. Adoum, and V. Lapoujade. External Blast Load on Structures Empirical Approach. *The 5th European LS DYNA Users Conference, Birmingham, UK*, 2005.

[100] H. Li, G. Ben-Dor, and Z. Y. Han. Analytical Prediction of the Reflected Diffracted Shock Wave Shape in the Interaction of a Regular Reflection with an Expansive Corner. *Fluid Dynamics Research*, 14(5), 1994.

[101] G. Lindkvist. ProSAir A Newly Developed Computational Model. 2006.

[102] P. M. Locking. The Trouble with TNT Equivalence. *The 26th International Symposium on Ballistics, Miami, USA*, pages 143–154, 2011.

[103] LS-Dyna. LS-Dyna. website available at https://www.lstc.com/products/ls-dyna, Accessed 2022.

[104] B. M. Luccioni and D. Ambrosini. Numerical Assessment of Blast Effects Scaling Procedures. Technical report, Asociacion Argentina de Mecanica Computactional, 2010.

[105] W. N. MacPherson, M. J. Gander, J. S. Barton, J. D. C. Jones, C. L. Owen, A. J. Watson, and R. M. Allen. Blast-Pressure Measurement with a High-Bandwidth Fibre Optic Pressure Sensor. *Measurement Science and Technology*, 11(2), 2000.

[106] W. Mercx, A. van den Berg, C. Hayhurst, N. Robertson, and K. Moran. Developments in Vapour Cloud Explosion Blast Modeling. In *Journal of Hazardous Materials*, volume 71, pages 301–319, 1999.

[107] C. Needham. *Blast Waves*. Springer, 2010.

[108] M. D. Netherton and M. G. Stewart. Probabilistic Modelling of Safety and Damage Blast Risks for Window Glazing. *Canadian Journal of Civil Engineering*, 36(8), 2009.

[109] M. D. Netherton and M. G. Stewart. The Effects of Explosive Blast Load Variability on Safety Hazard and Damage Risks for Monolithic Window Glazing. *International Journal of Impact Engineering*, 36(12), 2009.

[110] D. K. Ofengeim and D. Drikakis. Simulation of Blast wave propagation over a cylinder. *Shock Waves*, 7(5):305–317, 1997.

[111] H. J. Pasman, C. Fouchier, S. Park, N. Quddus, and D. Laboureur. Beirut Ammonium Nitrate Explosion: Are Not We Really Learning Anything? *Process Safety Progress*, 39(4), 2020.

[112] T. Payne, A. Williams, S. Rigby, and T. Worfolk. Large scale explosive arena trials - is your target being loaded correctly? *Institute of Explosive Engineers*, pages 10–16, 2016.

[113] PCB Piezotronics. Model 137B Pressure Sensor Installation and Operating Manual. Technical report, PCB Piezotronics, 2021.

[114] PCB Piezotronics. Model 113B ICPÂ® Pressure and Sensor Installation and Operating Manual. 2022.

[115] Photron. Photron FastCam - About Us, 2022.

[116] D. Powell, D. Bogosian, and L. Schwer. Mesh Sensitivity of Blast Wave Propagation. In *The 15th International LS-DYNAÂ® Users Conference Blast, Detroit, USA*, 2018.

[117] D. Preece. It's a Blast. Technical report, Global Technology Development, Orica USA Inc., 2009.

[118] D. K. Pritchard. A Review of Methods for Predicting Blast Damage from Vapour Cloud Explosions. *Journal of Loss Prevention*, 2(4), 1989.

[119] P. J. Rae and J. M. McAfee. The Blast Parameters Spanning the Fireball from Large Hemispherical Detonations of C-4. *Propellants, Explosives, Pyrotechnics*, 43(7):694–792, 2018.

[120] A. M. Remennikov. A Review of Methods for Predicting Bomb Blast Effects on Buildings. *Journal of Battelfield Technology*, 6(3):5–10, 2003.

[121] Denis D Rickman and Donald W Murrell. Development of an Improved Methodology for Predicting Airblast Pressure Relief on a Directly Loaded Wall. *Journal of Pressure Vessel Technology*, 129(1):195, 2007.

[122] W. Riedel, K. Fischer, A. Stolz, I. Haring, and M. Bachmann. Modelling the Vulnerability of Urban Areas to Explosion Scenarios. In *The 3rd International Conference on Protective Structures, Newcastle, Australia*. Springer, 2015.

[123] S. E. Rigby. *Blast Wave Clearing Effects on Finite-Sized Targets Subjected to Explosive Loads*. PhD thesis, University of Sheffield, 2014.

[124] S. E. Rigby, S. D. Fay, A. Tyas, Warren J. A, and S. D. Clarke. Angle of Incidence Effects on Far-Field Positive and Negative Phase Blast Parameters. *International Journal of Protective Structures*, 6(1):23–42, 2015.

[125] S. E. Rigby and Y. Gitterman. Secondary Shock Delay Measurements from Explosive Trials. *The 24th International Symposium on the Military Aspects of Blast and Shock, Halifax, Canada*, 2016.

[126] S. E. Rigby, R. Knighton, S. D. Clarke, and A. Tyas. Reflected Near-field Blast Pressure Measurements Using High Speed Video. *Experimental Mechanics*, (60):875–888, 2020.

[127] S. E. Rigby, T. J. Lodge, S. Alotaibi, A. D. Barr, S. D. Clarke, G. S. Langdon, and A. Tyas. Preliminary Yield Estimation of the 2020 Beirut Explosion Using Video Footage from Social Media. *Shock Waves*, 30(6):671–675, 2020.

[128] S. E. Rigby and P. W. Sielicki. An Investigation of TNT Equivalence of Hemispherical PE4 Charges. *Engineering Transactions*, 62(4):423–435, 2014.

[129] R. Robertson and W. E. Garner. Calorimetry of High Explosives. Technical report, Research Department, Royal Arsenal, Woolwich, 1923.

[130] B. Robins. *New Principles of Gunnery*. General Books LLC, London, 1742.

[131] T. Rose. *Air 3D Version 9 Users' Guide*. Cranfield University, Shrivenham, UK, 2006.

[132] T. A. Rose and P. D. Smith. An Approach to the Problem of Blast Wave Clearing. In *The 16th International Symposium on the Military Aspects of Blast and Shock, Oxford, UK*, 2000.

[133] T. A. Rose and P. D. Smith. Influence of the Principal Geometrical Parameters of Straight City Streets on Positive and Negative Phase Blast Wave Impulses. *International Journal of Impact Engineering*, 27(4):359–376, 2002.

[134] T. A. Rose, P. D. Smith, and J. H. May. The Interaction of Oblique Blast Waves with Buildings. *Shock Waves*, 16(1):35–44, 2006.

[135] M. Sadovskiy. *Mechanical Effects of Air Shockwaves from Explosions According to Experiments*. Nauka Press, 2004.

[136] L. Sadwin and M. Swisdak. The Energy of Airblast Waves. *The 22nd International Symposium on the Military Aspects of Blast and Shock, Bourges, France*, 2012.

[137] L. Sadwin, M. Swisdak, Y. Gitterman, and O. Lotan. Shock Wave Energy: Explosions in Air, Ground and Water. In *The 30th International Symposium on Shock Waves, Israel*, 2017.

[138] J. Shin, A. Whittaker, and D. Cormie. TNT Equivalency for Overpressure and Impulse for Detonations of Spherical Charges of High Explosives. *International Journal of Protective Structures*, 6(3):567–580, 2015.

[139] B. Simoens and M. Lefebvre. Influence of the Shape of an Explosive Charge: Quantification of the Modification. *Central European Journal of Energetic Materials*, 12(2):195–213, 2014.

[140] L. Skotny. Correct Mesh Size - A Quick Guide. *Enterfea Blog*, 2017.

[141] P. D. Smith. Blast Pressure Predictions Between Buildings. *Applied Acoustics*, 35(3):247–251, 1992.

[142] P. D. Smith and T. A. Rose. Blast Wave Propagation in City Streets - An overview. *Progress in Structural Engineering and Materials*, 8(1):16–28, 2006.

[143] P. D. Smith, T. A. Rose, and E. Saotonglang. Clearing of Blast Waves from Building Facades. *Proceedings of the Institution of Civil Engineers - Structures and Buildings*, 134(2):193–199, 1999.

[144] Steel Construction Institute. EMBIG: Energetics Material Blast Information Group, 2022.

[145] C. Stennett, S. Gaulter, and J. Akhavan. An Estimate of the TNT Equivalent Net Explosive Quantity of the Beirut Port Explosion Using Publicly Available Tools and Data. *Propellants, Explosives, Pyrotechnics*, 45(11):1675–1679, 2020.

[146] C. Stirling. Viper :: Blast.

[147] M. Swisdak and L. Sadwin. Airblast Equivalent Weight and Yield Determinations Based on Measurements of Energy and Other Blast and Wave Parameters. In *The 23rd International Symposium on the Military Aspects of Blast and Shock, Oxford, UK*, 2014.

[148] M. M. Swisdak. Explosion Effects and Properties Part 1 - Explosion Effects in Air. *Naval Surface Weapons Centre, White Oak Laboratory, Silver Springs, USA*, 1975.

[149] A. Tatlısuluoğlu and S. Beji. Blast Pressure Measurements of an Underwater Detonation in the Sea. *Journal of Marine Science and Application*, 20(4):706–713, 2021.

[150] Geoffrey Taylor. The Formation of a Blast Wave by a Very Intense Explosion. II. The Atomic Explosion of 1945. *Proceedings of the Royal Society A: Mathematical, Physical and Engineering Sciences*, 201(1065):175–186, 1950.

[151] D. Thompson, J. M. Janus, and E. Luke. Multi-Fidelity Tools for Blast Analysis in Urban Environments. Technical report, South East Region Research Initiative, 2011.

[152] K. Tomisaka. Rankine-Hugoniot Relation. Technical report, National Astronomical Observatory of Japan, 2007.

[153] A. Tyas. Experimental Measurement of Pressure Loading from Near-Field Blast Events: Techniques, Findings and Future Challenges. In *The 18th International Conference on Experimental Mechanics, Belgium*, 2018.

[154] A. Tyas. Blast Loading from High Explosive Detonation: What We Know and Don't Know. In *The 13th International Conference on Shock and Impact Loads on Structures, China*, 2019.

[155] A. Tyas, T. Bennett, J. Warren, and S. Fay. Prediction of Clearing Effects in Far Field Blast Loading of Finite Targets. *Shock Waves*, 21(2):111–119, 2011.

[156] A. Tyas, T. Bennett, J. Warren, S. Fay, and S. Rigby. Clearing of Blast Waves on Finite-Sized Targets - An Overlooked Approach. *Applied Mechanics and Materials*, 82:669–674, 2011.

[157] A. Tyas, J. J. Reay, S. D. Fay, S. D. Clarke, S. E. Rigby, J. A. Warren, and D. J. Pope. Experimental studies of the effect of rapid afterburn on shock development of near field explosions. *International Journal of Protective Structures*, 7(3), 2016.

[158] US Department of Defence. *UFC 3-340-02 Structures to Resist the Effects of Accidental Explosions*. US Department of Defence, 2008.

[159] A. C. Van Den Berg and A. Lannoy. Methods for Vapour Cloud Explosion Blast Modelling. *Journal of Hazardous Materials*, 34(2):151–171, 1993.

[160] P. Walter. Air-Blast and the Science of Dynamic Pressure Measurements. Technical report, PCB Piezotronics, 2004.

[161] P. Walter. Measuring Static Overpressures in Air Blast Environments. Technical report, PCB Piezotronics, 2008.

[162] C. Wu, G. Fattori, A. Whittaker, and D. J. Oehlers. Investigation of Air-Blast Effects from Spherical and Cylindrical Shaped Charges. *International Journal of Protective Structures*, 1(3), 2010.

[163] W. Xiao, M. Andrae, and N. Gebbeken. Air Blast TNT Equivalence Concept for Blast Resistant Design. *International Journal of Mechanical Sciences*, 185, 2020.

[164] W. Xiao, K. Chen, H. D. Xing, and B. L. Wang. Effect of Storage Temperature on Explosion Characteristics of RDX-Based Thermobaric Explosive. *Journal of Physics Conference Series*, 1507(2), 2020.

[165] Y. Yan, C. Youngsik, J. Lee, and K. Yun. Influence of the Shape of Explosive Charge on the Blast Wave Propagation. *MATEC Web of Conferences*, 54, 2016.